# USAAVLABS TECHNICAL REPORT 68-13A

# TWO-DIMENSIONAL TESTS OF AIRFOILS OSCILLATING NEAR STALL

## VOLUME 1

## SUMMARY AND EVALUATION OF RESULTS

By
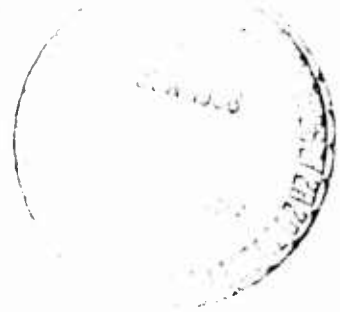
Jaan Liiva
Franklyn J. Davenport
Lewis Gray
Ivor C. Walton

Disclaimers

The findings in this report are not to be construed as an official Depart-
ment of the Army position unless so designated by other authorized
documents.

When Government drawings, specifications, or other data are used for
any purpose other than in connection with a definitely related Government
procurement operation, the United States Government thereby incurs no
responsibility nor any obligation whatsoever; and the fact that the Govern-
ment may have formulated, furnished, or in any way supplied the said
drawings, specifications, or other data is not to be regarded by impli-
cation or otherwise as in any manner licensing the holder or any other
person or corporation, or conveying any rights or permission, to manu-
facture, use, or sell any patented invention that may in any way be
related thereto.

Trade names cited in this report do not constitute an official endorse-
ment or approval of the use of such commercial hardware or software.


Disposition Instructions

Destroy this report when no longer needed. Do not return it to the
originator.

AD 670 957

TWO-DIMENSIONAL TESTS OF AIRFOILS OSCILLATING
NEAR STALL. VOLUME I. SUMMARY AND EVALUATION
OF RESULTS

Jaan Liiva, et al

Boeing Company
Philadelphia, Pennsylvania

April 1968

This report was prepared by Vertol Division, The Boeing Company, under the terms of Contract DA 44-177-AMC-438(T). It consists of results obtained from wind tunnel tests of airfoils oscillating near the stall angle of attack. The data were obtained at conditions comparable to those existing in present-day helicopters.

The object of this contractual effort was to obtain data on airfoils undergoing harmonic motion to serve as a basis for improvement of rotor theories. The unsteady aerodynamics data can provide a more realistic stall boundary and dynamic airloads if they are incorporated into present rotor theories.

The conclusions contained herein are concurred in by this command. The recommendations are sound. The report is published for the exchange of information and the stimulation of ideas.

Task 1F125901A14231
Contract DA 44-177-AMC-438(T)
USAAVLABS Technical Report 68-13A
April 1968

TWO-DIMENSIONAL TESTS OF AIRFOILS
OSCILLATING NEAR STALL

VOLUME I

SUMMARY AND EVALUATION OF RESULTS

D8-0678-1

By

Jaan Liiva
Franklyn J. Davenport
Lewis Gray
Ivor C. Walton

Prepared by

The Boeing Company
Vertol Division
Philadelphia, Pennsylvania

for

U. S. ARMY AVIATION MATERIEL LABORATORIES
FORT EUSTIS, VIRGINIA

## SUMMARY

This report presents the results of an experimental investigation of rotor blade dynamic stall. Forces and moments in two-dimensional flow on two typical helicopter rotor airfoils (NACA 0012 and Vertol 23010-1.58), in oscillatory pitch and vertical translation, were determined by measuring differential pressures. The Mach number, Reynolds number, and angle of attack prevailing in the retreating-blade stall region were investigated up to typical first-bending and first-torsion mode natural frequencies.

Pitch oscillation was found to increase the angle of attack at which stall occurred, with a consequent increase in maximum normal force. Hysteresis effects on the pitching moment resulted in negative aerodynamic damping of oscillations about mean angles of attack near the steady-flow stall value at Mach 0.2 and 0.4. At Mach 0.6, little or no such hysteresis appeared. The increase in usable angle of attack and maximum normal force due to airfoil camber was found to prevail under nearly all oscillatory conditions tested, as well as in steady flow.

Oscillatory translation at angles of attack near stall also showed increased maximum normal force for both airfoils. Furthermore, lag effects in the stall-unstall process were noted which could result in self-sustaining blade bending oscillations.

Additional tests were conducted with a torsionally flexible airfoil dynamic system, tuned to frequencies corresponding to typical rotor blade first-torsion mode values, and subjected to angle-of-attack oscillation at a frequency corresponding to a helicopter's 1/rev angle-of-attack change. Torsional oscillations due to stall were noted under several conditions.

## FOREWORD

# TABLE OF CONTENTS

# LIST OF ILLUSTRATIONS

# LIST OF SYMBOLS

| | |
|---|---|
| a | speed of sound, feet per second |
| b | airfoil semichord, feet |
| c | airfoil chord, feet |
| $C_D$ | airfoil drag coefficient |
| $\overline{C}_D$ | mean value of drag coefficient over an oscillation cycle |
| $C(k)$ | Theodorsen's function for unsteady flow |
| $C_L$ | airfoil lift coefficient, positive up |
| $C_M$ | airfoil pitching moment coefficient, positive nose-up |
| $C_N$ | airfoil normal force coefficient, positive up |
| $C_{N_{MAX}}$ | maximum value of normal force coefficient attained in oscillation cycle |
| e | distance from midchord of airfoil to pitch axis, in semichords |
| f | drive frequency of airfoil motion in pitch or translation oscillation, Hertz |
| $f_e$ | effective drag area, square feet |
| $f_T$ | tuned system resonant frequency, Hertz |
| h | translation position, positive up, semichords |
| $I_T$ | tuned system inertia, slug-ft$^2$ |
| k | $\pi fc/V$, reduced frequency parameter |
| $k_T$ | $\pi f_T c/V$, reduced frequency parameter of tuned system |
| M | tunnel free-stream Mach number |
| n | number of harmonic |
| $P_S$ | wind tunnel static pressure, pounds per square inch |

xiv

| | |
|---|---|
| $P_T$ | wind tunnel total pressure, pounds per square inch |
| $R$ | Reynolds number |
| $T_T$ | wind tunnel total temperature, degrees Rankine |
| $U$ | $\sqrt{(U_T{}^2 + U_P{}^2)}$, rotor blade airfoil velocity vector magnitude |
| $U_P$ | total of velocity components perpendicular to rotor tip path plane at a blade station, feet per second |
| $U_T$ | total of velocity components parallel to rotor tip path plane at a blade station, feet per second |
| $V$ | tunnel velocity, feet per second |
| $W$ | work function, foot-pounds |
| $x$ | airfoil chordwise location, measured from leading edge, feet |
| $y$ | airfoil surface location measured perpendicular to chord line, feet |
| $\alpha$ | instantaneous airfoil angle of attack, positive nose-up, degrees |
| $\alpha'$ | first differential of $\alpha$ with respect to pitch reference |
| $\alpha''$ | second differential of $\alpha$ with respect to pitch reference |
| $\alpha_o$ | mean angle of attack, degrees, positive for nose-up |
| $\alpha_{STALL}$ | angle of attack corresponding to $C_{N_{MAX}}$, degrees |
| $\gamma_T$ | torsional Locke number |
| $\delta\alpha$ | elastic deflection of tuned system, degrees |
| $\Delta\alpha$ | magnitude of forced pitching motion, degrees |
| $\Delta C_P$ | differential pressure coefficient |
| $\Delta h$ | magnitude of forced translation motion, semichords |

xv

| | |
|---|---|
| $\Delta P$ | differential pressure, pounds per square inch |
| $\Delta W_\alpha$ | $(2\pi^2 f \Delta\alpha^2)^{-1} \oint C_M d\alpha$, work-per-cycle coefficient for pitching oscillation |
| $\Delta W_h$ | $(2\pi^2 f \Delta h^2)^{-1} \oint C_N dh$, work-per-cycle coefficient for translation |
| $\zeta$ | damping as fraction of critical damping |
| $\theta$ | pitch and translation motion reference angle, degrees |
| $\theta_A$ | rotor blade airfoil section geometric angle of attack, degrees |
| $\mu'$ | rotor blade tip speed ratio |
| $\rho$ | density of air, slugs per cubic foot |
| $\phi$ | $\tan^{-1} U_p/U_T$, induced angle of attack of rotor blade, degrees |
| 1/rev, 3/rev, etc. | one per revolution, three per revolution, etc. |
| $(\bar{\ })$ | wind tunnel axis system |

# INTRODUCTION

Contemporary helicopters frequently fly with the rotor blade
partially stalled in some regions of the azimuth. This is
caused by the combined effects of reduced dynamic pressure on
the retreating side of the disc and the requirement for roll
equilibrium. Furthermore, in the reverse-flow region, the
blade actually moves through the air with the trailing edge
foremost. Consequently, an increase in aircraft forward speed
without a corresponding increase in rotor rpm implies en-
largement of the region where stall may be a problem. In fact,
retreating blade stall is generally the factor which limits
helicopter speed, regardless of the engine power available.
The capability to predict the effects of blade stall accurately
is therefore a vital factor in the successful development of
the full speed potential of a helicopter.

Stall prediction is much more complex on helicopter rotors
than on conventional aircraft wings, because of the highly
variable aerodynamic environment of the rotor blade as it
moves around the azimuth. This environment is complex because:

1.  The angle of attack is influenced by blade motion,
    cyclic pitch, and the complex induced-flow field
    associated with the blade vortex system.

2.  The blade is practically never subjected to a simple
    flow approaching it at right angles to its edges.
    Normally, there is a substantial component of wind
    velocity along the blade. This is analogous to the
    effect of sweepback on conventional wings, which is
    known to have considerable influence on stall behavior.

3.  There is the effect of unsteady flow on the behavior
    of the blade aerodynamic forces.

Attempts to predict the effects of blade stall on performance
by using steady-state airfoil characteristics with stall and
Mach number accountability in a strip theory analysis have been
unsuccessful; the onset of stall is predicted too early.

This is shown in Figure 1 for the H-21 rotor, which was tested
in the 40- by 80-foot wind tunnel at Ames Research Center[1].
The theory predicts stall at a much lower value of lift than
the wind tunnel test data. Simple modifications to the perfor-
mance theory, consisting of the deletion of stall in the $C_L$
data up to an angle of attack of 20 degrees (the drag and
pitching moment data are left unchanged), have provided the
means for predicting rotor performance adequately; this is
shown in Figure 1 by the dotted line. However, the angle of

1
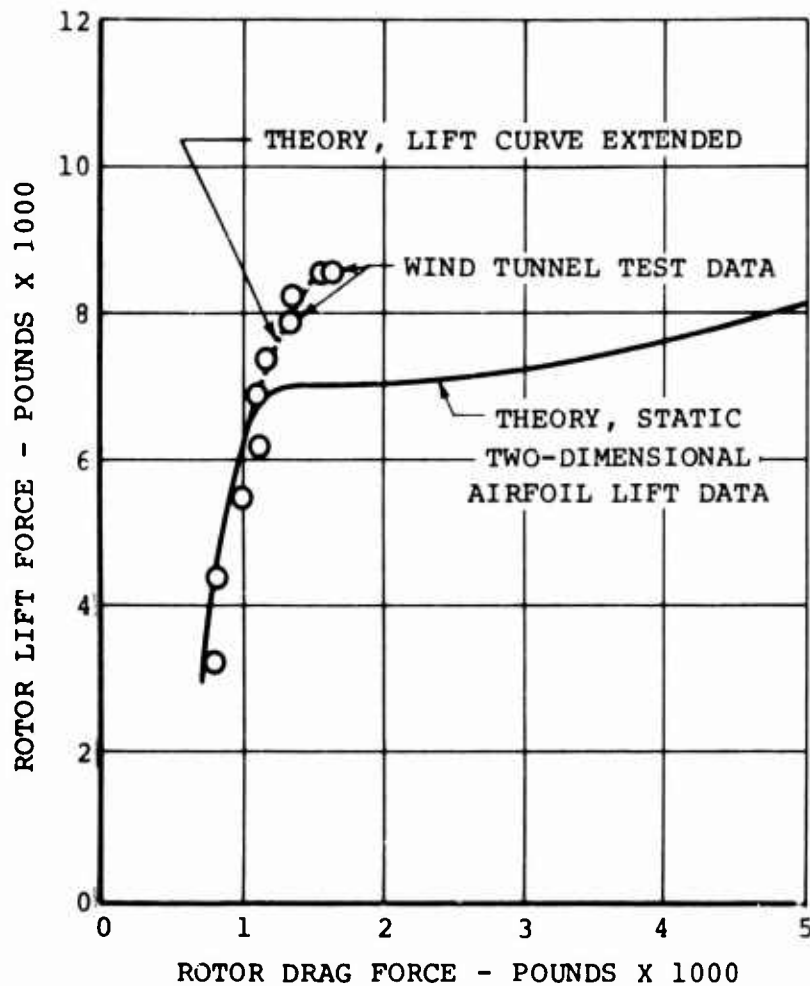
NOTES: 1. TEST CONDITIONS:
   A. $\theta_{.75} = 15°$
   B. $\mu' = 0.34$
   C. $M_{(1)(90)} = 0.716$

2. REFERENCE: NACA TN 4367

3. THEORY COMPENSATED BY AN INCREMENTAL DRAG FORCE DUE TO THE UNCERTAIN LEVEL OF WALL INTERFERENCE AND UNKNOWN CONTRIBUTION OF ROTOR HUB DRAG.

Figure 1.   Rotor Drag Correlation for H-21 Rotor.

2

attack for stall on the rotor blade is somewhere between static stall and the value of 20 degrees which was chosen for the analysis, and the rotor stall limit must therefore be determined separately by testing a similar model or a full-scale rotor in a wind tunnel.

It has been suggested by Harris[2] that the increase in the maximum $C_L$, above the static stall values, can be caused by radial flow or unsteady aerodynamic effects. Radial flow effects were included in a performance analysis, but they did not increase $C_L$ sufficiently to correlate theory with test data; stall was still predicted too early.

Halfman's test data[3] on a pitching airfoil show that the maximum lift experienced by an airfoil oscillating through stall can be substantially higher than the two-dimensional static value. Dynamic effects, then, are the most likely reason for the stall delay exhibited by a helicopter rotor blade.

Another problem is also important for safety reasons. Flight test experience has indicated that large blade torsional oscillations can be encountered before severe vibration warns the pilot of stall, especially under high weight conditions. Moreover, this can happen before the speed limit due to maximum available engine power is reached.

This phenomenon involves interaction of the blade's torsional elastic behavior with its aerodynamic pitching moment ($C_M$). Under the high-$\alpha$, unsteady-flow conditions in question, $C_M$ behaves in a highly nonlinear way. Therefore, to provide a basis for predicting the onset and severity of such oscillations, experimental $C_M$ data for those conditions are needed.

A literature search (see SELECTED BIBLIOGRAPHY) reveals that even though many wind tunnel tests have been performed to evaluate the effects of oscillatory motion on airfoil loads, most of them have been aimed at establishing effects on airplane wings; thus, they were carried out under test conditions and for model configurations which are not directly applicable to helicopter rotor blades.

The only such data directly applicable (pitching about quarter-chord, at realistic Mach and Reynolds numbers) were obtained by Carta. His data, however, remain unavailable except for some average damping curves and the few normal force and pitching moment curves published[4,5]. Halfman's data, already noted, did cover both pitching and translation motion of a typical helicopter airfoil. However, the Mach number range was not high enough, and the pitch axis was too far aft.

Model and full-scale rotor tests are another source of lift and pitching moment data. However, such tests are highly

three-dimensional, and it is difficult to separate the
contributions of radial flow from those of unsteady flow.
Furthermore, the angle of attack is a very uncertain quantity.
These data are still valuable in that they can provide an
ultimate check on the analytical methods which must be developed
to use nonsteady two-dimensional airfoil data.

To provide this needed capability to predict stall under
dynamic conditions, both for rotor loads and for performance
analyses, the program to wind tunnel test oscillating airfoils
reported herein was undertaken. Its objective was to provide
a comprehensive framework of experimental data around which
theories of dynamic stall can be developed.

## SELECTION OF TEST CONDITIONS AND VARIABLES

The model characteristics and the operating conditions required for a comprehensive series of tests designed to isolate and clarify the influence of unsteady flow on rotor blade stall are reviewed in this section.

The five items to be defined are:

1. Mode of testing (i.e., two- versus three-dimensional flow)

2. Airfoil configuration

3. Model scaling

4. Airfoil motion

### TEST MODE

The purpose of this test program was to isolate the effects of time-varying angle of attack on rotor stall. A two-dimensional flow has all the main characteristics which will create the pressure distribution traits responsible for boundary layer separation. A two-dimensional wind tunnel also provides very close control of airfoil angle and motion with respect to the relative wind; therefore, such a facility was a natural choice.

The absence of a centrifugal force field and of a fluctuating spanwise component of free-stream flow can have only secondary effects on the results below and at stall. Their influence on the blade surface pressures arises through changes in boundary layer thickness due to spanwise variations in pressure or velocity. These changes are small compared to the blade surface motions of interest here.

### AIRFOIL CONFIGURATION

To establish a link to previous work and to provide a data base against which more advanced airfoil sections can be measured, the NACA 0012 (modified) was the first airfoil chosen for testing. The modifications consist of a symmetrical leading-edge fairing (corresponding to a typical anti-icing boot) and a flat sheet metal trailing-edge extension. The resulting configuration is identical to the rotor blade section used on the CH-47A helicopter. An advanced airfoil, of the type used on the CH-47B, was chosen for comparison. This airfoil has a camber line similar to the NACA 230 and a thickness ratio of about 10 percent. A cuspate trailing edge similar to that of the first airfoil is used. The second airfoil was also tested with a 3-degree upward deflection of the trailing edge, which

5

flight test experience has shown to be desirable.  Airfoil contours and coordinates are shown in Figure 2.

## MODEL SCALING

Three basic parameters govern the scaling of the model.  These are the Mach number (M), Reynolds number (R), and reduced frequency (k).

$$R = \frac{Vc}{\nu} \tag{1}$$

$$M = \frac{V}{a} \tag{2}$$

$$k = \frac{\pi f c}{V} \tag{3}$$

For full aerodynamic similarity, the Mach number and the Reynolds number for the model and the full-scale rotor blade must be identical.

$$\frac{(R)_{MODEL}}{(R)_{FULL\ SCALE}} = \frac{(Vc)_{MODEL}}{(Vc)_{FULL\ SCALE}} \times \frac{(\nu)_{FULL\ SCALE}}{(\nu)_{MODEL}} \tag{4}$$

$$\frac{(M)_{MODEL}}{(M)_{FULL\ SCALE}} = \frac{(V)_{MODEL}}{(V)_{FULL\ SCALE}} \times \frac{(a)_{FULL\ SCALE}}{(a)_{MODEL}} \tag{5}$$

Equations (4) and (5) are satisfied by testing at full-scale velocity in a pressurized wind tunnel with air as the testing medium.  Since the tunnel size dictated a model chord of 27 percent of full-scale size, the test section total pressure and the kinematic viscosity were adjusted to provide full-scale Reynolds numbers.

Figure 3 shows the Mach and Reynolds numbers used for these tests.  Figure 4 shows the advancing and retreating tip Mach number conditions typical of current and advanced-design helicopter rotors.  Mach numbers from 0.3 to 0.5 are of special interest at the tip of the retreating blade near the 270-degree azimuth.  However, conditions at other points (highest angles of attack are often reached at approximately 300 degrees) require the somewhat wider band of 0.2 to 0.6 Mach number chosen for these tests.

For dynamic similarity, the reduced frequency for the model and full-scale blade must be identical.  Since the velocity V was determined by aerodynamic considerations, the requirement for dynamic similarity can be satisfied as follows:

6
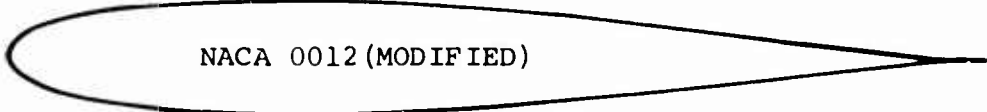
NACA 0012 (MODIFIED)

| x/c | y/c |
|-----|-----|
| 0 | 0 |
| 0.0110 | 0.0170 |
| 0.0220 | 0.0230 |
| 0.0330 | 0.0270 |
| 0.0540 | 0.0340 |
| 0.0760 | 0.0390 |
| 0.1087 | 0.0445 |
| 0.1521 | 0.0493 |
| 0.2065 | 0.0527 |
| 0.2500 | 0.0542 |
| 0.3043 | 0.0547 |
| 0.3478 | 0.0541 |
| 0.4130 | 0.0520 |

| x/c | y/c |
|-----|-----|
| 0.4564 | 0.0499 |
| 0.5000 | 0.0472 |
| 0.5434 | 0.0439 |
| 0.6086 | 0.0383 |
| 0.6521 | 0.0343 |
| 0.6955 | 0.0300 |
| 0.7607 | 0.0230 |
| 0.8042 | 0.0181 |
| 0.8477 | 0.0127 |
| 0.8911 | 0.0070 |
| 0.9346 | 0.0011 |
| 1.000 | 0.0011 |

LEADING-EDGE RADIUS = 0.0143
$x = 0.0143$
$y = 0.0$
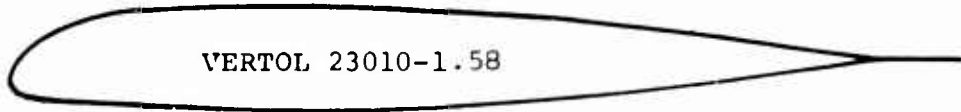
VERTOL 23010-1.58

| x/c | $y/c_U$ | $y/c_L$ |
|-----|---------|---------|
| 0 | -0.0251 | 0.0215 |
| 0.0056 | -0.0070 | 0.0336 |
| 0.0096 | -0.0028 | 0.0361 |
| 0.0135 | 0.0008 | 0.0374 |
| 0.0254 | 0.0097 | 0.0394 |
| 0.0333 | 0.0145 | 0.0401 |
| 0.0571 | 0.0253 | 0.0419 |
| 0.0967 | 0.0369 | 0.0443 |
| 0.1462 | 0.0451 | 0.0471 |
| 0.1957 | 0.0489 | 0.0497 |

| x/c | $y/c_U$ | $y/c_L$ |
|-----|---------|---------|
| 0.2452 | 0.0499 | 0.0517 |
| 0.2848 | 0.0499 | 0.0523 |
| 0.3937 | 0.0479 | 0.0503 |
| 0.4729 | 0.0444 | 0.0464 |
| 0.5521 | 0.0396 | 0.0412 |
| 0.6313 | 0.0335 | 0.0346 |
| 0.7502 | 0.0223 | 0.0228 |
| 0.8293 | 0.0137 | 0.0139 |
| 0.9086 | 0.0046 | 0.0047 |
| 0.9440 | 0.0010 | 0.0011 |
| 1.000 | 0.0010 | 0.0011 |

LEADING-EDGE RADIUS = 0.0158
$x = 0.0158$
$y = -0.0215$

Figure 2. Test Airfoil Coordinates.
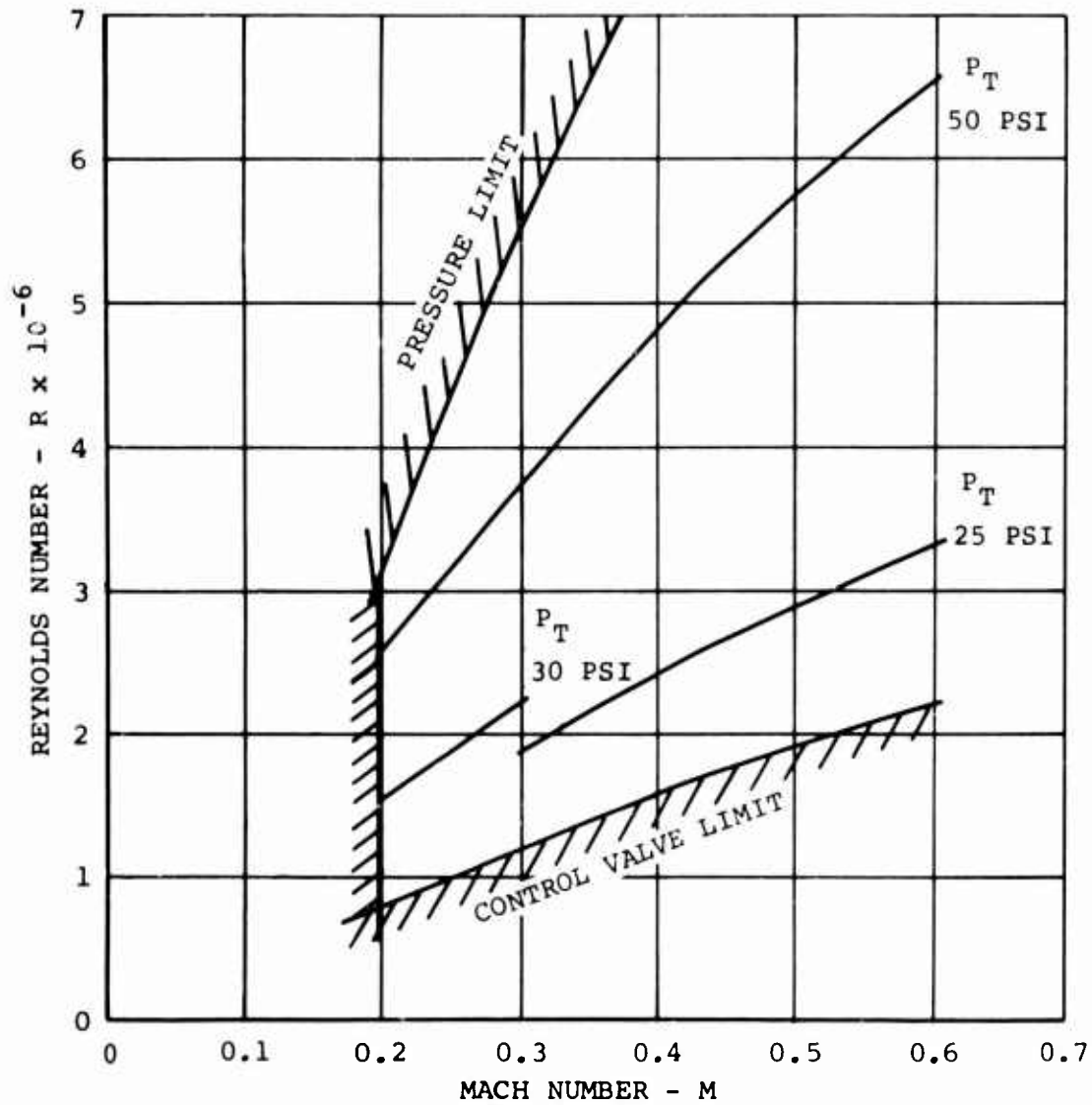
Figure 3. Reynolds Number Variation With Mach Number
for Wind Tunnel.

8
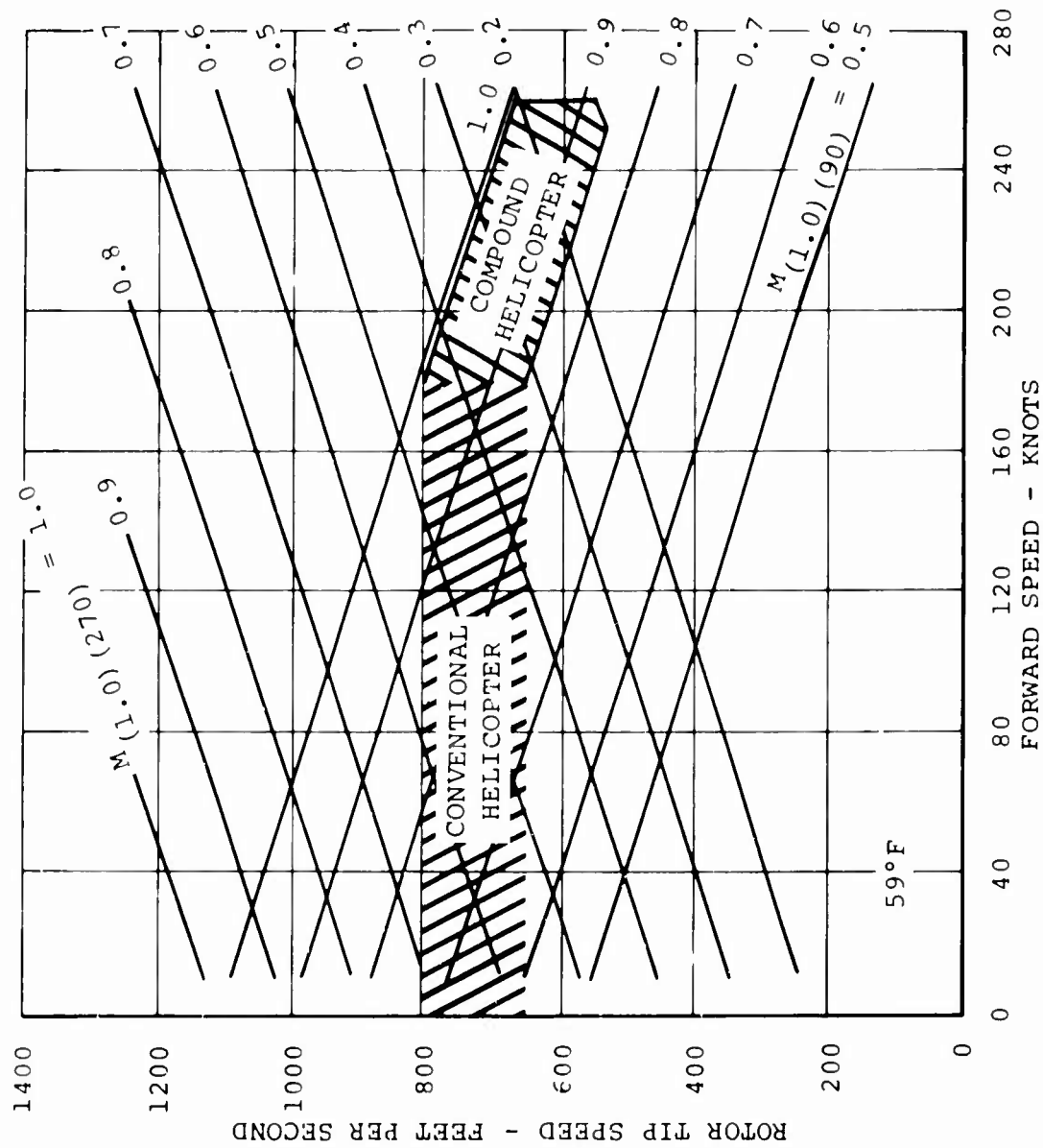
Figure 4. Present and Envisioned Helicopter Operating Region.

9

$$\frac{(k)_{\text{MODEL}}}{(k)_{\text{FULL SCALE}}} = \frac{(fc)_{\text{MODEL}}}{(fc)_{\text{FULL SCALE}}} \tag{6}$$

This was achieved by increasing the model oscillation frequency in proportion to the decrease in model chord. The testing frequencies and amplitudes of motion are discussed in the next section.

## AIRFOIL MOTIONS

Before considering what kinematic characteristics will be required of the model, the following should be noted concerning the question of frequency scaling between the airfoil model and the actual rotor.

Aerodynamic similarity requires that the time to execute a given motion, expressed as a ratio to the time for the airstream to move one semichord, should be the same for the model as for the rotor blade. It can easily be shown that if this quantity is matched (along with the Mach and Reynolds numbers), then complete two-dimensional aerodynamic similarity is obtained. For periodic motions, this characteristic time is used to nondimensionalize the frequency to obtain k, the reduced frequency (sometimes called the Strouhal number).

To investigate the required airfoil kinematics, consider first the rotor blade relative-wind vector diagram sketched below.



VELOCITIES AND ANGLES
REFERRED TO TIP PATH
PLANE AXES
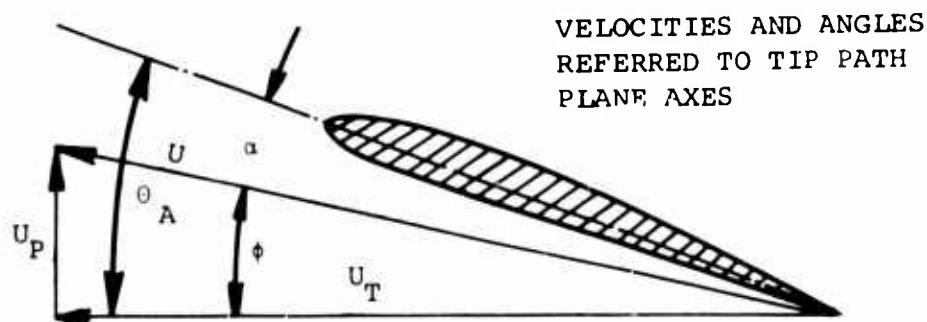
The following time variations appear in the parameters shown:

1. $U_T$

    a. Varies sinusoidally at 1/rev because of aircraft forward speed

10

    b. Varies at higher frequencies (but very low amplitude) because of chord bending

    c. Varies irregularly because of vortex effects

2. $U_P$

    a. Has no 1/rev variation since axes are referred to plane of no flapping

    b. Varies at frequencies of 2/rev and higher because of flap bending at appreciable amplitude

    c. Varies irregularly because of vortex effects

3. $\theta_A$

    a. Varies at 1/rev because of cyclic pitch and/or flapping motion (accepting the classical equivalence between flapping and feathering)

    b. Varies at higher frequencies (4/rev or higher) because of blade torsional motion

It should be noted in regard to $\theta_A$ that typical hub and rotor blade designs have both the pitch bearing axis and the shear center near, or slightly forward of, the quarter-chord point; therefore, that location on the airfoil chord line was chosen as the center of rotation for pitch oscillations.

For the rotor blade, $U$, $\phi$, and $\alpha$ are dependent variables which can be deduced from the three quantities already discussed. For the wind tunnel model, the independent variables can also be taken as $U_T$, $U_P$, and $\theta_A$. (In the discussion below, the corresponding wind tunnel variables will be denoted by $\bar{U}_T$, $\bar{U}_P$, and $\bar{\theta}_A$ to avoid confusion.) $\bar{U}_T$, $\bar{U}_P$, and $\bar{\theta}_A$ are subject to certain restrictions because of mechanical or operational limitations of the model or test facility; i.e.,

1. $\bar{U}_T$ may not oscillate.

2. $\bar{U}_P$ is limited to sinusoidal variations of amplitude $f\Delta h$ about a mean value of zero. Furthermore, as f increases, the available $\Delta h$ will be limited by strength and vibration considerations, and $\Delta h$ cannot exceed 0.31 chord in any case.

3. $\bar{\theta}_A$ may oscillate over a large range of amplitude and frequency at any desired mean value; however, $\bar{\theta}_A$ and $\bar{U}_P$ cannot oscillate at the same time.

11

Within these constraints, which of the time-varying parameters listed above can be studied meaningfully?  Consider them in the order given:

1. Direct simulation of $U_T$ variation by $\bar{U}_T$ is obviously ruled out.  However, it is conceivable that $\alpha$ variations due to changes in $U_T$ (item 1a) at fixed $U_P$ might be simulated by $\bar{\theta}_A$ oscillations at constant $\bar{U}_T$. (A substantial average negative $U_P$ must prevail on a rotor producing propulsive force at high speed.) This possibility was explored analytically using unsteady-flow potential theory.  It was concluded that such a simulation would not be meaningful, because of time lag effects due to the shedding of counter-vortexes.

2. $U_P$ variation due to flap bending (item 2b) can be simulated and is of interest.  Appropriate frequencies and amplitudes are discussed in a following paragraph (Blade Elastic Motion Study).  Item 2c was considered to be beyond the scope of the work undertaken in this effort.

3. The 1/rev variation of $\theta_A$ (item 3a) can easily be simulated by appropriate $\bar{\theta}_A$ oscillations.  Dynamic lift curve behavior above static stall, under these conditions, was one of the two main concerns prompting this investigation.  Item 3b, higher frequency $\theta$ variations, can also be studied by $\bar{\theta}_A$ motions; this is the second principal reason for undertaking this work. Frequencies, amplitudes, and other aspects of the motion are also discussed in the next major paragraph.

It will not be necessary again to discuss relative wind, angle of attack, or other elements of the airfoil model as distinct from those of the rotor blade in the same context.  Therefore, the notation used in the remainder of this report will conform to the usual wind tunnel practice;  i.e., $\alpha$ (instead of $\bar{\theta}_A$) will refer to the angle between airfoil chord line and the wind tunnel centerline, and V (instead of $\bar{U}_T$) will refer to test section wind speed.

## BLADE ELASTIC MOTION STUDY

A computer analysis was made of rotor blade aeroelastic motions for a variety of blade configurations and flight conditions.  The ranges of amplitude and frequency of those results were used as guides in defining test conditions.

The results were as follows:

1. Pitching motion about the airfoil quarter-chord at amplitudes of 2.5 degrees and 5 degrees and frequencies corresponding to the range from 4/rev to 6/rev were found to be sufficient to cover the effects of blade torsional oscillations. To permit clear definition of trends with frequency, it was also found necessary to conduct tests of pitching motions at 2/rev and 3/rev. The higher frequency pitching tests, together with 1/rev oscillations at amplitudes up to 7.5 degrees, provided thorough coverage of the ranges of interest in rotor technology.

2. Plunging motions of 0.3 and 0.45 semichord amplitude, at a frequency corresponding to 2/rev, were found to be sufficient to cover the effects of blade bending. To establish trends with frequency, tests were also found to be desirable at 1/rev.

## STALL OF A SIMULATED TORSIONALLY FLEXIBLE BLADE

When stall occurs, the actual pitching motion of a rotor blade element will generally be much more complex than a simple harmonic oscillation. Because rotor blades are usually very limber in torsion, the large nose-down pitching moment normally associated with stall can cause a rapid and substantial negative elastic twist. This leads to loss of lift due to reduced angle of attack and other complications. (Harris and Pruyn discuss this in their paper[2].) Under some circumstances, self-sustaining limit-cycle oscillations (or stall flutter) may occur, as discussed by Carta[4].

Motions of two distinct types appear to be involved: (1) the 1/rev sinusoidal variation due to cyclic pitch control, and (2) torsional oscillations which if present would be expected to occur at a frequency close to the first torsional natural frequency of the blade (in the range from 4/rev to 6/rev). These motions are superposed on the 1/rev motion. Their amplitude and their persistence with time will depend on the blade dynamic characteristics and on the amplitude and mean value of the 1/rev background motion.

In order to show the combined effects of the two kinds of motion, it was decided to conduct tests of a tuned system, in which the airfoil is mounted on a torsion spring through which the background 1/rev motion is transmitted. The spring stiffness was varied to give a range of natural frequencies from four to six times the background frequency.

13

The data from these tests also serve a second purpose: they represent a comparatively simple dynamic system on which mathematical models constructed from the data obtained in forced sinusoidal motion may be tried out.

## TEST FACILITIES, DATA RECORDING, AND REDUCTION SYSTEMS

A detailed description of the test facility, apparatus, and data reduction system is presented in Volume II of this report. A short summary is presented here.

### TEST FACILITIES

The variable density, two-dimensional 1-by-3-foot test section of the Boeing 4-by-4-foot supersonic wind tunnel was used for these tests. The tunnel total pressure and the resulting air density were varied to simulate full- and half-scale Reynolds numbers for a typical transport helicopter rotor blade.

#### Pitch Mechanism

The pitch oscillating mechanism is shown in Figure 5. A flywheel with an eccentrically mounted, interchangeable cam drives a crank which is connected to the airfoil by a torsion spring for the tuned system, or by an adapter for direct drive. A hydraulic motor supplies the power. An eddy-current damper was used with the tuned system for safety.

#### Vertical Translation

A system similar to the pitch mechanism was used for the translation tests. Airfoil endplates were required with the translating mechanism to cover the slots in the tunnel walls. These end plates caused flow separation at the tunnel wall which was eliminated by using wall boundary layer control.

#### Models and Instrumentation

The model airfoils were constructed of a steel center spar with sheet metal leading and trailing edges. The span of each wing was nominally 12 inches and the chord was 6.38 inches. Fourteen miniature differential-pressure transducers were used to obtain the chordwise pressure distribution. The natural frequency of the installed transducers was at least 1030 Hertz (Hz) with a damping factor of 0.45.

### DATA RECORDING SYSTEM

All data, both airfoil pressure and tunnel test condition information, were recorded on two FM wideband tape recorders. A time code and a 1/rev pulse recorded on both tapes provided tape synchronization. In addition, all parameters were recorded on oscillograph tape for instant data monitoring. Included were $C_N$ and $C_M$, obtained by integrating the pressures with an analog computer. The data recording flow path is shown in Figure 6.
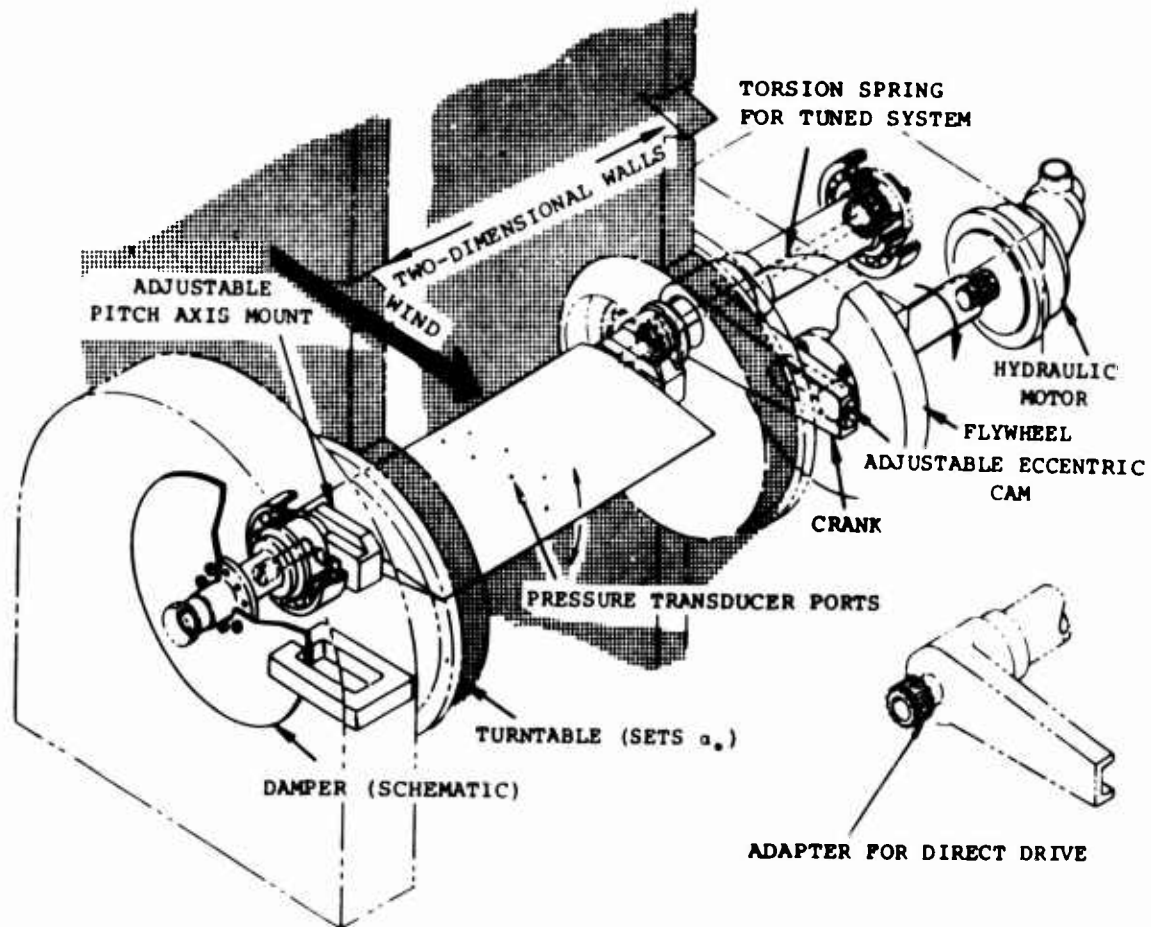
15

Figure 5. Pitch Oscillating Mechanism.
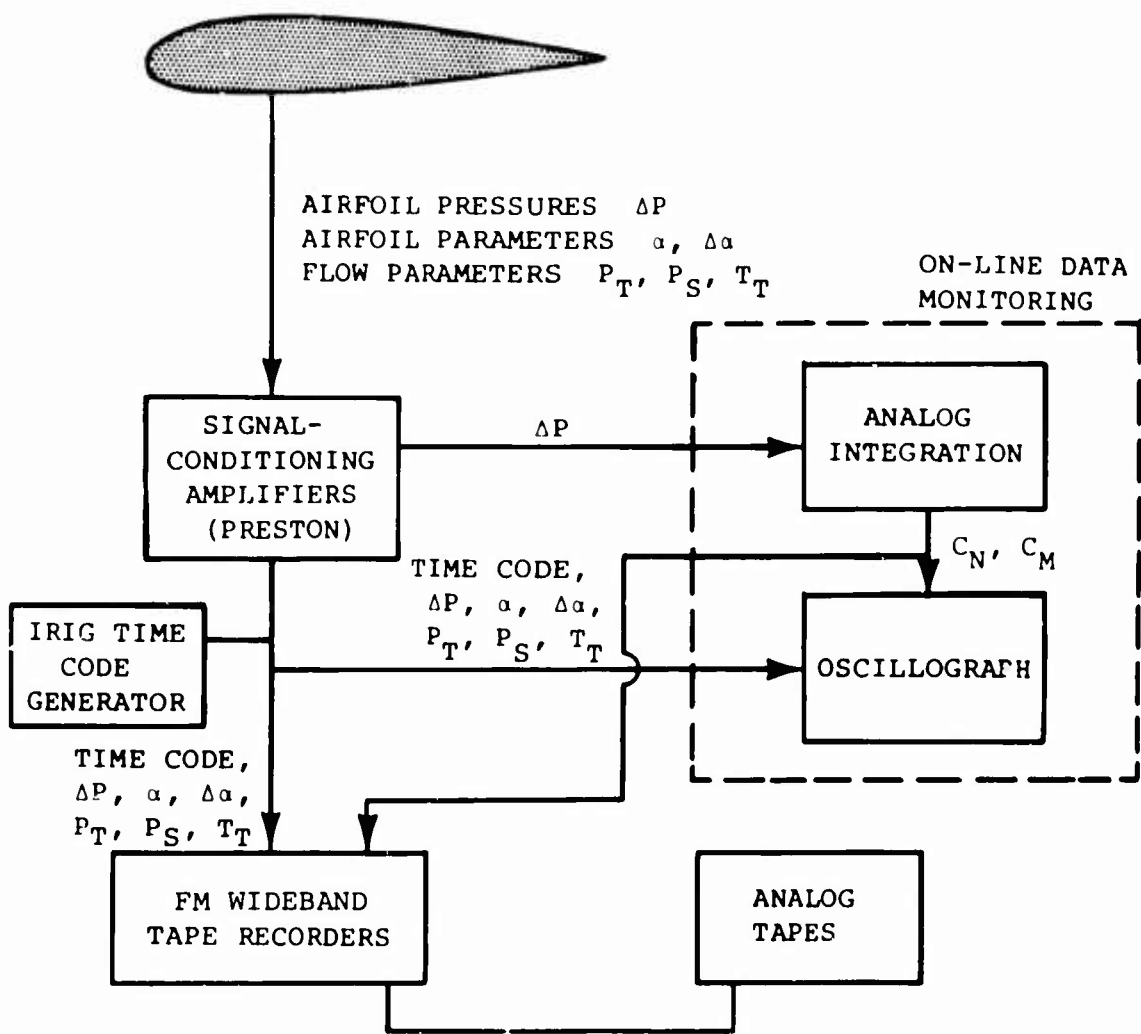
Figure 6.  Data Recording System.

## DATA REDUCTION SYSTEM

Nearly 800 individual test points were taken in a series of
four tests. The total number of individual data readings
was close to 10 million, since the data for 10 cycles were
averaged and approximately 40 points were read per cycle. To
handle this large volume of data, the recorded analog informa-
tion was digitized and processed on a digital computer, using
the basic flight test data reduction programs which were used
by Pruyn[6] for the "Tandem Rotor Airloads Measurement Program".
The pressure data were integrated to obtain time histories of
$C_N$, $C_M$, and W, the work or damping parameter, and the average
cycle damping. The flight test data plotting system, which is
integral with the data reduction system, was used to plot
approximately 80 percent of the $C_N$ and $C_M$ versus $\alpha$ data.

## EXPERIMENTAL RESULTS

### FORCED PITCHING OSCILLATION

The forced pitching oscillation data points cover three airfoil
configurations (symmetrical, cambered, and cambered with reflex)
for mean angles of attack from 0 to 25 degrees, amplitudes from
2.5 to 7.5 degrees, Mach numbers from 0.2 to 0.6, and reduced
frequencies from 0.042 to 0.720.

The effects of the flow and oscillation parameters on the $C_N$
and $C_M$ versus $\alpha$ behavior of the Vertol 23010-1.58 airfoil are
presented in Figures 7 through 12. (The general features and
trends are very similar for both the cambered and the symmet-
rical sections.) The significant differences in behavior of the
airfoils are then discussed, and data for the NACA 0012 profile
are presented which illustrate those differences.

### Effect of Mean Angle of Attack

Figure 7 presents a set of $C_N$ and $C_M$ versus $\alpha$ traces for 5-
degree amplitude oscillations of the 23010-1.58 airfoil at
$M = 0.4$ and $k = 0.06$. A sequence of increasing $\alpha_o$'s is shown
and compared with steady-$\alpha$ data.

The first pair of traces, $\alpha_o = 7.33$ degrees, shows the charac-
teristic elliptical shape centered on the steady-$\alpha$ line of
stall-free flow. The displacements from steady-$\alpha$ data are con-
sistent with potential theory. The next pair, at $\alpha_c = 9.63$
degrees, shows the first signs of stall in the figure-eight
shapes of both $C_N$ and $C_M$. At the high-$\alpha$ end of the cycle, loops
are formed in a clockwise sense.

For $C_M$, the area enclosed by the trace and the sense of motion
around the loops have important physical significance. The net
work done by the airfoil on the surrounding air is proportional
to the integral

$$W = \oint C_M \, d\alpha. \tag{7}$$

This integral is proportional to the area enclosed by the trace
and is positive for a counterclockwise (CCW) circuit. If the
circuit encloses a substantial area in a clockwise (CW) sense,
the contribution of that area is negative; i.e., it represents
energy extracted from the airstream by the airfoil. Net energy
extraction in a cycle (negative damping) implies that the rotor
blade oscillation in which it occurred would tend to increase
in amplitude. This is precisely the condition for flutter.

The third pair, at $\alpha_o = 12.22$ degrees, shows substantial stall
effects; e.g., large departures from zero $C_M$ and considerable
loss of lift. Some aspects of these traces worthy of special
note are:

19

1. The angles of attack at which $C_M$ and $C_N$ break are clearly higher than the steady-$\alpha$ values. $C_N$ breaks at 16 degrees and $C_M$ at 15 degrees, where both break at 14 degrees in steady flow.

2. A large CW loop is evident in the middle of the $C_M$ trace. The net damping for this cycle is negative. However, a CCW loop has appeared at the high-$\alpha$ end of the cycle, indicating that as $\alpha_o$ increases, there will be a return to more stable conditions.

3. There is a substantial lag in the reestablishment of attached flow after $\alpha$ has dropped below the steady-state flow stall level.

The traces for $\alpha_o$ = 14.92 degrees show further development of the same features. The CCW loop at high $\alpha$ has now become large enough to balance the big CW loop in the center, and the damping is only slightly negative. For $\alpha_o$ = 17.51 degrees, the net damping is again positive. It is worth noting that the angles for the $C_N$ and $C_M$ break have remained at 17 and 15 degrees, respectively, for the last three conditions discussed.

The final set, at $\alpha_o$ = 24.57 degrees, shows a condition of fully developed stall at all times. The mechanism of flow separation and reattachment no longer creates the loop shape required for feeding energy into the airfoil dynamic system.

## Effect of Pitching Frequency

Figure 8 shows $C_N$ and $C_M$ traces for the 23010-1.58 airfoil at a sequence of increasing frequencies for M = 0.4, $\alpha_o$ = 12.5 degrees, and $\Delta\alpha$ = 5 degrees. (The angles are nominal values; $\Delta\alpha$ actually increases from 4.83 degrees to 5.65 degrees as k goes from 0.062 to 0.355, because of the dynamics of the oscillating mechanism). The $\alpha_o$ chosen here is of particular significance because it is in the region of highest negative damping.

The most significant trend with frequency is the collapse of the $C_N$ hysteresis loop into a thin ellipse. The resulting trace runs parallel to and slightly below the static $C_N$ versus $\alpha$ curve because $C_N$ is lower during the decreasing-$\alpha$ part of the cycle than it is during the increasing-$\alpha$ part, contrary to theory.

The flattening of the loop may be explained as the result of two different phenomena. The first is the postponement of the onset of stall to the point where $\alpha$ stops increasing, evident at k = 0.124 and above. This is reasonable in view of the reduction of the apparent angle of attack at the leading edge

20

because of the upward motion of the airfoil. (Effectively, pitching motion applies camber to the boundary conditions governing the flow about the airfoil, in direct proportion to pitch rate.) The second phenomenon is an apparent upper limit to the time rate-of-change of lift.

The $C_N$ curve is displaced to a lower level because stall recovery is not complete until the second half of the increasing-$\alpha$ cycle is reached. A theoretical trace for stall-free flow is shown on the plot (Figure 8) for $k = 0.355$ to confirm the above point.

The $C_M$'s also show increasing postponement of stall as frequency goes up. The $C_M$ break always occurs earlier in cycle time than the $C_N$ break. This tendency of moment stall to respond less to pitch rate than does lift stall is apparently universal.

As the $\alpha$ for moment stall goes up, the dynamic $C_M$ overshoots the static-stall $C_M$ level by an increasing margin. Ultimately, however, an upper bound to the time rate-of-change again appears, moderating the overshoot and postponing the return to potential-flow $C_M$ levels. Therefore, the CW loop in the $C_M$ trace grows with increasing k until all portions of the cycle contribute to negative damping. At the highest k's, however, the rate-of-change limit discussed above begins to reduce the loop size.

The potential-flow $C_M$ ellipse has been added to the $k = 0.355$ $C_M$ graph. In this case, the test results follow closely the theoretical line over the entire upward-pitching half cycle.

Since the behavior of the chordwise pressure distribution (to be discussed later) indicates that attached flow prevails only over the increasing-$\alpha$ part of the cycle, the agreement with theory of that part of the moment trace can be expected.

Figure 9 shows $C_N$ and $C_M$ as functions of airfoil pitch reference angle. (These curves may be considered as functions of time, but note that the scale varies inversely with the frequency.) The concepts of lift and moment stall discussed above are better illustrated in this type of plot. It is also significant that, although the $C_N$ versus $\theta$ behavior approaches the sinusoidal behavior of unstalled flow, at high frequencies the $C_M$ still shows stall effects up to the highest frequency of this test.

### Effect of Pitch Amplitude. Maximum $\alpha$ Fixed

The $C_N$ and $C_M$ traces for three different amplitudes of oscillation at $M = 0.4$ and $k = 0.124$ are compared in Figure 10. Since the maximum $\alpha$ and the frequency of oscillation are the same for each case, the differences in $C_N$ and $C_M$ behavior

21

above $\alpha = 15$ degrees are caused by pitch rate effects ($d\alpha/dt$ being proportional to $\Delta\alpha$). $C_N MAX$ increases significantly with increased $d\alpha/dt$. Pitching moment break is also delayed by the higher $d\alpha/dt$ of the large-amplitude oscillation. In addition, since the 2.5-degree oscillation does not extend into the $\alpha$ region below static stall, nearly the whole moment curve contributes to negative damping. For the larger amplitude oscillation both positive and negative damping are present, resulting in a net positive damping for $\Delta\alpha$ of 7.5 degrees and a negative damping for $\Delta\alpha$ of 5 degrees.

Effect of Mach Number

Figures 11 and 12 show sequences of $C_M$ and $C_N$ traces at $f = 16$ Hertz (scale 1/rev) and $\Delta\alpha = 5$ degrees for increasing $\alpha_0$ at $M = 0.2$ and $M = 0.6$. They should be considered along with the corresponding data for $M = 0.4$, already presented in Figure 7.

Together, these three sequences illustrate airfoil response to the 1/rev $\alpha$ variation of a rotor blade at the Mach number range appropriate to the retreating blade. The questions of greatest concern in that response are:

1. Under what conditions does $C_N$ show abrupt and/or substantial reductions from its potential-flow level?

2. Under what conditions does $C_M$ show large deviations from zero, and how big are the deviations?

At $M = 0.2$, the trace for $\alpha_0 = 12.28$ degrees shows no evidence of stall, either in $C_N$ or in $C_M$. At this point, large stall effects were evident at $M = 0.4$. Even at $\alpha_0 = 14.97$ degrees, an $\alpha$ of 20 degrees is reached before stall, which is later precipitated by the adverse effect of nose-down pitch rate (effective inverse camber). As usual, $C_M$ begins to decrease before $C_N$, but it does not overshoot the static level, and it varies at a moderate rate.

At $\alpha_0 = 17.53$ degrees, more spectacular events occur when $\alpha$ reaches its maximum. The $C_M$ drops very rapidly to -0.32, three times the static-stall value. Its recovery is fast, but this impulsive loading could evoke a strong torsional response in a rotor blade. The $C_N$ begins its maneuver by going up, not down. The reason for such unusual behavior is probably connected with the fact that potential-flow conditions had been carried to an exceptionally high $\alpha$ before breakdown occurred. The pressure distribution for this condition will be examined later.

22

The potential-flow lift level is not achieved at any point in the cycle for the $\alpha_0 = 19.78° C_N$ trace. This accounts for the comparatively quiescent behavior of $C_M$.

At M = 0.6, a completely different pattern prevails. The whole set of $C_N$ and $C_M$ traces is characterized by minimal deviations from the static values over the entire range of $\alpha_0$'s tested, because of the very low reduced frequency (17 Hertz corresponds to k = 0.04 at this speed, as opposed to 0.12 at M = 0.2). Furthermore, the static $C_N$ and $C_M$ curves change gradually with $\alpha$, and they are free from the discontinuities evident at lower Mach numbers. The reasons for the continuous changes through stall at M = 0.6 for both airfoils will be discussed in a later section.

## Effects of Reynolds Number

The Reynolds number was decreased to a value corresponding to half scale (60 percent for M = 0.2) for several test conditions by reducing the total pressure in the test section. No curves are shown, because no noticeable differences between half-scale and full-scale data were found. There was one exception: at M = 0.2, differences were observed when the tunnel was operating at its low-speed limit and the angle of attack was doubtful; however, these differences are not considered to be meaningful.

## Effect of Airfoil Symmetry

Figure 13 presents a sequence of traces for the NACA 0012 (modified) symmetrical airfoil oscillating +5 degrees about $\alpha_0 = 12.3$ degrees. The Mach number is 0.4 and the frequency varies from k = 0.065 to k = 0.371. This sequence can be compared directly to that given in Figure 8 for the cambered airfoil.

At the lowest frequency (equivalent to 1/rev), the traces show substantially earlier stall than was evident for the 23010-1.58 airfoil. In fact, they strongly resemble the $\alpha_0 = 15$-degree curves for that section (Figure 8, fourth pair).

As the frequency goes up, the $C_N$ loop tends to flatten, much as it did for the 23010-1.58 airfoil. At the same time, however, significantly larger $C_M$ excursions are evident. A minimum $C_M$ of -0.3, which does not decrease with further increases in frequency, is reached near k = 0.2. Moreover, recovery from this large negative value occurs later in the cycle as the frequency is increased. Thus, the CW area in the loop, and therefore, the negative damping, is greater for the symmetrical than for the cambered airfoil.

23

Figure 14 shows the influence of Mach number on the stalling response of the symmetrical airfoil at f = 16 Hertz (equivalent to 1/rev). At M = 0.2 and $\alpha_0$ = 12.3 degrees, large stall effects are evident in both $C_N$ and $C_M$, whereas the cambered section showed essentially perfect potential-flow behavior under the same conditions. (See Figure 11, second pair of traces). At M = 0.6, the dynamic effects have essentially disappeared, and both $C_N$ and $C_M$ remain close to the static values. In this respect, the cambered and symmetrical sections are very similar.

## Effect of Trailing-Edge Reflex

The 23010-1.58 airfoil was tested with its trailing-edge tab bent upward (reflexed) at an angle of 3 degrees. The $C_N$ and $C_M$ traces were found to show no appreciable differences from those for the airfoil with a straight trailing edge, aside from the small overall shift in $C_M$. This agrees with the steady-state test data. It is therefore concluded that the favorable effects noted for the reflex feature on cambered blades are not associated with changes in stall behavior.

## SUMMARY OF KEY RESULTS FROM THE PITCH OSCILLATION TESTS

Figure 15 shows the highest $C_N$ values attained in pitch oscillation for the Vertol 23010-1.58 airfoil. The Mach 0.4 and 0.6 lines are significant boundaries, since they were derived from data groups where changes to $\alpha_0$ did not significantly increase the maximum $C_N$. In the case of the Mach 0.2 line, it was apparent that higher $\alpha_0$'s than those tested here would have given higher maximum $C_N$'s for k's above 0.124; therefore, that line does not represent an actual limit. This is indicated by the change in slope of the 0.2 Mach line at k = 0.525, where the $\alpha_0$ = 25-degree data begin to dominate the $\alpha_0$ = 17.5-degree data used for the rest of the M = 0.2 line.

The frequency trends clearly show the influence of dynamic effects in increasing the maximum $C_N$. The strong effect of Mach number in suppressing attainable $C_N$ is also clear.

Figure 15 shows similar curves for the NACA 0012 (modified) airfoil. The same frequency trends are apparent, but at Mach 0.4 the $C_N$ limit is substantially lower than for the cambered section.

Damping characteristics of the Vertol 23010-1.58 airfoil are presented in Figures 16 and 17 as a ratio to theoretical damping. The theoretical damping equations are derived in Appendix I and are based on incompressible nonsteady aero-dynamic theory. In Figure 16, the reduced frequency is held constant at k = 0.24. Increasing the Mach number causes the damping parameter to cross into negative values at lower $\alpha_0$'s, until compressibility alters the damping characteristics of the airfoil sufficiently to prevent a net negative damping for the

24

cycle. At Mach 0.6 the lowest value of negative damping is
60 percent of the theoretical unstalled value.

In Figure 17, the dimensional frequency is held constant in-
stead of the reduced frequency as in Figure 16. The data shown
are for f = 96 Hertz (6/rev), corresponding to a typical rotor
blade's torsional natural frequency. This plot shows that
negative damping exists only for a very narrow range of Mach
numbers for this amplitude of oscillation; since the Mach
number on a rotor blade varies widely along the blade's
length, the contribution to the total damping of the blade
will normally come from a limited part of the blade.

Because of the nonlinear character of stall, the damping
cannot be expected to be independent of amplitude. This is
clearly shown by the lower part of Figure 18. In the $\alpha_o$ range
where instability is present, larger amplitude motion leads to
a more damped condition. This could lead to limit-cycle
oscillations at the amplitude which gives zero damping. The
upper part of Figure 18 shows the influence of amplitude on
maximum $C_N$. Excursions beyond static stall are increased by
oscillation amplitude because of the higher pitch rate.

The effect of camber is illustrated in Figure 19, where the
frequency is held constant at a typical first torsional mode
value. The beneficial effect of camber is apparent at all
Mach numbers, either in the form of a higher $\alpha_o$ before the
damping becomes negative or in the form of a lower level of
negative damping.

DRAG IN PITCHING OSCILLATION

The problem of measuring the instantaneous drag of an airfoil
under unsteady-flow conditions is much more difficult than that
of finding the lift. Time-lag and mixing effects rule out
using the wake-momentum survey method except for getting an
average value. The use of a balance had been impractical for
$C_N$ and $C_M$ because of the complexity of the dynamic response;
the same argument would apply for $C_D$. It would be conceivable
to measure the form drag from pressure measurements, i.e., by the
same technique as for instantaneous $C_N$. However, many more
transducers would be required because of the sensitivity of
$C_D$ to details of the leading-edge pressure. Furthermore, to
obtain $C_N$ and $C_C$ (chord force) at the same time, it would be
necessary to measure $\Delta P$'s with respect to a known reference
value, instead of merely taking $\Delta P$'s across the airfoil.
Finally, the skin-friction component would not register in this
system.

Therefore, it was decided to measure only average drag values
by using a slowly traversing pitot-static probe to survey the

25

moment defect in the wake. Drag data were obtained for the Vertol 23010-1.58 airfoil only. All drag data are summarized in Figure 20.

The dashed line shows $C_D$ under steady-$\alpha$ conditions. The dotted lines are extrapolations of the low-$\alpha$ (fully attached flow) data representing hypothetical $C_D$'s for conditions where dynamic effects have postponed stall. The results of the oscillatory drag measurements show that the average $C_D$ goes up with frequency between 16 Hertz and 48 Hertz at both Mach numbers.

Quasi-steady, average values of drag have been computed from the steady data for comparisons, by using the following equation:

$$\bar{C}_D = \frac{1}{2\pi} \oint C_D (\alpha) \, d\alpha, \tag{8}$$

where $\alpha$ is the instantaneous angle of attack. Two different values of $C_D$ were calculated at the higher mean angle of attack. In the first case, the steady-state drag values were used directly. In the second, the drag was assumed to follow the dotted line in Figure 20 when $d\alpha/dt$ was positive, and the steady-state solid line when $d\alpha/dt$ was negative. In this way the effect of stall delay could be estimated. At Mach 0.4, it is seen that the second method gives a more realistic value, since the pitching oscillation at this Mach number does actually delay stall until $\alpha$ stops increasing. At Mach 0.6, the second method underpredicts $C_D$. This is reasonable, since the similarity of the dynamic $C_N$ and $C_M$ traces to the static values implies that $C_D$ would be unchanged as well.

Figure 20 also shows typical shapes of total pressure profiles. It should be noted that under some conditions, dynamic effects can actually produce negative drag, as in the case of a bird in flight. Such an effect is visible in the center of the 16-Hertz trace. Further study of such phenomena is beyond the scope of this report.

## FORCED VERTICAL TRANSLATION

Tests were run at frequencies corresponding to 16 Hertz (1/rev) and 32 Hertz (2/rev), Mach numbers from 0.2 to 0.6, geometric angles of attack from 0 to 20 degrees, and amplitudes ($\Delta h$'s) from 0.31 to 0.62 semichord.

The $C_N$ and $C_M$ traces will be presented first, followed by a discussion on damping and the maximum $C_N$'s attained during a cycle.

26

## Effect of Angle of Attack and Frequency

Figure 21 shows the effect of $\alpha_o$ (geometric $\alpha$, relative wind due to airfoil motion not included) on $C_N$ and $C_M$ for vertical translation. Fixed parameters are: $\Delta h = 0.30$, $k = 0.067$ (1/rev), and $M = 0.4$. The data at $\alpha_o = 5.02$ degrees and 9.82 degrees show no sign of stall. At $\alpha = 12.25$ degrees, $C_N$ and $C_M$ both show stall at the middle of the downstroke. Stall is caused by the increase in the effective $\alpha$ due to the vector addition of plunge rate with tunnel velocity. As was the case for pitching motions, $C_N$ stalls later than $C_M$.

For plunging motion, the net work performed by the airfoil over a cycle is given by

$$W = \oint C_N \, dh. \tag{9}$$

This is proportional to the area enclosed in the $C_N$ versus $\alpha$ trace, and is positive (stable) for a CCW circuit.

In the $\alpha_o = 12.25$-degree case, only a small area of negative damping appears at the left of the $C_N$ trace. At the next $\alpha_o$, 14.65 degrees, the airfoil is at its static-stall angle. On the upstroke, when dh/dt is positive and the effective $\alpha$ is reduced, the airfoil remains unstalled. At maximum positive h and during the negative dh/dt part of the cycle, the airfoil is fully stalled. This results in negative damping. The $C_M$ trace also shows the effects of stall. However, the total pitching moment change is only -0.12, the value for static stall, and no overshoot in pitching moment is present.

The traces shown on Figure 22 are at twice the frequency (2/rev) of the plots in Figure 21. The area in the $C_N$ loops at low mean angle of attack has increased, as nonsteady potential-flow theory predicts. At $\alpha_o = 12.46$ degrees, $C_N$ and $C_M$ both show stall effects beginning at h = 0 on the downstroke. Nevertheless, negative damping does not result because the airfoil remains stalled until the middle of the upstroke. The stall at $\alpha_o = 14.88$ degrees occurs at the end of the first quarter of the cycle, but the slow variation of $C_N$ with time gives attached flow only during the last half of the upstroke. There is a substantial reduction in damping compared to the low-$\alpha$ case, but it remains positive. The large $C_M$'s shown here may be significant for rotor dynamics, through effects on torsional oscillation.

## Effect of Mach Number

Some typical $C_N$ and $C_M$ traces at f = 33 Hertz (2/rev) are shown in Figures 23 and 24 at Mach number 0.2 and 0.6, respectively. There is no evidence of stall up to the highest $\alpha_o$ tested at Mach 0.2. A systematic change is evident in the $C_M$ traces

27

for M = 0.2. These traces lie on lines sloping downward to the right and enclose little or no area. This is the effect of the noncirculatory loading caused by plunge acceleration.

The slope of the line agrees very well with the potential theory value ($dC_M/dh = 0.048$ at this frequency). The tilt was hardly noticeable at M = 0.4 because it is proportional to the square of the reduced frequency. At M = 0.4, $dC_M/dh$ would have been only -0.012.

At M = 0.6, there is a substantial amount of load rearrangement, as evidenced by the moment hysteresis loops. At this Mach number, the effect of increasing $\alpha$ is to flatten the potential-flow ellipse on the $C_N$ versus h plot. This severely limits the variation of lift with h. No figure-eight features of appreciable magnitude appear in either the $C_N$ or the $C_M$ traces; this can be ascribed to the absence of sharp breaks in the static data, as in the case of pitching motion.

## Effect of Amplitude

Figure 25 shows the effect of a 50-percent increase in translation amplitude on the $C_N$ and $C_M$ versus $\alpha$ traces. From comparison of these loops with the third set of data in Figure 21, it is clear that the general characteristics of the data are preserved when the amplitude is increased.

## Effect of Airfoil Symmetry

Figure 26 shows $C_N$ and $C_M$ traces for the NACA 0012 (modified) airfoil in plunging motion at 32 Hertz (h = 0.24), Mach 0.2, and $\Delta h = 0.31$. At $\alpha_0 = 10$ degrees (well below stall), the traces are practically identical to those for the 23010-1.58 airfoil. At 12.5 and 15 degrees, however, very substantial stall effects appear; the $C_N$ loop becomes somewhat irregular, its center sagging to a level of 1.0 or less, and a large drop in $C_M$ appears at the end of the downstroke. This is in strong contrast to the behavior of the cambered airfoil under the same conditions. Data at M = 0.4 are not shown, since variance from the behavior of the 23010-1.58 airfoil was less striking, although stall effects were more prevalent. At Mach 0.6, no noticeable differences were found between the airfoils.

## SUMMARY OF KEY RESULTS OF VERTICAL TRANSLATION TESTING

### Maximum Normal Force Data

Figure 27 shows the maximum $C_N$'s obtained during tests in the
plunging motion mode. The values reached were very insensi-
tive to the frequency and amplitude of motion, though the
maxima were generally reached at conditions corresponsing to
the largest rate of change of instantaneous $\alpha$ (with respect to
the relative wind). At Mach 0.2, no maximum was reached for
the 23010-1.58 section for the $\alpha_0$'s tested. The value shown
is extrapolated.

Both airfoils show a $C_N$ increase over the steady-flow value,
ana the effect of larger Mach number is, as usual, to suppress
the $C_N$ attainable. The higher stall angle of the 23010-1.58
airfoil is apparent in its consistent increment of 0.2 in $C_N$
over the symmetrical section.

### Damping in Plunge

The tests reported here are the first known to the authors in
which negative average damping was observed in translation
motion. These tests were conducted at a much larger $\Delta h$ and
at higher Mach numbers than any previous tests. This is pro-
bably why neither Halfman[3] nor Rainey[7] measured negative
damping.

Figure 28 shows damping in plunge for the Vertol 23010-1.58
airfoil section as a function of geometric $\alpha_0$ for M = 0.4 and
M = 0.6. For angles well below the static-stall level, damping
at M = 0.4 remains near the theoretical value. This is con-
sistent with lift variation at the rate corresponding to a
stall-free, lift-curve slope. The beginning of the loss of
damping is apparent at 12.3 degrees; above 15 degrees, zero or
negative damping prevails. The largest negative value occurs
when $\alpha_0$ is just at the stall point and the plunging motion
varies the aerodynamic $\alpha$ just enough to cross the lift-curve
discontinuity. (The $C_N$ and $C_M$ traces for the cycle are shown
in Figure 21.)

At Mach 0.6, the loss of damping occurs at a lower $\alpha_0$, but no
large negative values were observed. This is consistent with
a $C_N$ versus $\alpha$ relationship in which lift has practically
ceased to vary. This agrees with the steady-flow $C_N$ data and
the $C_N$ and $C_M$ versus $\alpha$ curves of Figure 52. No stall was
observed for this profile at Mach 0.2. Therefore, the damping
was always observed to be near the theoretical level and is
not shown.

29

Figure 29 shows similar data for the symmetrical airfoil. The damping drops off at a lower $\alpha_0$ than for the cambered profile at Mach 0.4, but near the same point at Mach 0.6. The maximum negative value reached was only half that of the NACA 23010-1.58 airfoil. Presumably, this is a consequence of the smaller discontinuity in the $C_N$ versus $\alpha$ curve.

Both the symmetrical and the cambered airfoils show progressively less severe negative damping for larger h excursions. This implies the possibility of limit-cycle bending oscillations of rotor blades.

## DYNAMIC EFFECTS ON CHORDWISE LOADING

Considerable insight into the processes governing stall, $C_N$ and $C_M$ breaks, and negative damping can be gained by examining $\Delta C_p$ time histories and chordwise load distributions. To provide a background for comparison with dynamic results, and to explain the existence of separate branches on the $C_N$ and $C_M$ versus $\alpha$ curves, chordwise loadings for steady-flow conditions will be examined first.

### Chordwise Loadings Under Static Conditions

Figure 30 shows how Mach number determines whether discontinuities will be present on the moment and normal force curves. Pressure distributions are shown for angles of attack just below and just above the $C_N$ or $C_M$ break at Mach 0.4 and at Mach 0.6. At Mach 0.4, the loading is seen to be of the classical potential-flow type before stall. The large negative $d(\Delta C_p)/dx$ implies that the upper surface pressure must rise rapidly just aft of the leading edge. The result of a slight increase in $\alpha$ is to aggravate this adverse pressure gradient, precipitating stall. The redistribution of load is drastic: $C_N$ drops by 20 percent and $C_M$ falls to about 0.1. The flatness of the $\Delta C_p$ curve is symptomatic of a large region of separated flow, filled with turbulent eddies.

Compare those results with the Mach 0.6 loadings: a completely different phenomenon operates in this case. The pressure distributions for both angles of attack imply a favorable pressure gradient forward of 10-percent chord. This is due to transonic effects. Supersonic expansion around the leading edge causes increasing local air velocity and falling pressure until a shock is reached near 15-percent chord.

When $\alpha$ increases, the flow is able to adjust to the change by a small readjustment of the expansion/shock system. Slightly weakened pressure recovery results, leading to small increases in negative pitch moment and in $C_N$. The Mach 0.6 flow is thus free of discontinuities, though changes in slope in $dC_N/d\alpha$ and $dC_M/d\alpha$ do occur.

## Loadings During Pitching Oscillations

### Effect of Frequency

Figure 31 shows pressure, normal force, and pitching moment variations with time for the Vertol 23010-1.58 airfoil oscillating at 16 Hertz. Even at this comparatively low frequency, substantial postponement of stall is evident on the $C_N$ and $C_M$ curves. Note also that the $\Delta C_p$ nearest the leading edge (0.01c) remains substantially greater than the $\Delta C_p$ further down the chord throughout the period of stall.

Figure 32 shows a sequence of chordwise loadings at 20-degree intervals in the cycle. Theoretical steady-flow loading profiles are shown for comparison. Note that the measured loadings match the theoretical shapes with great precision when stall is not present.

Figures 33 and 34 show data similar to those of Figures 31 and 32, except that the frequency here is 96 Hertz. The dynamic influence on $C_N$ and $C_M$ is dramatic. The $C_N$ trace now forms a passable sinusoid, not very different from the quasi-steady, potential-flow line. However, the presence of stall is evident on the $C_M$ curves. The chordwise loadings show a slight but noticeable difference from the steady-flow theoretical shapes over the increasing-$\alpha$ range. This is caused by effective additional camber due to pitch rate.

### Effect of Mach Number

It has been noted that particularly violent fluctuations of force and moment occurred when dynamic effects were strong enough, because of low Mach number, to delay stall. An exceptionally large $C_N$ was reached in this case. Figure 35 shows the loading variation on the Vertol 23010-1.58 airfoil as the flow breaks down at $\alpha = 22.5$ degrees (16 Hertz, Mach 0.2). The differential pressure across the aft portion of the blade is three times larger than for steady-flow stall.

The effect of Mach number on high-frequency oscillatory loadings is shown by Figures 36 through 39, which form a complete sequence when considered with Figures 31 and 32. At Mach 0.2, the pressure profiles shown in Figure 37 are completely free of visible signs of stall. At every $\alpha$, $\Delta C_p$ falls steadily toward the aft portion of the airfoil.

Oscillations at 96 Hertz from Mach 0.4 have already been discussed. In that case, dynamic effects were not able

31

to eliminate substantial stalling. At Mach 0.6, the
situation is again different. Good pressure recovery
appears to prevail under all conditions. The influence
of nose-down pitch rate as effective inverse camber is
discernible in the loading profiles corresponding to
nose-down motion. Then, the expansion/shock effect is
exaggerated, and almost complete unloading of the aft
part of the section results from this high Mach number.
Steady-flow tests often show such loadings. (See
Reference 8 for examples of this.)

Effect of Airfoil Symmetry

Figures 40 and 41 show time histories and chordwise
loadings for the NACA 0012 (modified) airfoil oscil-
lating at 80 Hertz in a Mach 0.4 flow. The most striking
difference in the results shown for this cambered sec-
tion is the complete loss of the leading-edge pressure
peak when stall occurs. This is characteristic of the
symmetrical airfoil under all conditions tested. It is
partly responsible for the consistently larger negative
stalled $C_M$'s.

Note also how a $\Delta C_p$ wave appears to travel down the air-
foil in the period from 80 to 200 degrees of the cycle.
This wave could be the result of the shedding of a strong
vortex from the leading edge, which, in turn, is a con-
sequence of the loss of pressure peak already discussed.
This is the other contributor to the increased negative
$C_M$ values observed for the symmetrical section.

Loadings in Translation Motion

Figures 42 and 43 show typical effects of plunging oscillation
on the cambered airfoil loadings, while Figures 44 and 45 give
corresponding data for the symmetrical airfoil. The angle of
attack selected for the NACA 0012 plot is deliberately lower,
since approximately equal margins from stall were desired.

The results in both cases are consistent with those observed
for pitching oscillations. Note especially the wider $C_M$
excursion of the 0012, and also its more serious loss of
leading-edge suction.

COMPARISON WITH THEORETICAL RESULTS

Experimental force and moment derivatives for both the symme-
trical and the cambered airfoils are compared with theore-
tically predicted values in Figure 46. The theoretical data
and the wind tunnel wall corrections were calculated with a
computer program which was supplied by NASA[9]. The theory was
based on thin airfoil representation with the effects of

32

compressibility and the tunnel walls (method of images) included. Test data are presented only for small $\alpha_o$'s, since the viscous and transonic flow effects which appear at high values of $\alpha_o$ cannot be predicted analytically.

## Pitching Motion

The experimental values of the dynamic-lift curve slope are lower than the theoretical ones in all cases. This agrees with the universally noted reduction of the static-lift curve slope caused by viscosity. The trends to higher values of $|C_N|/|\alpha|$ with increasing Mach number agree well with the predictions. The $C_N$ phase agrees well at Mach 0.2, but at 0.4 and 0.6 the experimental results lag by as much as 18 degrees. No explanation for this discrepancy is now available. More of such lag is apparent in the case of the Vertol 23010-1.58 than for the NACA 0012 (modified). This is caused by separation effects on the lower surface near the leading edge.

Pitching moment derivatives also show generally good agreement, but again they show some reduction in magnitude. The same thing was noted by Halfman[3] and is attributed to viscosity.

The trend with Mach number is identical for both experimental and theoretical data. The $C_M$ phase of the symmetrical airfoil moment agrees with theory within 7 degrees. For the cambered airfoil, the difference between theory and test is 20 degrees, at low reduced frequency. This is caused by a slight rearward shift of the aerodynamic center from the quarter-chord point for the additional loading due to oscillations. The 20-degree difference in phase represents a shift of only 0.8-percent chord, owing to the extreme sensitivity of the pitching moment phase to the location of the pitch reference center.

## Vertical Translation

The test data for $C_N$ and $C_M$ in translation are compared with theory in Figure 47. The agreement of the $C_N$ and $C_M$ slopes with oscillatory $\alpha$ is very good except at very low values of k for the cambered airfoil, where the $C_M$ magnitude response is again much larger than theory predicts. This can be expected, since the behavior of the cambered airfoil at k's of 0.03 will be essentially quasi-steady, and the aerodynamic center of the cambered airfoil is not on the quarter-chord.

There is a 20-degree difference in the oscillating $C_N$ phase between theory and test for the symmetrical airfoil. There is also a 15-degree difference between the $C_N$ phases of the symmetrical and cambered airfoils. No such difference was noted for $C_M$; no explanation for this is known at the present time. The difference between theory and test for the moment phase can be explained by an offset of the center of pressure

33

from the quarter-chord. Again, the $C_M$ phase is very sensitive, if moments are taken about an axis near the aerodynamic center.

## COMPARISON WITH PREVIOUS RESULTS

### United Aircraft Corporation Oscillation Data

Average pitch damping per cycle is compared with Carta's results in Figure 48. The range of $\alpha_0$ for negative damping agrees well, but the tests reported here indicate a lower minimum value than do the UAC experiments.

The test program reported here had the benefit of automated data reduction methods. Therefore, all of the results shown are averaged from at least five consecutive cycles. In the case of the symmetrical airfoil data, ten cycles were used. The UAC results were manually processed, so only one cycle per test point could be covered. Therefore, differences are to be expected.

### CH-47A Dynamic Airloads Data

$C_M$ data from the dynamic airloads tests[10] are compared with symmetrical airfoil data from this report in Figure 49. The tunnel test point was chosen to represent the Mach and $\alpha$ conditions on the retreating side of the rotor disc (M = 0.4, $\alpha_0$ = 10 degrees + 5 sin $\theta$) and the pitch reference position has been shifted to agree with the stall point of the flight test data. The agreement between test and theory is remarkable, both in the magnitude of the $C_M$ change with stall and in the duration of stall. Both the wind tunnel and the flight test data show a partial reattachment at the 270-degree azimuth position followed by a further stall. The flight test data show a 6 to 7/rev oscillation on the advancing side, which is probably elastic response in the first torsion mode. The nose-down pitching moment of the flight test data in the 60- to 180-degree azimuth range may be due to the higher Mach number for those data.

## TIME HISTORIES OF STARTS AND STOPS FOR PITCHING OSCILLATION

A complete time history of forced pitch oscillation from beginning to end was recorded for ten data points. Since the data from these tests span many records and many cycles of oscillations, they are not reducible by the computer programs developed for the airfoil in steady oscillation; therefore, they are not included in the data listings.

Time history plots from the analog traces have been scanned for unusual behavior. Nothing worthy of note has been found.

34

## PITCH OSCILLATION OF AN AIRFOIL SYSTEM WITH A TORSIONAL DEGREE OF FREEDOM

Because of the widely varying aerodynamic parameters, such as the reduced frequency and Mach number, along a rotor blade in forward flight, the stall-induced torsional oscillations of a whole blade cannot be simulated in a wind tunnel. Another complication is the fact that the blade is not executing simple sinusoidal pitching motion at the conditions of greatest interest. Rather, it is producing a combination of the 1/rev basic angle-of-attack change (discussed in the blade motion studies section), with varying amounts of higher frequency elastic motions superimposed. These elastic pitching and translation deflections modify the angle of attack. Of these elastic motions the response of the first torsional mode is of most interest, since it can be forced to large deflections by stall effects.

Therefore, the approach taken in this series of tests was to simulate a representative blade section by spring-mounting the airfoil, which was tuned to 4 to 6/rev (64 to 96-Hertz model scale), and by driving the angle of attack at 1/rev (16-Hertz model scale) with the system used for forced pitching tests.

Oscillations in the first torsional mode for a rotor blade are governed by a second-order differential equation of the form

$$\alpha'' + \alpha = \frac{1/2 \rho V^2 (2b) \ (area)}{I_T \ f_T^2} \ C_M \ (\alpha, \ \alpha' \ldots). \tag{10}$$

The conditions required for aerodynamic similarity are:

1. A correct Mach number to simulate the aerodynamic environment of the retreating blade.

2. A Reynolds number in the two- to six-million range

3. A reduced frequency corresponding to rotor 1/rev for the background pitch motion contribution to $\alpha$, $\alpha'$, etc.

4. The elastic torsional frequency must be four to six times the background frequency.

The condition for dynamic similarity requires that the coefficient of $C_M$ on the right-hand side of the equation for the rotor blade motion match the corresponding coefficient in the equation for airfoil system motion. That coefficient is called the torsional Locke number and is denoted here by $\gamma_T$.

$\gamma_T$ can also be written as

$$\gamma_T = \frac{2 \rho b^4}{I_T} \left[ \frac{V}{f_T b} \right]^2 = \frac{2 \rho b^4}{I_T} \left[ \frac{1}{k_T} \right]^2. \tag{11}$$

35

The factor $k_T$, the reduced torsional natural frequency, is dictated by aerodynamic similarity and can be simulated easily in a tunnel. $I_T$ was determined by model strength requirements, and the resulting value of $2\rho b^4$ (span)$/I_T$ was low by a factor of 10. The result of this difference is a reduction to the model's displacement to 10 percent of the full-scale level due to a given aerodynamic force.

While the model tests will not provide full-scale deflections, they can provide the following important results:

1. The tests can predict the onset of stall-induced oscillations, because these depend on the 1/rev $\alpha$ variation.

2. The tests can provide data with which analytical formulations of the effects of stall on rotor blades can be checked in a dynamic system described by the torsional equation.

The pitch response data from the tuned system tests are presented in Figures 50 and 51. Only the Vertol 23010-1.58 airfoil was tested in this manner for the test conditions listed in Tables IX and X in Volume II.

## Effect of Mean Angle of Attack and Mach Number

The amplitude of the maximum elastic pitch response is directly related to the angle for static stall as shown in Figure 50 for Mach numbers 0.4 and 0.6. The maximum higher harmonic $\delta\alpha$, rather than the fourth, fifth, or sixth harmonic of the tuned system, has been plotted because the peak response frequency of the system is affected by damping and by the slight variations in the 1/rev driving frequency. All pitch response data have been multiplied by $k_T^2$, which is the dominant term in Locke number ($b^4/I_T$ is constant for the model). The elastic response is decreased by changing the Mach number from 0.4 to 0.6. This agrees with the conclusions drawn from forced pitch oscillation tests.

The higher harmonic response for $C_N$ and $C_M$ is in general agreement with the $\alpha_o$ response. At mean angles of attack where the motion does not experience stall effects, the higher harmonic pitch response rapidly approaches the background levels measured in the forced pitch oscillation testing.

36

## Effect of System Resonant Frequency

Figure 50 shows the effect of changing the system resonant frequency from 64 to 99 Hertz (4 to 6/rev). The increase in response is spectacular for the 4/rev system. This shows that the response to stall is highly dependent on the stiffness of the system.

## Effect of Driving Amplitude

Two pitch-driving amplitudes were tested ($\alpha = \pm 5$ degrees and $\alpha = \pm 7.5$ degrees). The effect on pitch response is shown in Figure 51 for $M = 0.4$ at a tuned frequency of $f_T = 80$ Hertz. The 2.5-degree $\alpha_0$ shift between the two curves indicates a primary dependence of the pitch response on the stall behavior of the motion and not on the driving amplitude.

## Effect of Locke Number

A few test points were obtained at 50-percent total pressure in the test section. This test has the combined effects of reducing the Reynolds number and the Locke number, $\gamma_T$. Since the forced pitch oscillation data did not show differences with Reynolds number, the primary effect of the lower pressure was to change $\gamma_T$. In all cases, the elastic $\alpha$ response was decreased with a decrease in $\gamma_T$.

## Effect of External Damping

Two levels of external damping were used during the tests. The effect of external damping is shown in Figure 51 for the $\alpha_0$ for maximum response. The maximum elastic response was decreased by a factor of three with the application of full damping ($\zeta = 0.10$).

## CONCLUSIONS

1.  Pitching motions at the amplitudes and frequencies typical
    of blade elements of helicopter rotors strongly affect the
    limits of aerodynamic normal force due to stall.  The maxi-
    mum normal force coefficient  in all cases shows an
    increase which grows with frequency but which declines as
    the Mach number approaches 0.6.

2.  The margin of maximum normal force for cambered over
    symmetrical airfoils which has been observed in the past
    under steady-flow conditions prevails under dynamic
    pitching conditions as well.

3.  Dynamic effects postpone symptoms of stall in airfoil pitch-
    ing moment also.  However, the increase in angle of attack
    for development of substantial nose-down pitching moment
    is generally smaller than the increase in $\alpha$ for normal
    force break.

4.  Pitching oscillations at angles of attack where flow separa-
    tion occurs can result in a net input of energy from the
    passing airstream to the airfoil dynamic system.  (In the
    case of a rotor blade, this would imply increasing ampli-
    tude of oscillation.)  This negative damping diminishes
    for larger amplitudes of oscillation.  It is sensitive to
    Mach number, but it disappears for all practical purposes
    on increasing Mach number to Mach 0.6.

5.  The cambered airfoil shows an advantage of 3 to 6 degrees
    in angle of attack over the symmetrical airfoil at Mach
    numbers where negative damping can occur.  Camber also
    reduces the magnitude of the pitching moments developed.

6.  Oscillatory vertical translation (plunge) can result in
    increased maximum normal force over steady-flow conditions.

7.  The steady-flow advantage of camber in maximum normal force
    coefficient carries over into dynamic stall in plunge.

8.  Plunging motion at the amplitudes and frequencies
    pertinent to helicopter rotor blades produces negative
    damping over narrow ranges of angle of attack at Mach
    0.2 and Mach 0.4.

9.  The effects of negative damping in pitch and plunge are
    strongly related to discontinuities in the static normal
    force and pitching moment curves.  These discontinuities
    are caused by leading-edge stall.  At Mach 0.6, where
    transonic effects eliminate leading-edge stall, damping is
    reduced below the potential flow level but remains positive.

## RECOMMENDATIONS

1. The stall behavior data presented in this report should be analyzed with a view to mathematical description. Such a description is a necessary first step in the practical application of these data to rotor dynamic and aerodynamic analyses.

2. Thin airfoils as proposed for advanced-technology helicopter rotors should be tested under dynamic conditions to establish their damping and normal force characteristics.

3. A program of analysis should be undertaken to develop a detailed understanding of the flow processes affecting dynamic stall, such as local supersonic flow and vortex shedding. The program would require supplemental experimental work in flow visualization and the measurement of absolute pressures to define local flow Mach number on the airfoil surfaces.
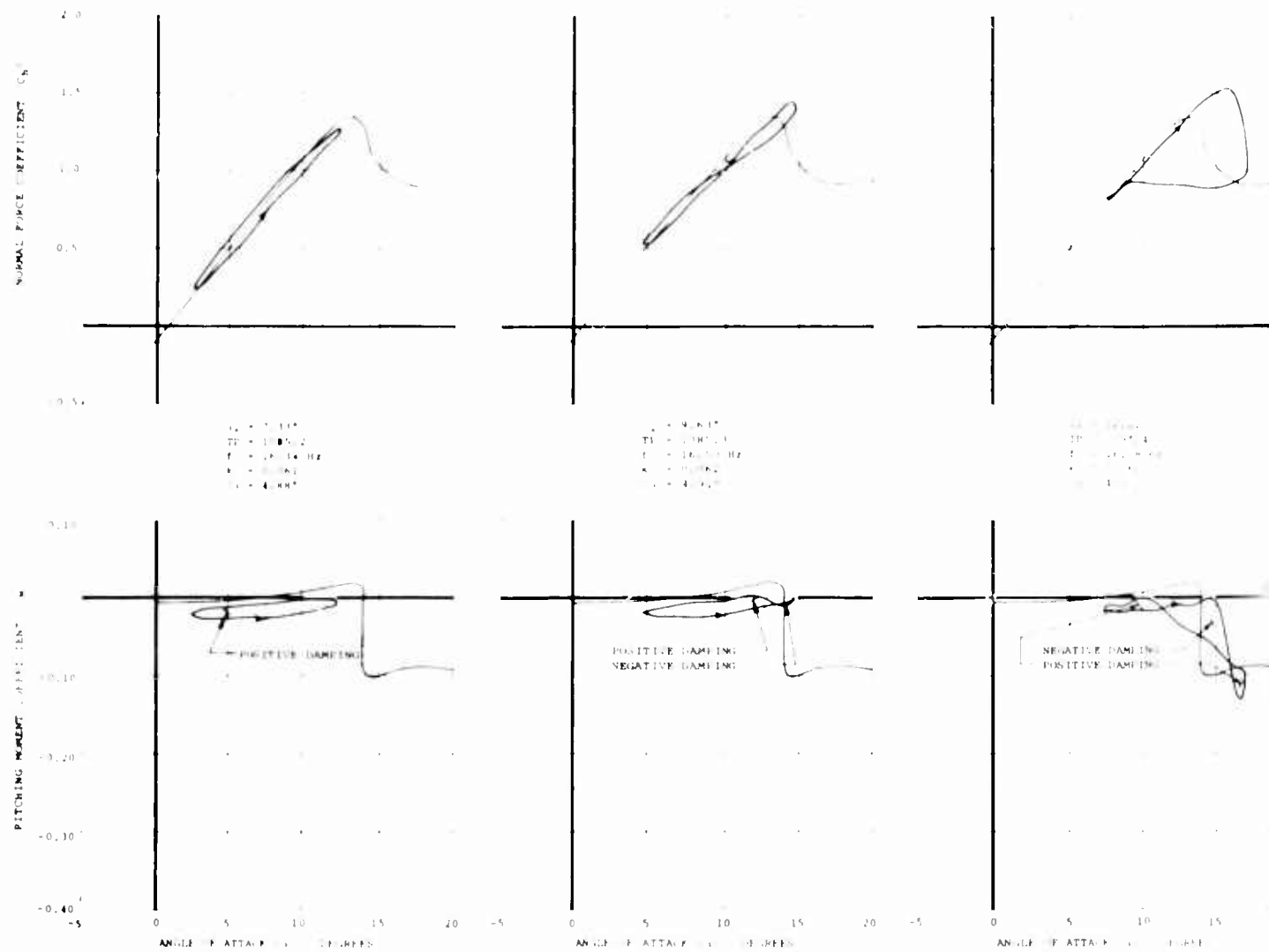
Figure 7. Dynamic $C_N$ and $C_M$ Versus $\alpha$ for Pitch Oscillation of Vertol 23010-1.58 Airfoil at M = 0.4, f = 16 Hertz, and $\Delta\alpha$ = 5°.
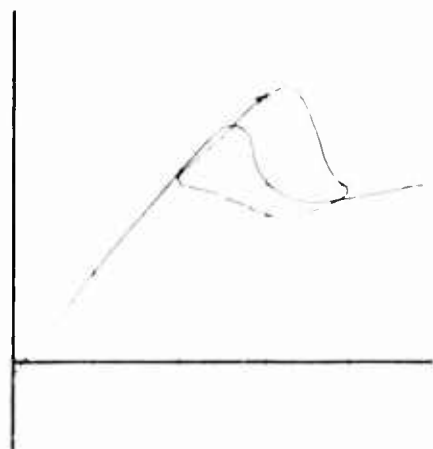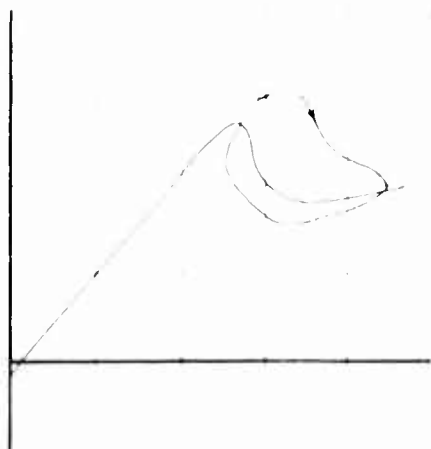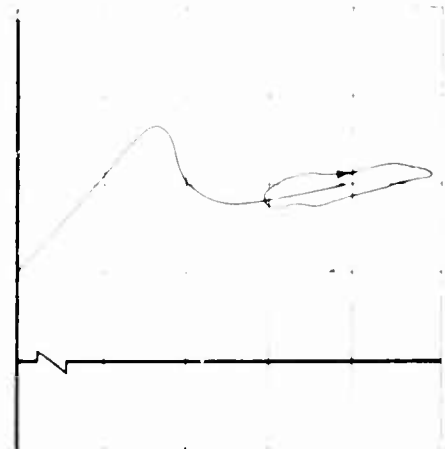
NEGATIVE DAMPING

POSITIVE DAMPING

NEGATIVE DAMPING

POSITIVE DAMPING

POSITIVE DAMPING
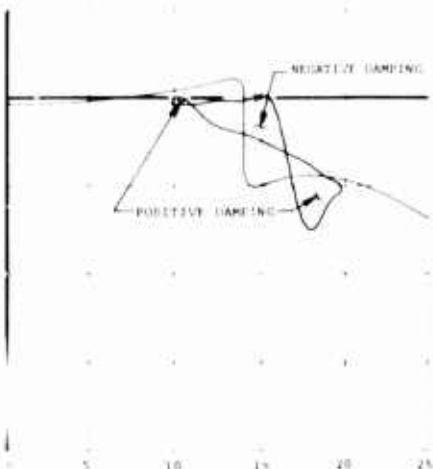
ANGLE OF ATTACK (α) - DEGREES
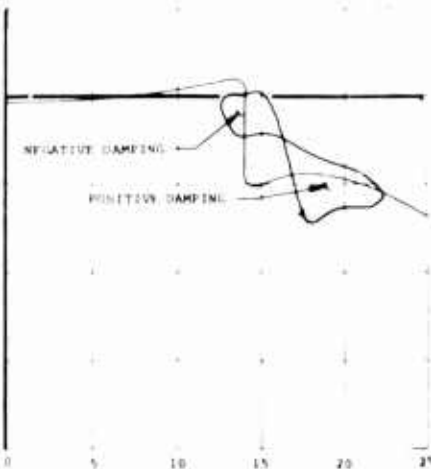
ANGLE OF ATTACK (α) - DEGREES
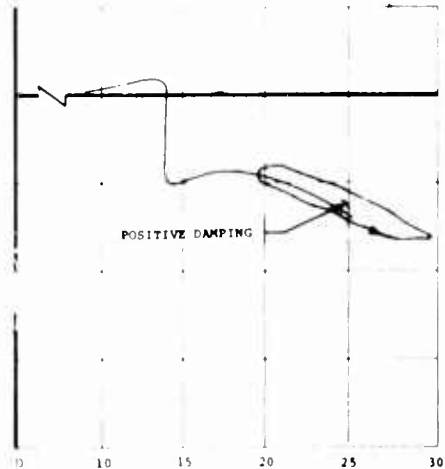
ANGLE OF ATTACK (α) - DEGREES

B.
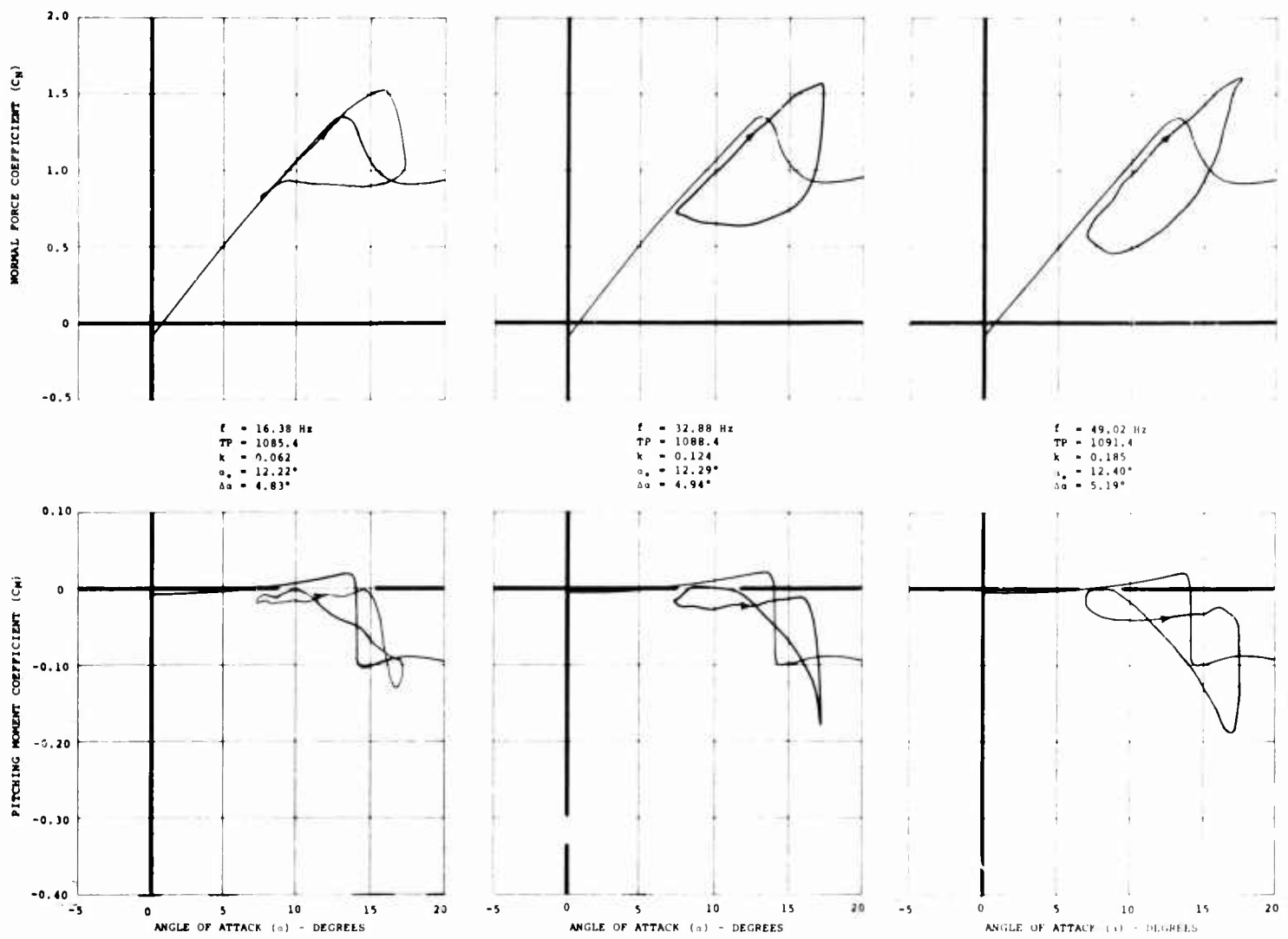
**Figure 8.** Effect of Frequency on Dynamic $C_N$ and $C_M$ for Vertol 23010-1.58 Airfoil at $M = 0.4$, $\alpha_0 = 12.25°$, and $\Delta\alpha = 5°$.

43

f = 63.37 Hz
TP = 1092.4
k = 0.238
$a_e$ = 12.33°
$\Delta a$ = 5.31°

f = 80.33 Hz
TP = 1098.4
k = 0.302
$a_e$ = 12.28°
$\Delta a$ = 5.63°

f = 94.34 Hz
TP = 1102.4
k = 0.355
$a_e$ = 12.45°
$\Delta a$ = 5.65°

THEORY

THEORY

ANGLE OF ATTACK (a) - DEGREES

ANGLE OF ATTACK (a) - DEGREES

ANGLE OF ATTACK (a) - DEGREES
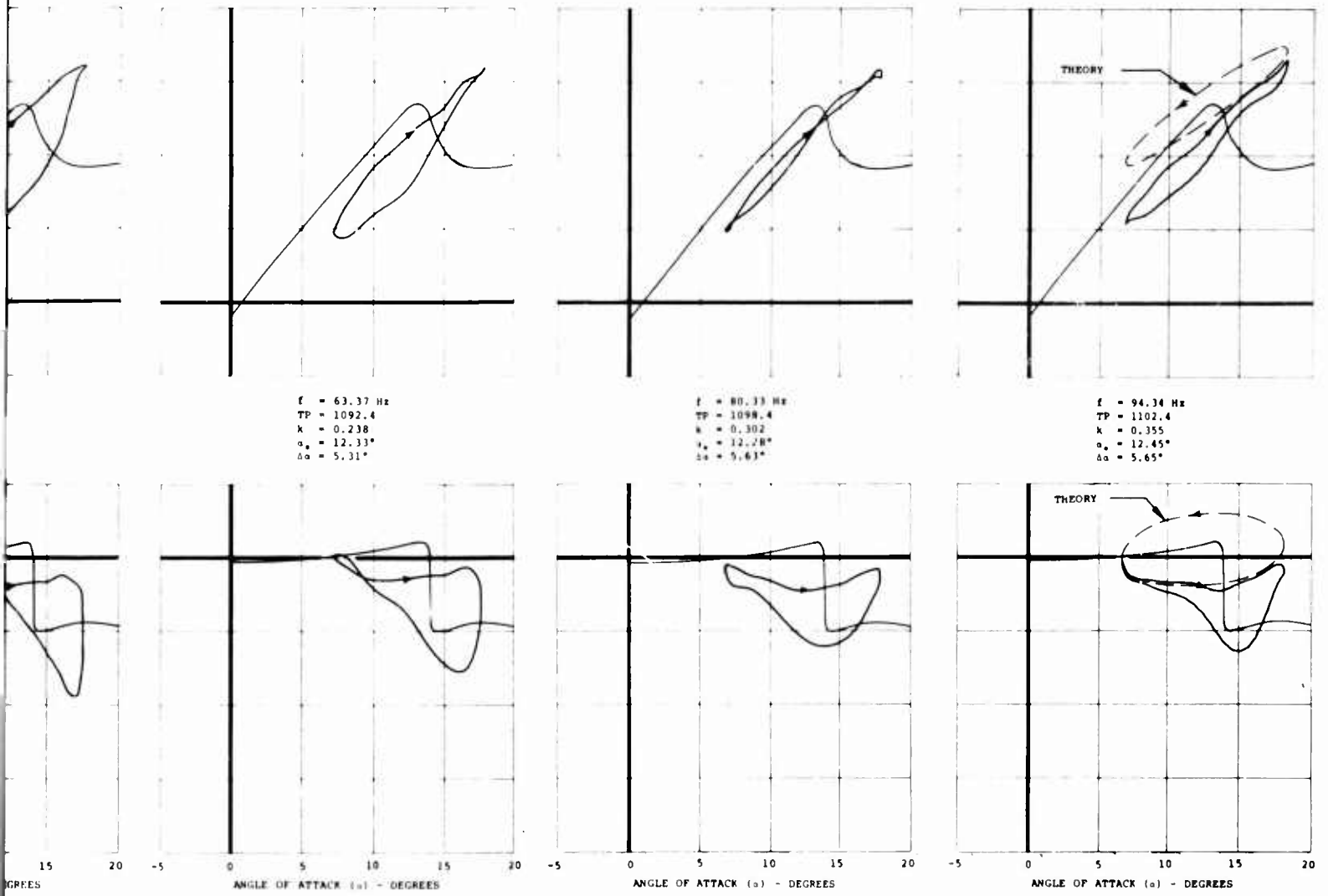
B.
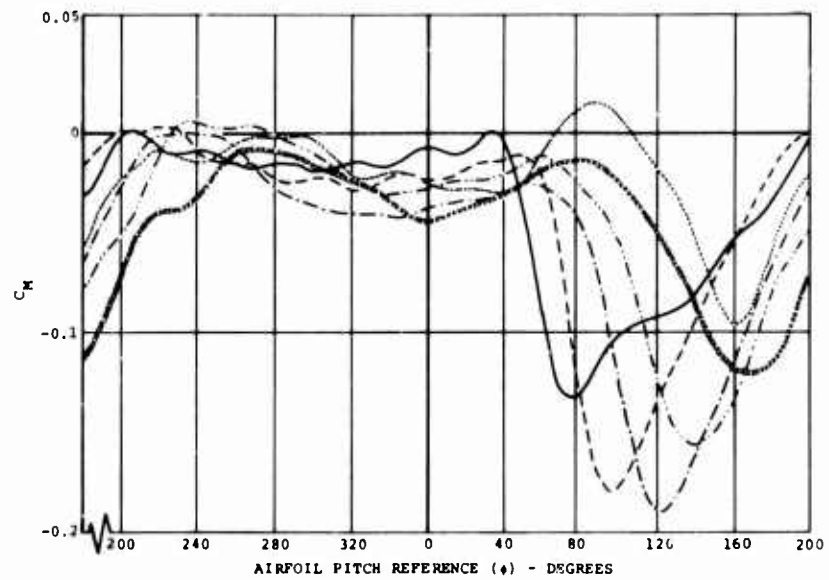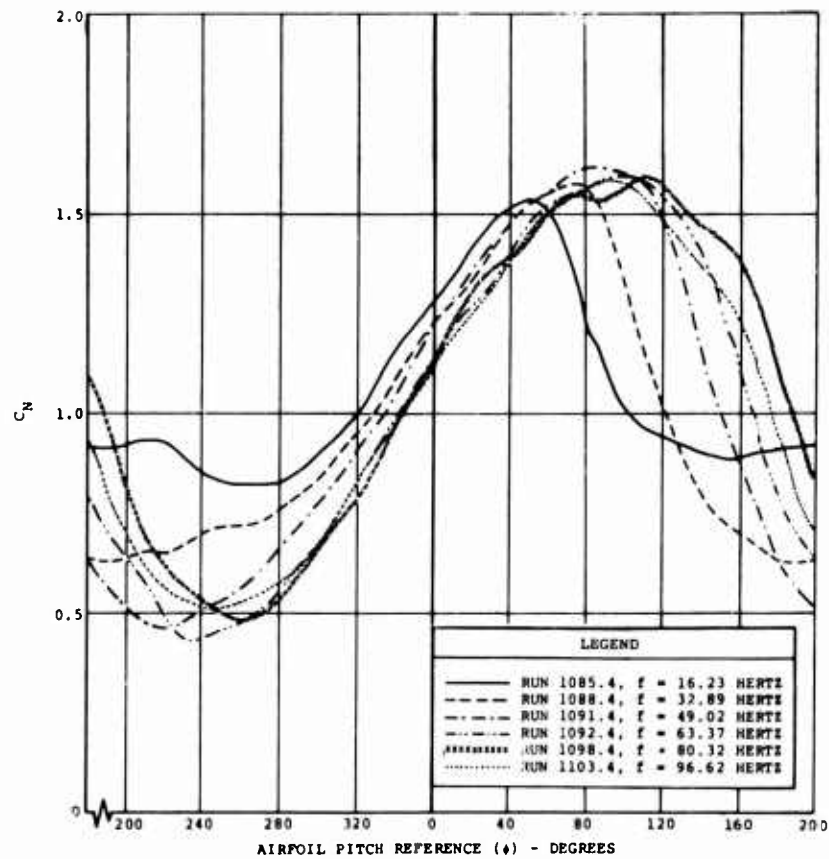
Figure 9. Effect of Frequency on $C_N$ and $C_M$ Time History at Stall for Vertol 23010-1.58 Airfoil at $M = 0.4$, $\alpha_o = 12.3°$, and $\Delta\alpha = 5°$.

45
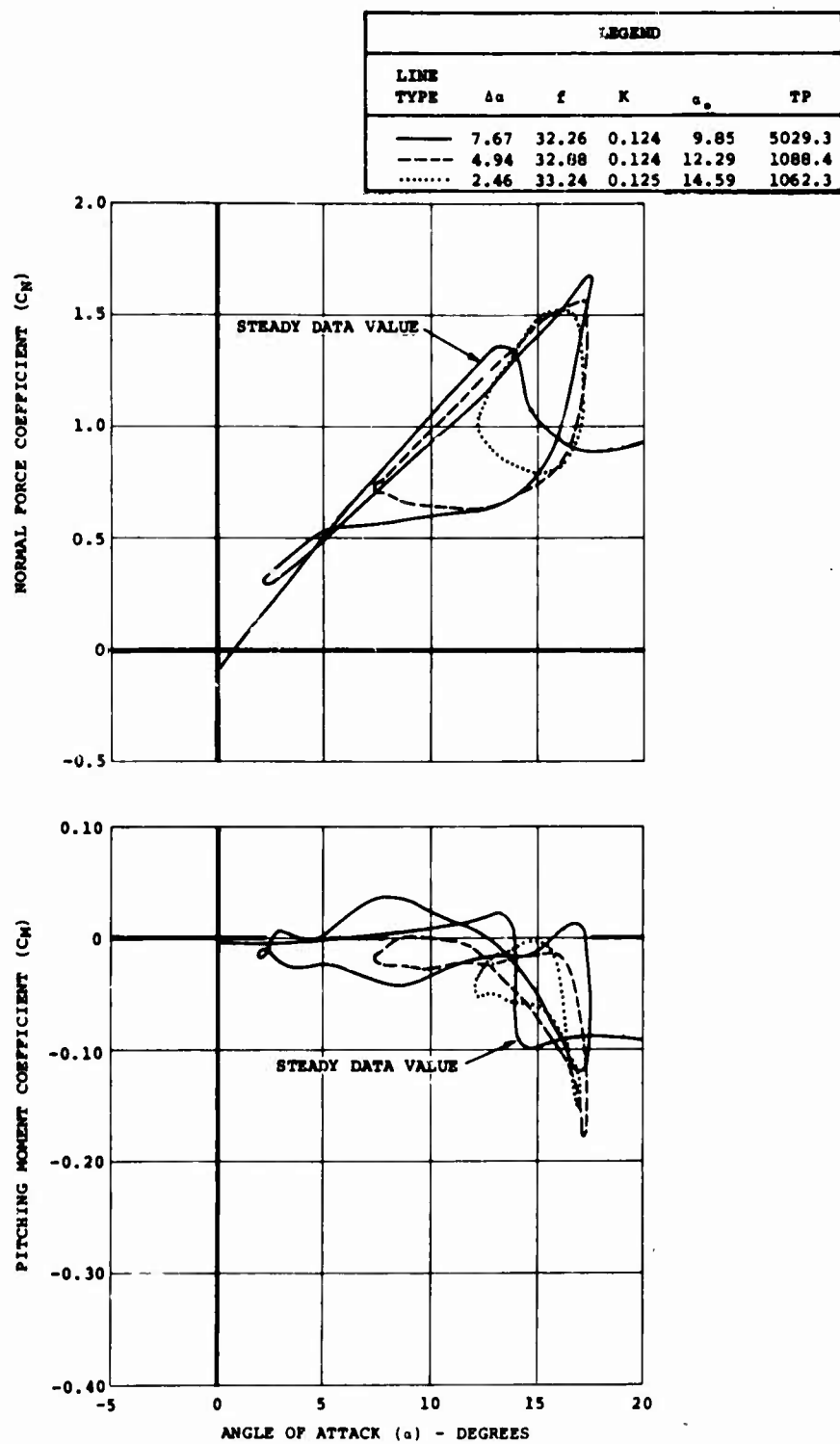
Figure 10. Amplitude of Oscillation Effect on Vertol
23010-1.58 Airfoil at M = 0.4 and f = 32 Hertz.

46

NORMAL FORCE COEFFICIENT ($C_N$)

2.0

1.5

1.0

0.5

0

-0.5

$\alpha_o$ = 0.02°
TP = 1086.1
f = 16.34 Hz
k = 0.121
$\Delta\rho$ = 4.88°

$\alpha_o$ = 12.28°
TP = 1094.4
f = 16.53 Hz
k = 0.123
$\Delta\alpha$ = 4.98°

$\alpha_o$ = 14.97°
TP = 1149.1
f = 16.37 Hz
k = 0.122
$\Delta\alpha$ = 4.98°
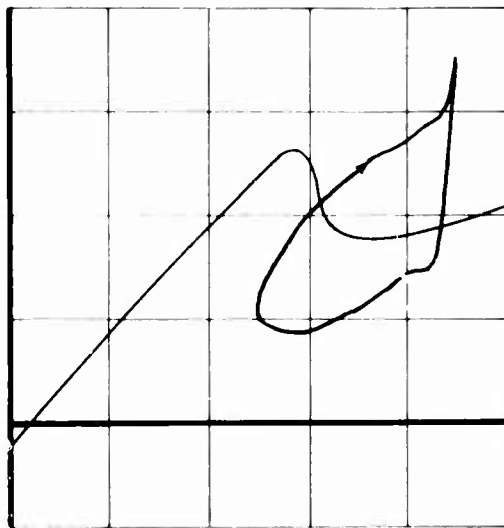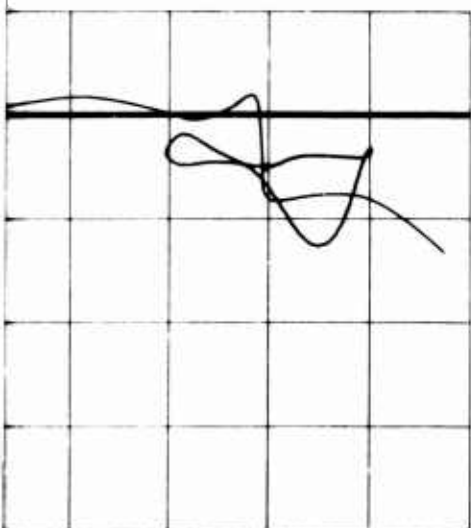
PITCHING MOMENT COEFFICIENT ($C_M$)

0.10

0

-0.10

-0.20

-0.30

-0.40

-5    0    5    10    15    0
ANGLE OF ATTACK ($\alpha$) - DEGREES

-5    0    5    10    15    20
ANGLE OF ATTACK ($\alpha$) - DEGREES

0    5    10    15
ANGLE OF ATTACK ($\alpha$) -

Figure 11.   Dynamic $C_N$ and $C_M$ Versus $\alpha$ for Vertol 23010-1.58
Airfoil at M = 0.2, f = 16 Hertz, and $\Delta\alpha$ = 5°.

47

A.

|  | | |
|---|---|---|
| $\alpha_0 = 14.97°$ | $\alpha_0 = 17.53°$ | $\alpha_0 = 19.78°$ |
| TP = 1148.1 | TP = 1148.2 | TP = 5036.4 |
| f = 16.37 Hz | f = 16.37 Hz | f = 15.11 Hz |
| k = 0.122 | k = 0.122 | k = 0.115 |
| $\Delta\alpha = 4.98°$ | $\Delta\alpha = 4.89°$ | $\Delta\alpha = 4.80°$ |

ANGLE OF ATTACK (α) - DEGREES
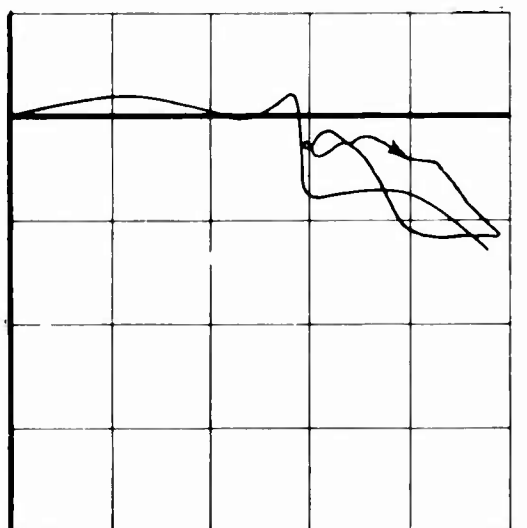
ANGLE OF ATTACK (α) - DEGREES

ANGLE OF ATTACK (α) - DEGREES

B.

Figure 12. Dynamic $C_N$ and $C_M$ Versus $\alpha$ for Vertol 23010-1.58
Airfoil at M = 0.6, f = 16 Hertz, and $\Delta\alpha$ = 5°.
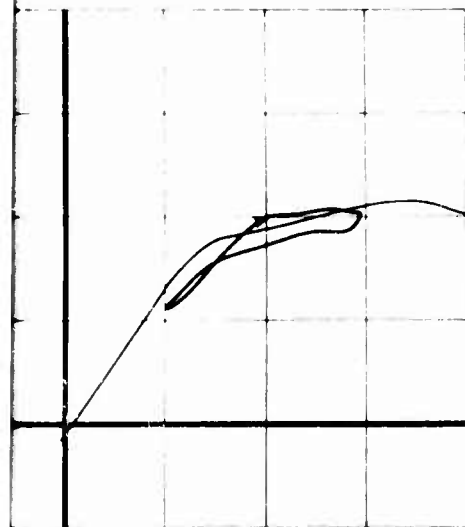
49

A)

$\alpha_o = 9.62°$
TP = 1083.3
f = 16.81 Hz
k = 0.043
$\Delta\alpha = 4.77°$

$\alpha_o = 12.19°$
TP = 1084.1
f = 16.00 Hz
k = 0.041
$\Delta\alpha = 4.79°$
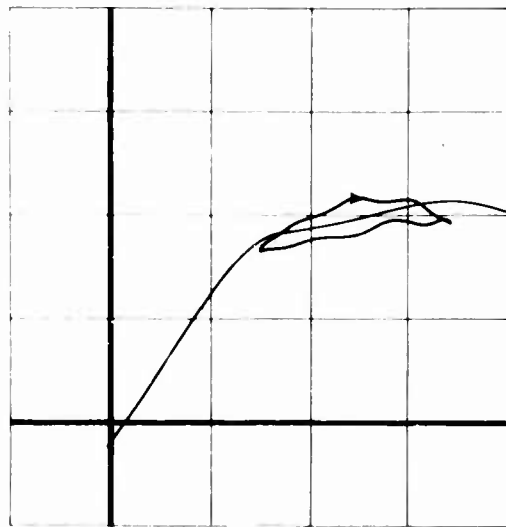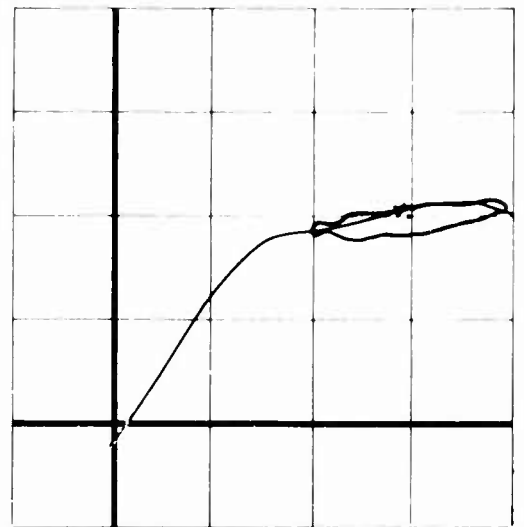
$\alpha_o = 14.83°$
TP = 1145.1
f = 16.58 Hz
k = 0.042
$\Delta\alpha = 4.81°$
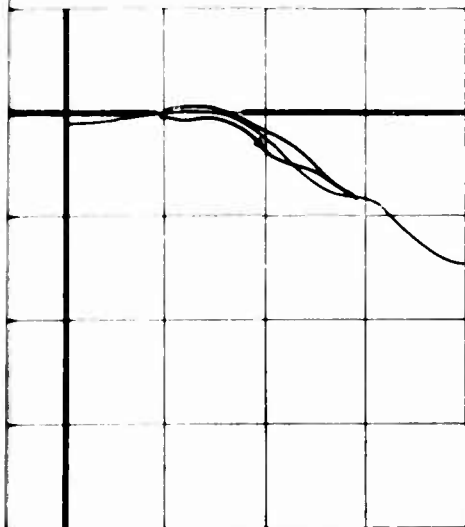
ANGLE OF ATTACK (α) - DEGREES
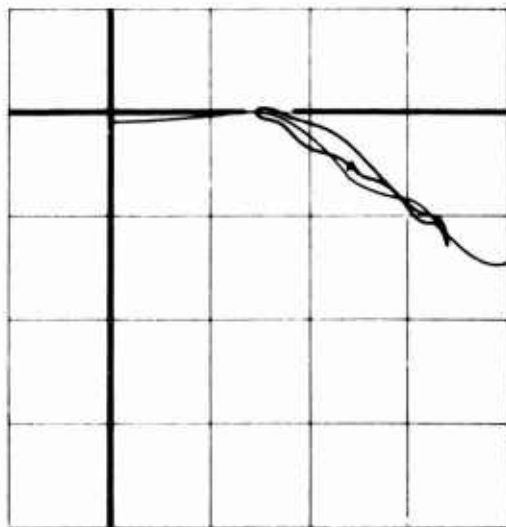
ANGLE OF ATTACK (α) - DEGREES
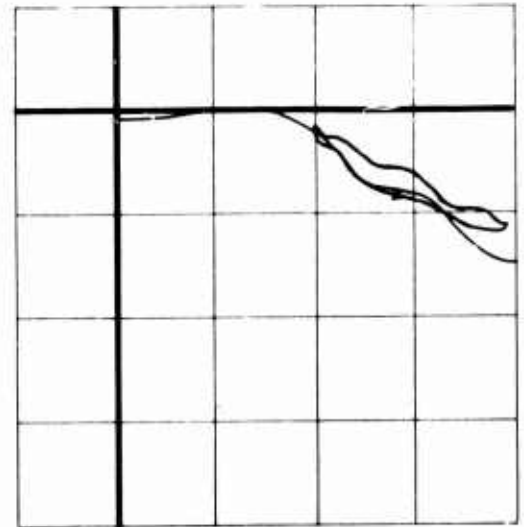
ANGLE OF ATTACK (α) - DEGREES

B.
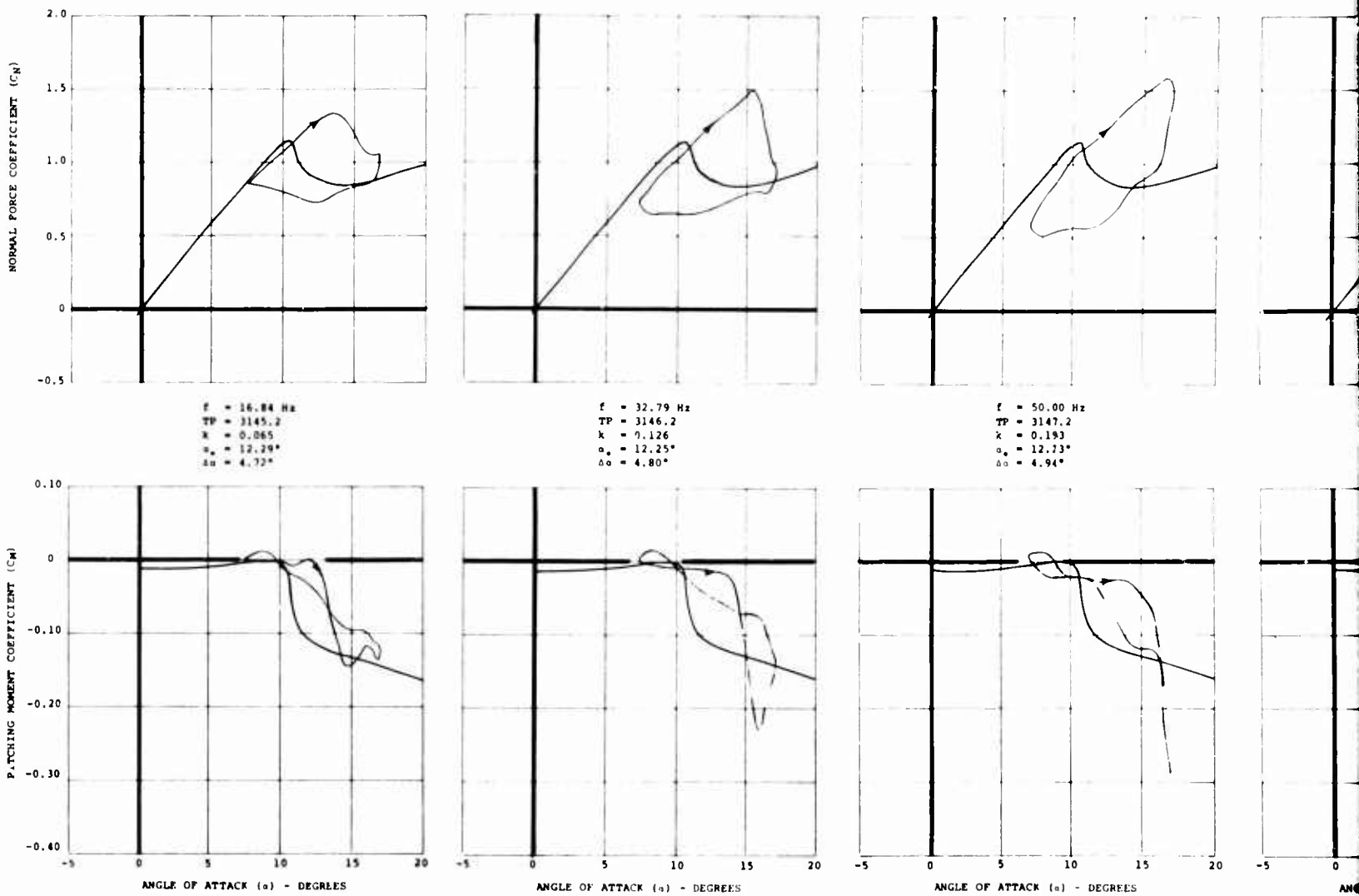
Figure 13.   Effect of Frequency on Dynamic $C_N$ and $C_M$ for NACA 0012 (Modified)
Airfoil at M = 0.4, f = 16 Hertz, and $\alpha_0$ = 12.25°.
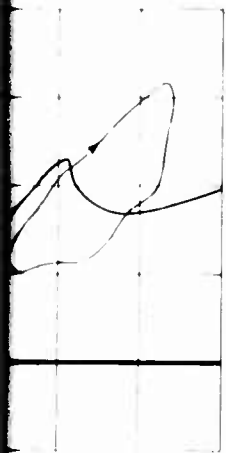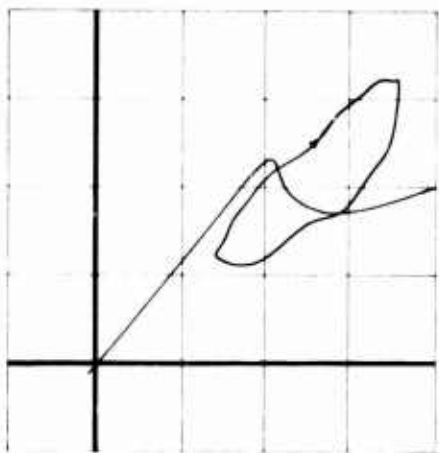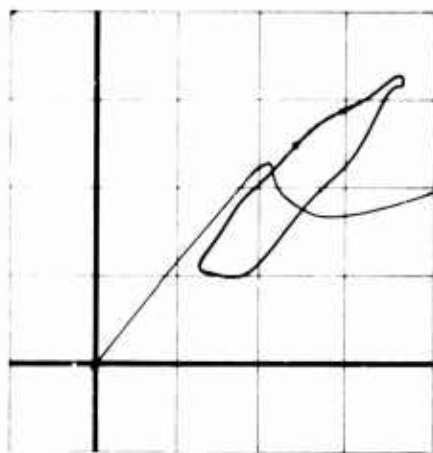
51

A.

10      15      20     -5      0      5      10      15      20     -5      0      5      10      15      20     -5      0      5      10      15      20
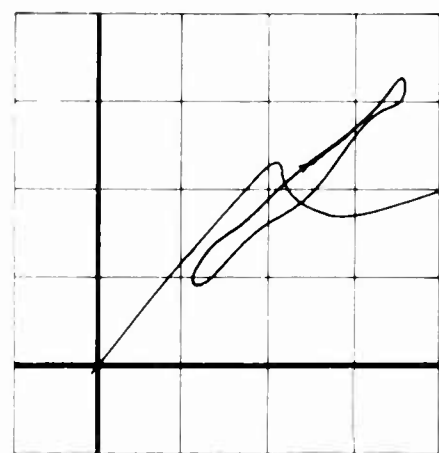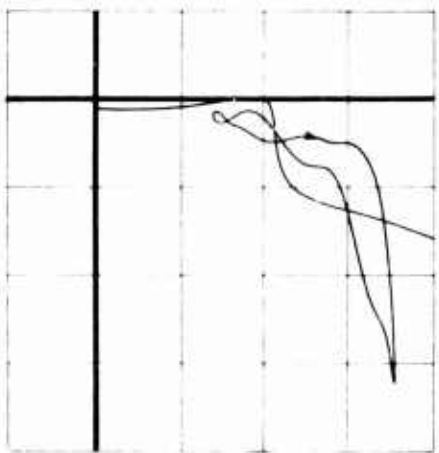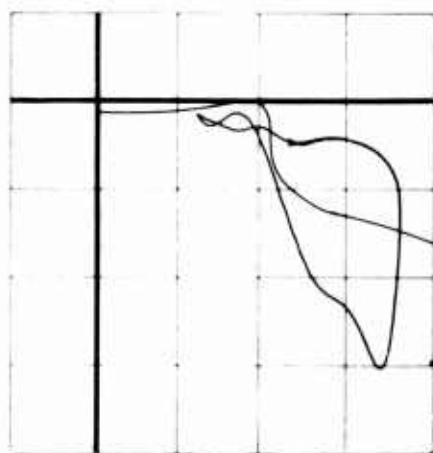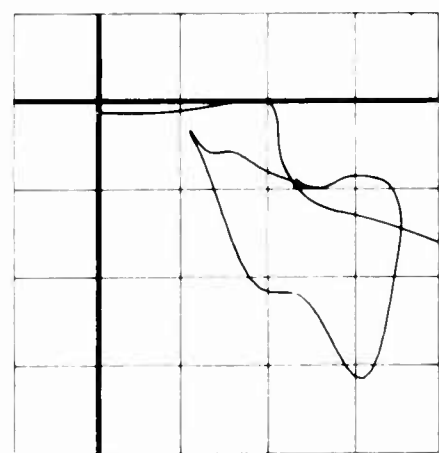
(α) - DEGREES        ANGLE OF ATTACK (α) - DEGREES        ANGLE OF ATTACK (α) - DEGREES        ANGLE OF ATTACK (α) - DEGREES

Modified)

B.
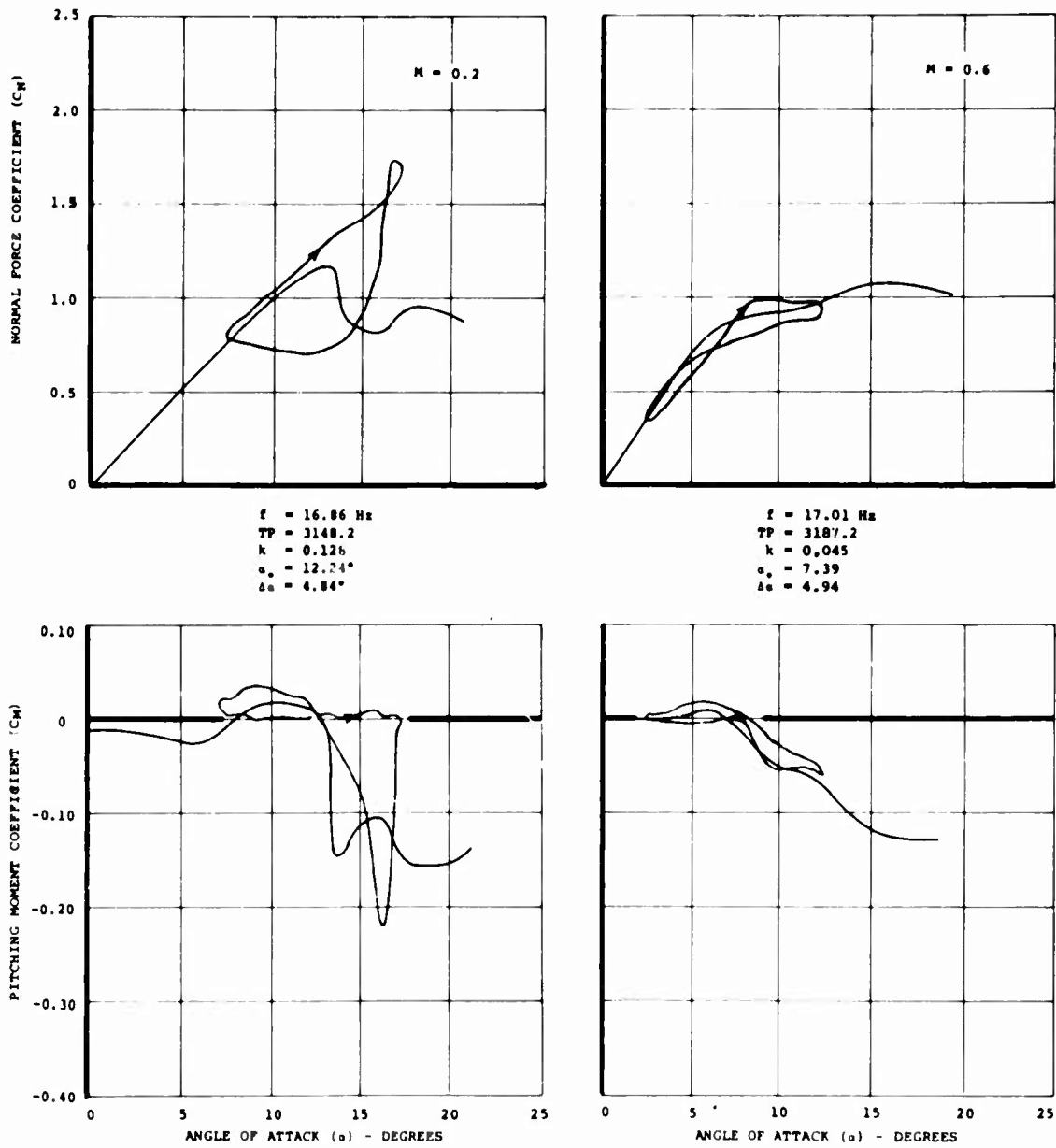
Figure 14. Effect of Mach Number on Dynamic $C_N$ and $C_M$ for the NACA 0012 (Modified) Airfoil at $f$ = 16 Hertz.

NOTES:   VERTOL 23010-1.58

1.   $\alpha_0 = 17.5°$ and $25°$ (M = 0.2)
2.   $\alpha_0 = 17.5°$ (M = 0.4)
3.   $\alpha_0 = 12.5°$ (M = 0.6)
NACA 0012 (Modified)
4.   $\alpha_0 = 17.5°$ and $25°$ (M = 0.2)
5.   $7.5 < \alpha_0 < 17.5°$ (M = 0.4)
6.   $\alpha_0 = 10°$ (M = 0.6)
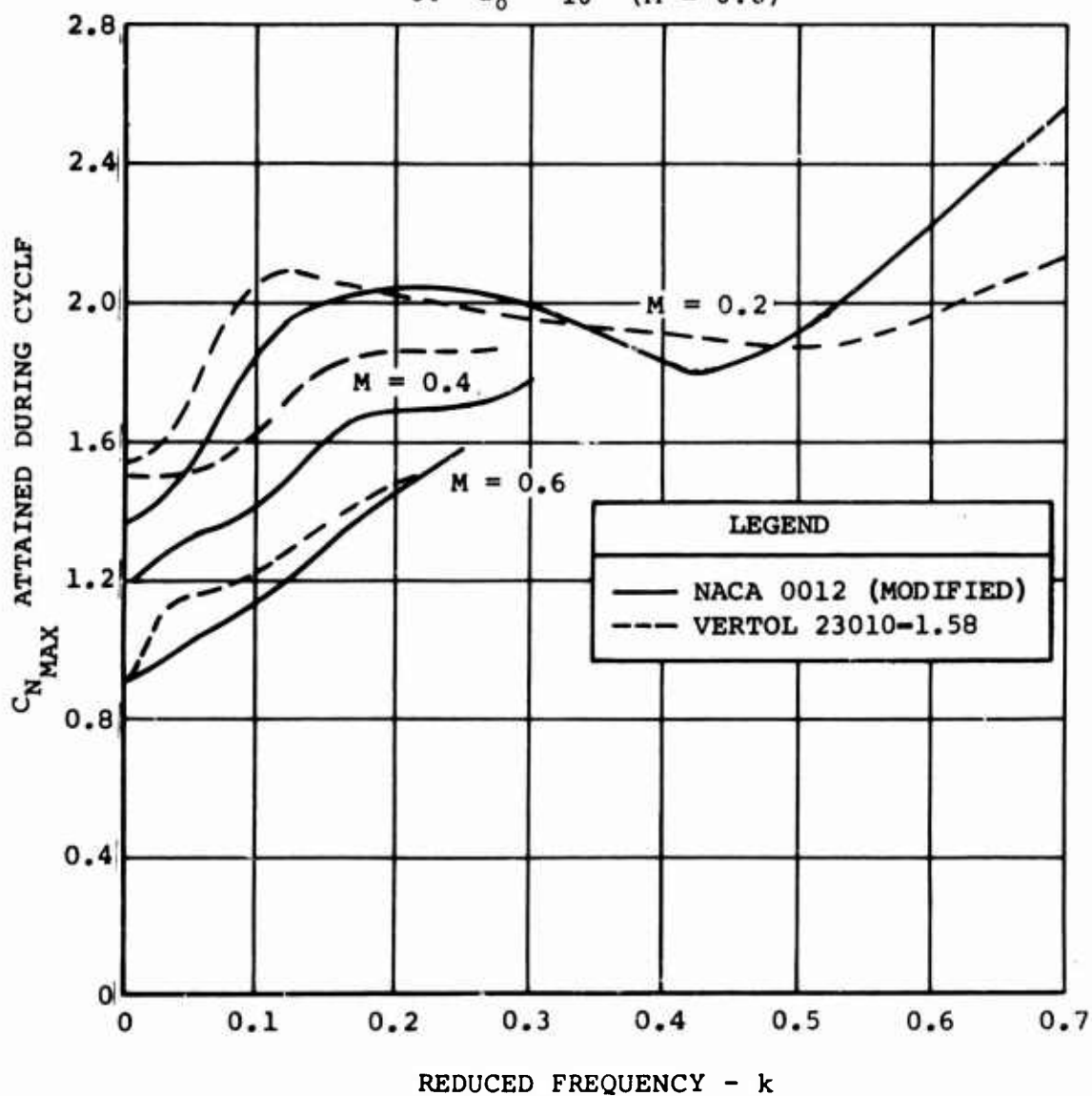
Figure 15.   Maximum Normal Force Attained During These
Tests for Pitch Oscillation at $\Delta\alpha = 5°$.

54
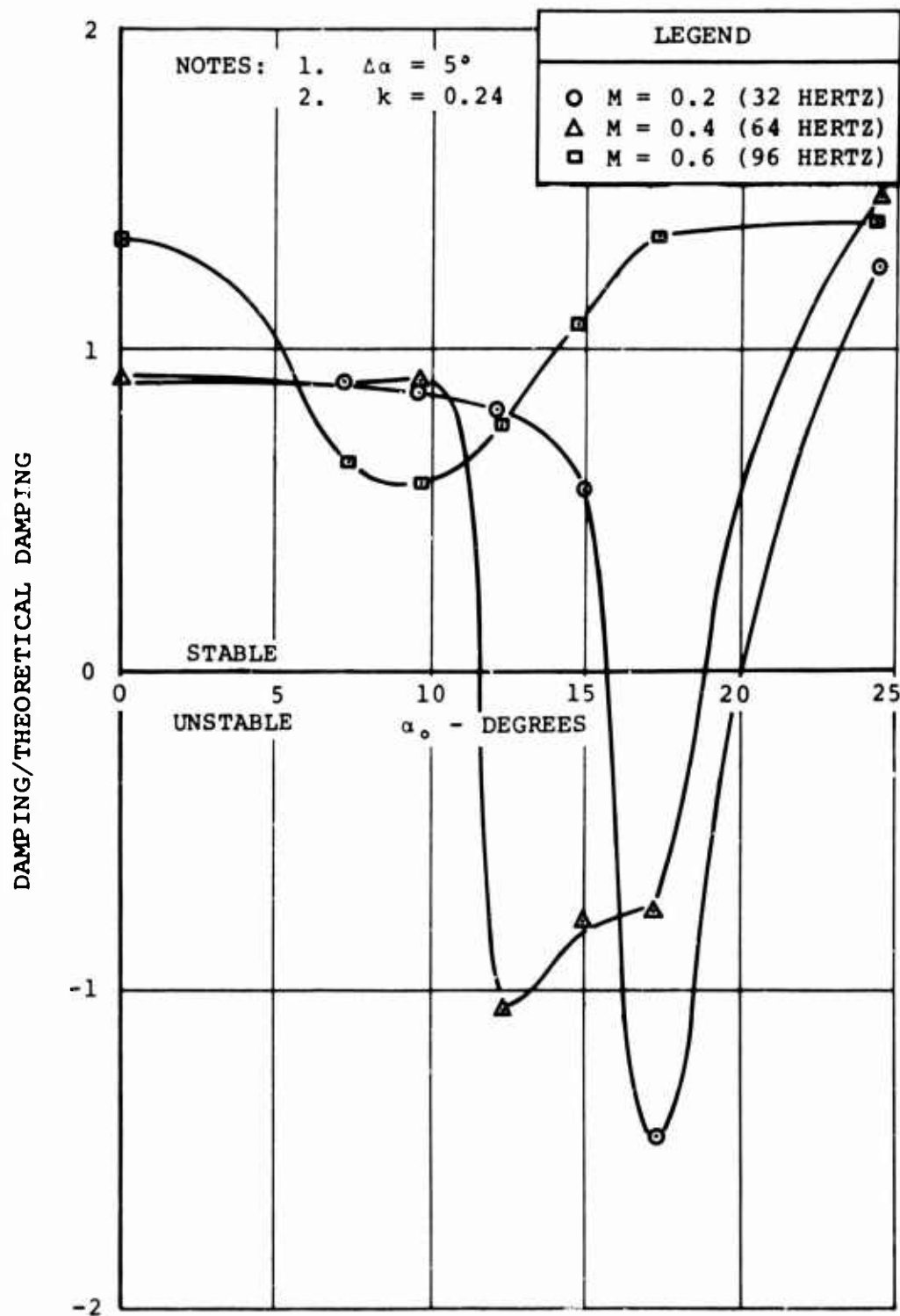
Figure 16. Effect of Mach Number on the Aerodynamic Pitch Damping of Vertol 23010-1.58 Airfoil.
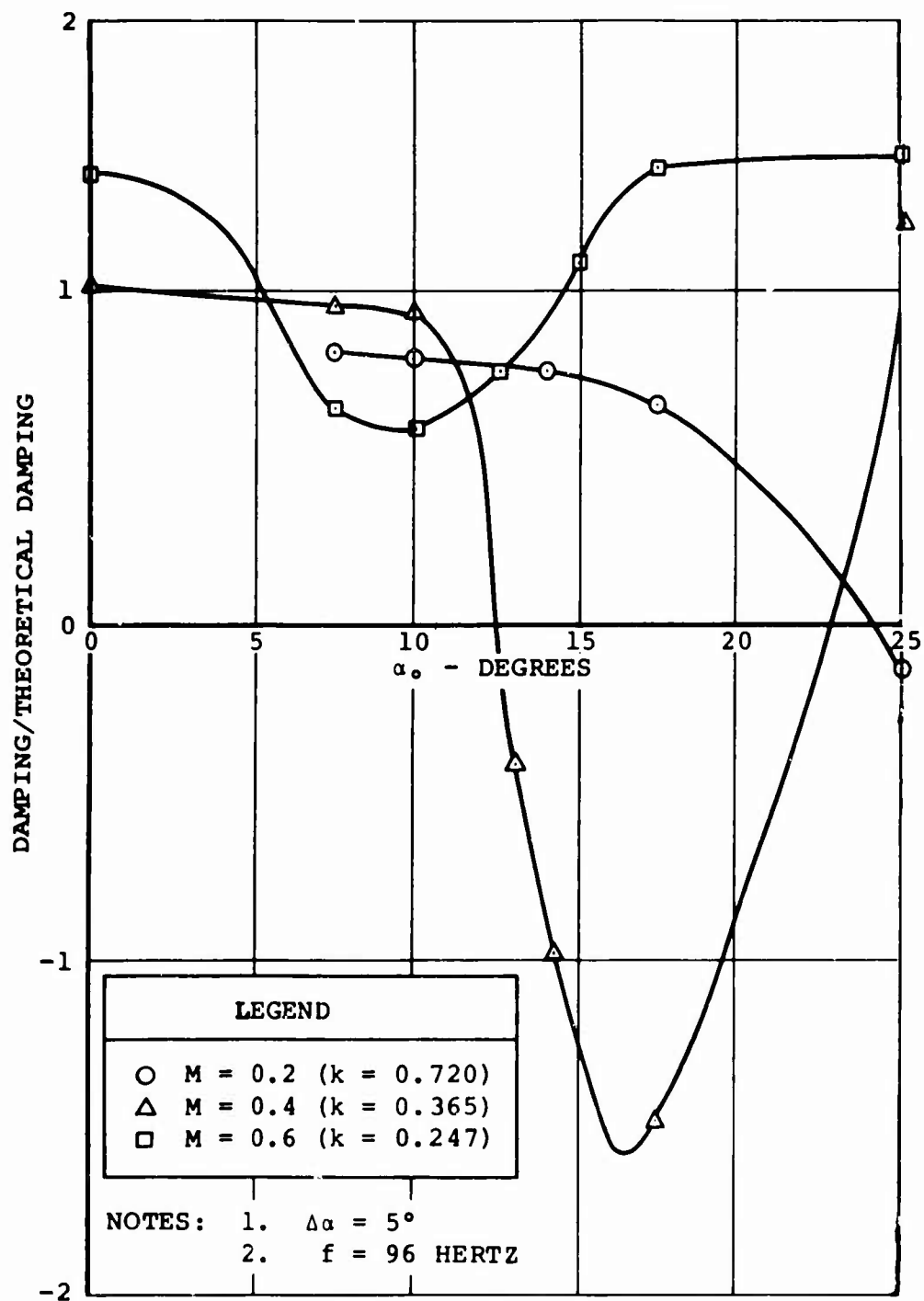
Figure 17. Effect of Mach Number on the Aerodynamic Pitch
Damping of Vertol 23010-1.58 Airfoil at Constant
Frequency.

56
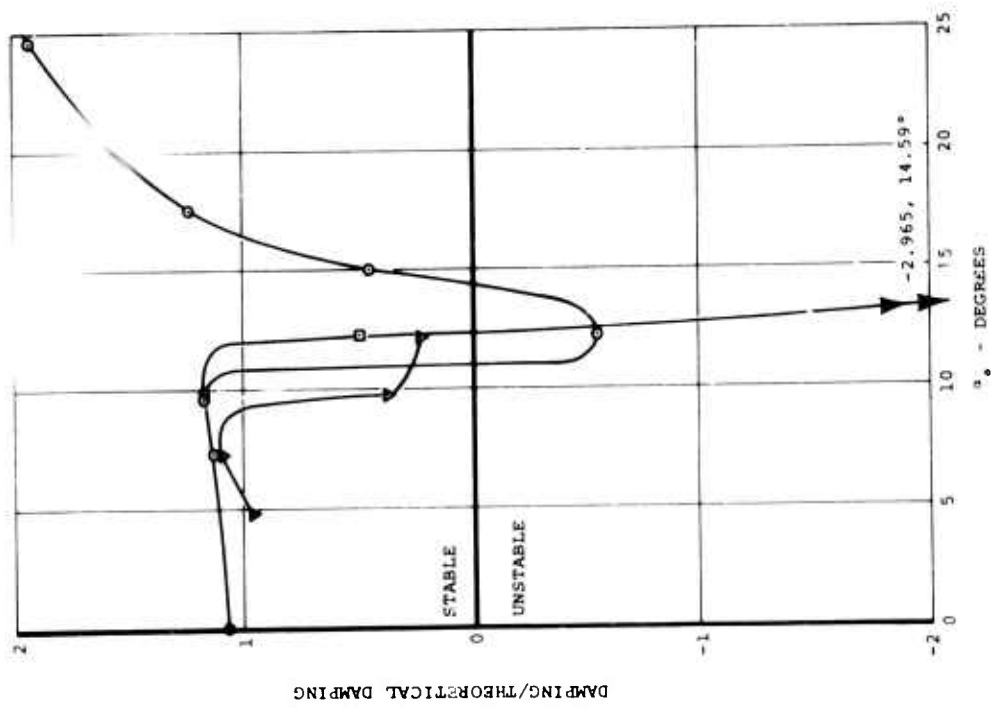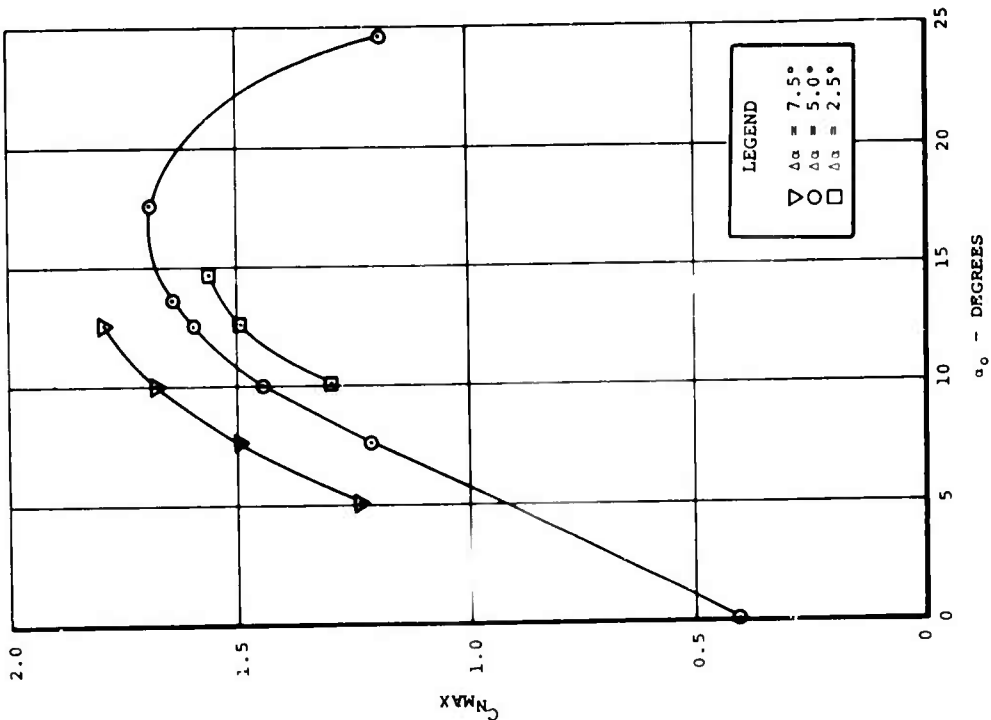
Figure 18. Amplitude of Oscillation Effect on $C_{N_{MAX}}$ and Damping for Vertol 23010-1.58 Airfoil at M = 0.4 and f = 16 Hertz.

57
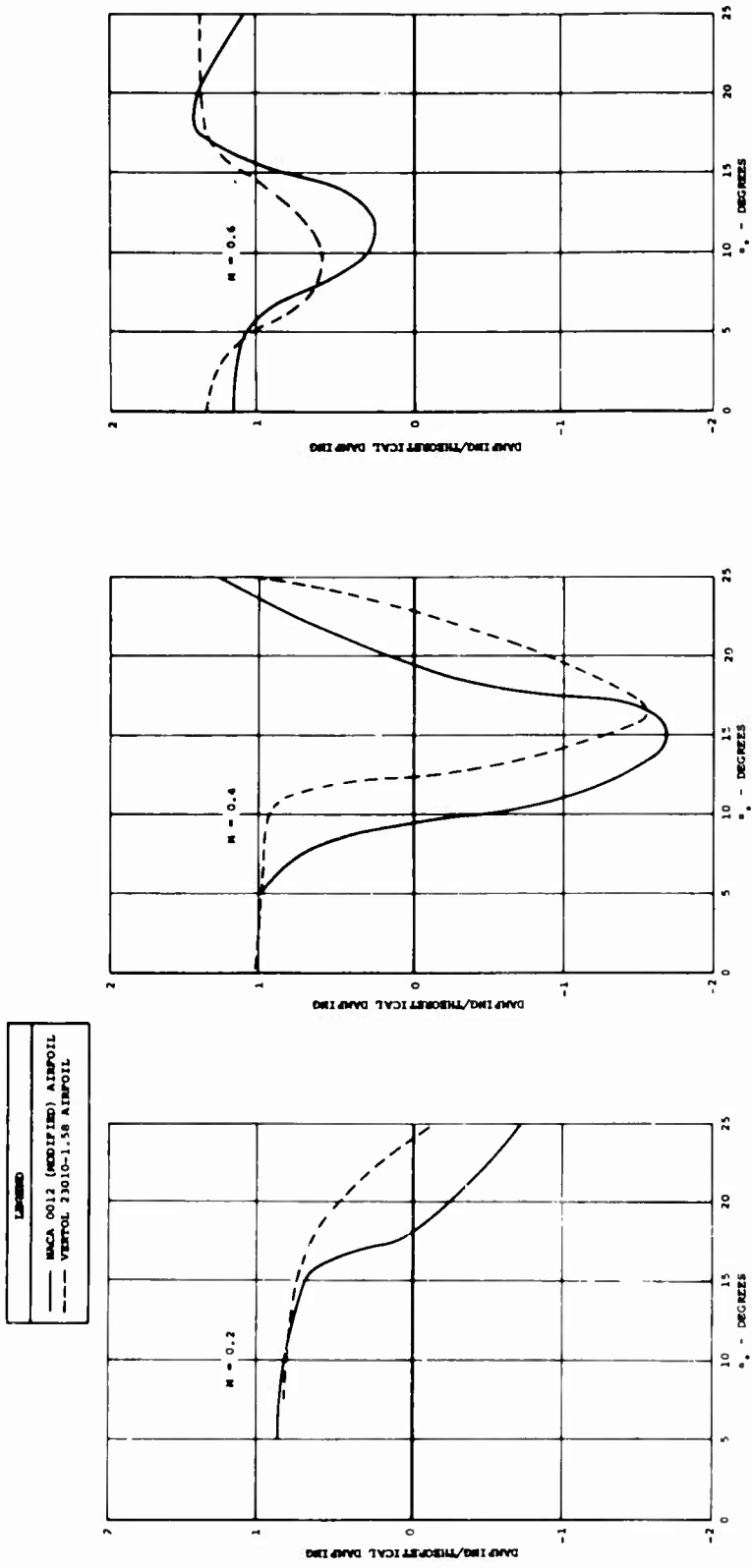
Figure 19. Comparison of Pitch Damping at f = 96 Hertz
and Δα = 5° for Vertol 23010-1.58 and
NACA 0012 (Modified) Airfoils.
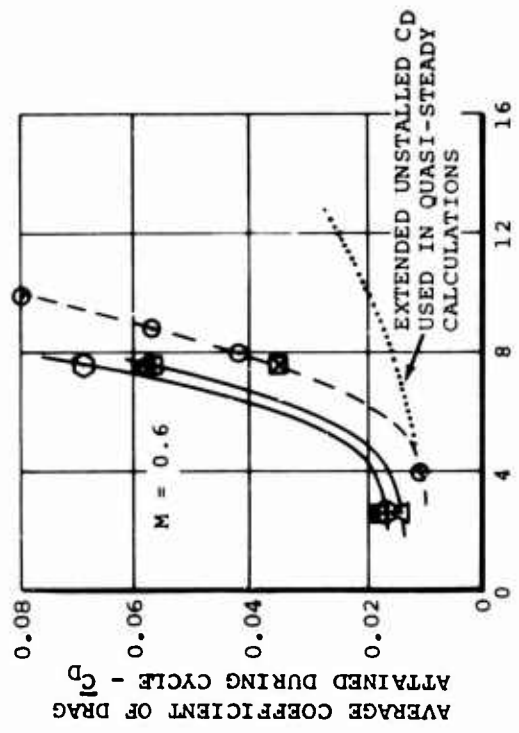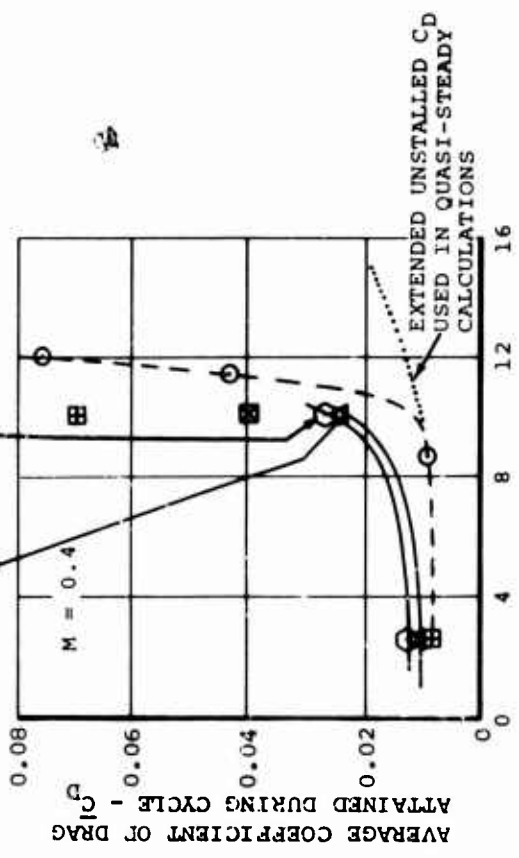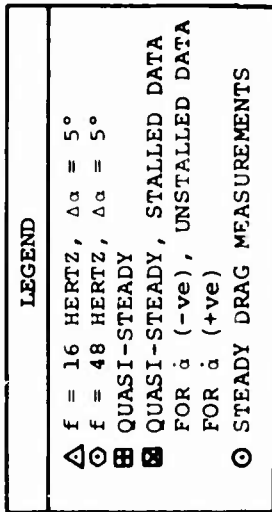
Figure 20. Oscillatory and Steady Drag Data for Vertol 23010-1.58 Airfoil From Wake Traverse Measurements.

59

Figure 21. Dynamic $C_N$ and $C_M$ Versus h for Vertol 23010-1.58 Airfoil at M = 0.4, f = 17 Hertz, and $\Delta h = 0.304$.

61

A.
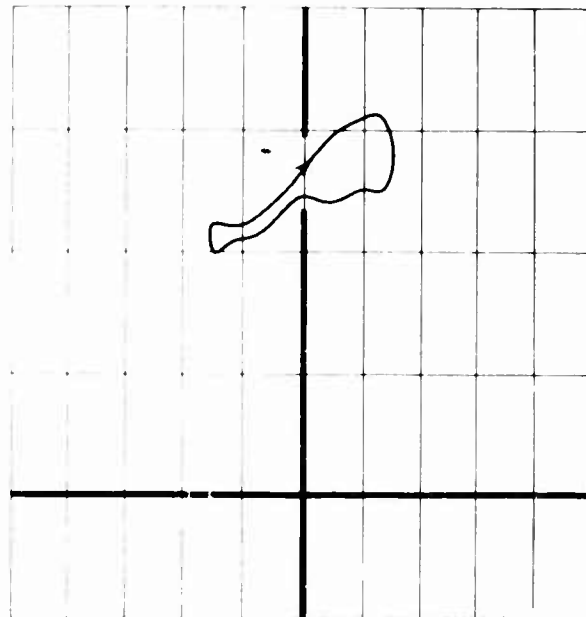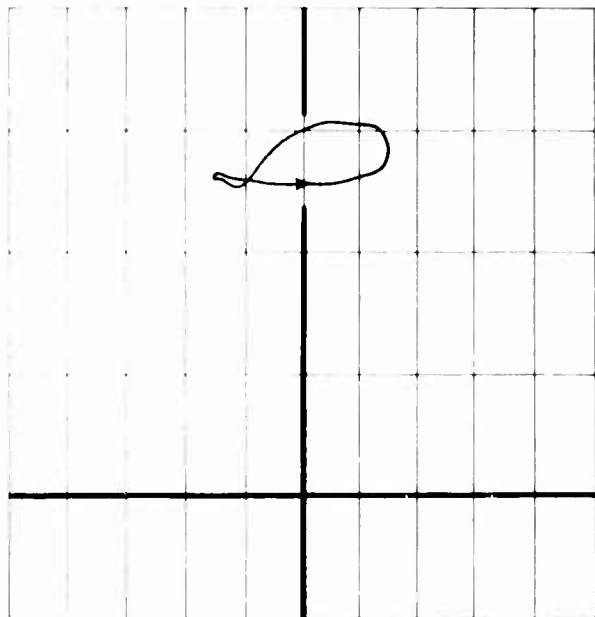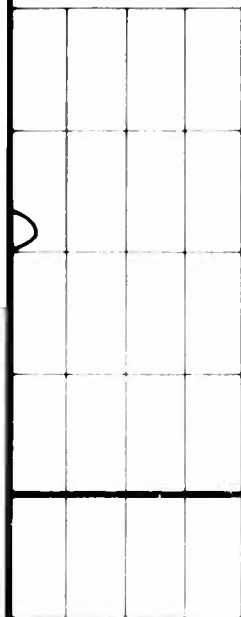
$$\alpha_o = 12.25°$$
$$TP = 4025.3$$
$$f = 17.24 \text{ Hz}$$
$$k = 0.068$$
$$\Delta h = 0.306$$

$$\alpha_o = 14.65°$$
$$TP = 4025.4$$
$$f = 17.24 \text{ Hz}$$
$$k = 0.068$$
$$\Delta h = 0.306$$
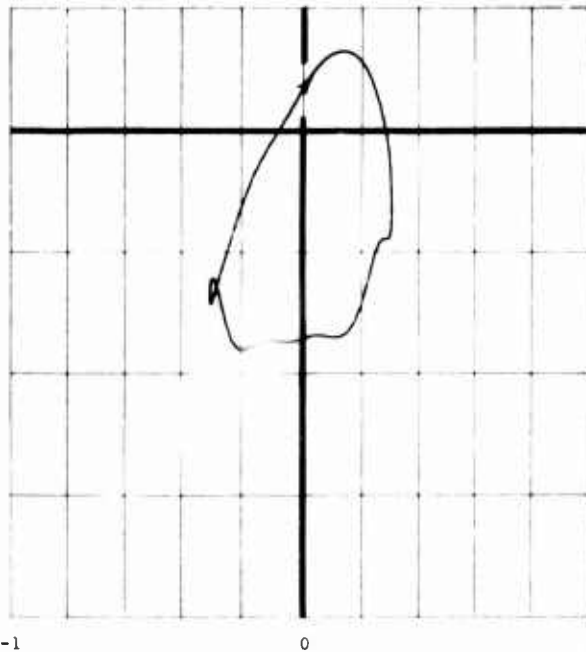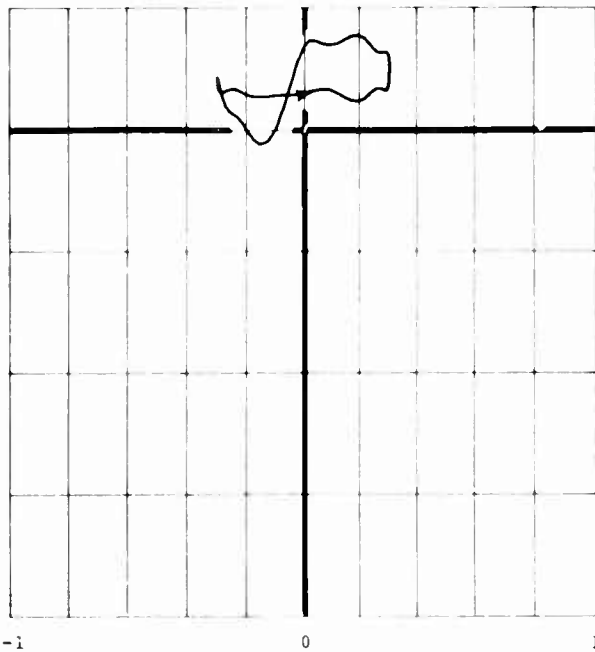
ON (h)

TRANSLATION POSITION (h)

TRANSLATION POSITION (h)
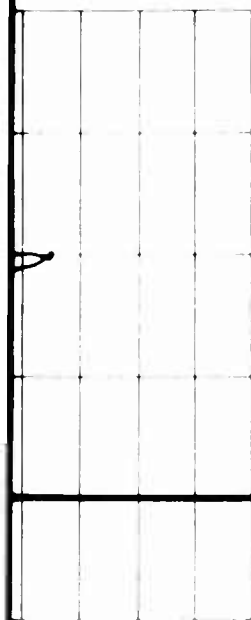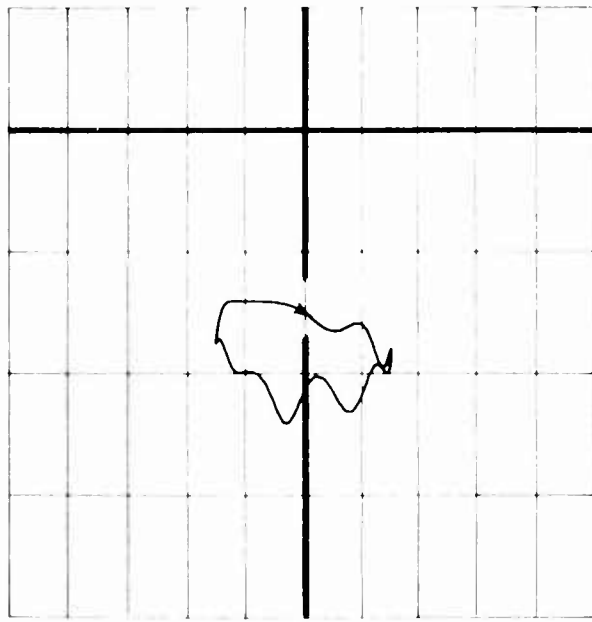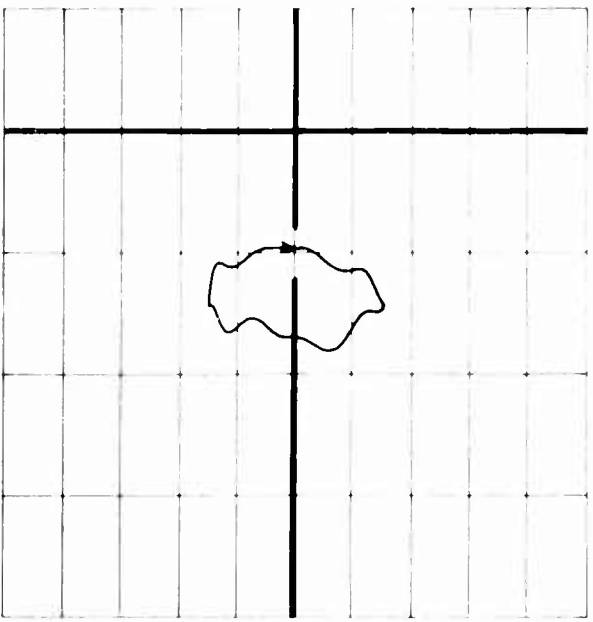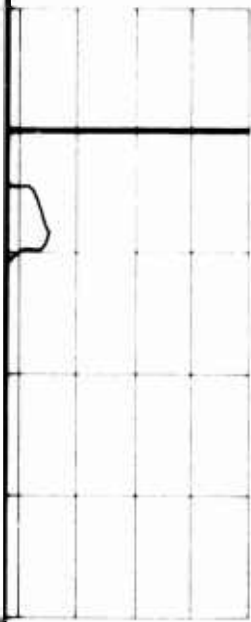
58
04.

B.
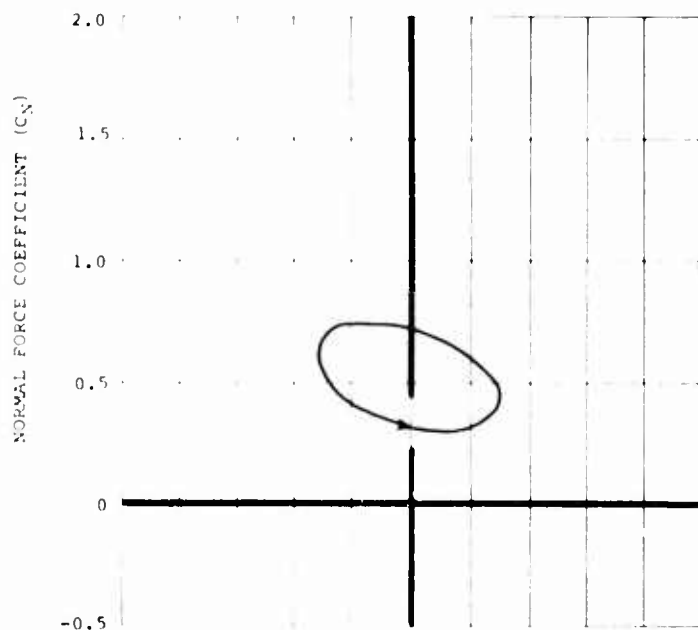
Figure 22.  Dynamic $C_N$ and $C_M$ Versus h for Vertol 23010-1.58
Airfoil at M = 0.4, f = 33 Hertz, and $\Delta h$ = 0.306.

63

A.
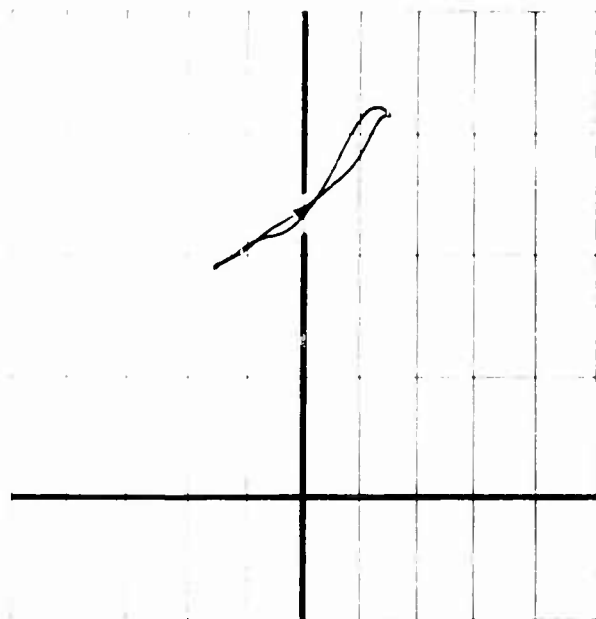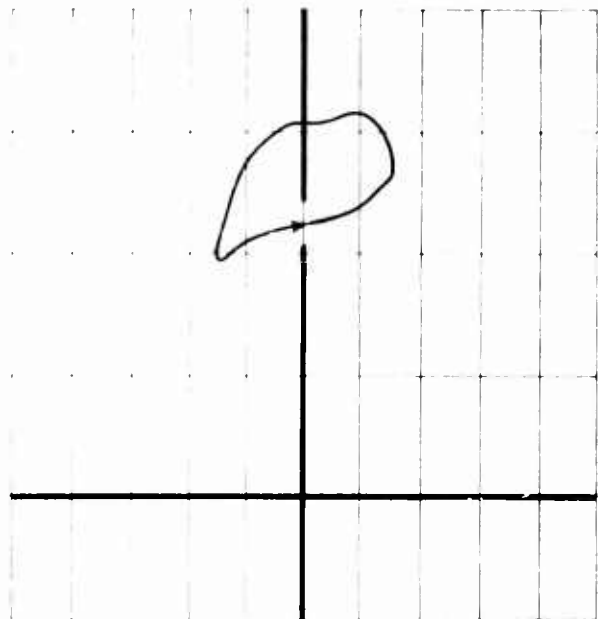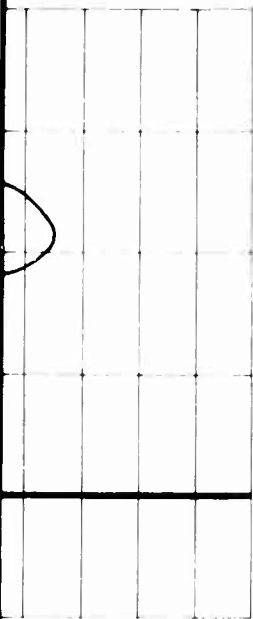
$$\alpha_o = 12.46°$$
$$TP = 4028.3$$
$$f = 30.96 \text{ Hz}$$
$$k = 0.121$$
$$\Delta h = 0.306$$

$$\alpha_o = 14.88°$$
$$TP = 4028.4$$
$$f = 32.89 \text{ Hz}$$
$$k = 0.128$$
$$\Delta h = 0.306$$
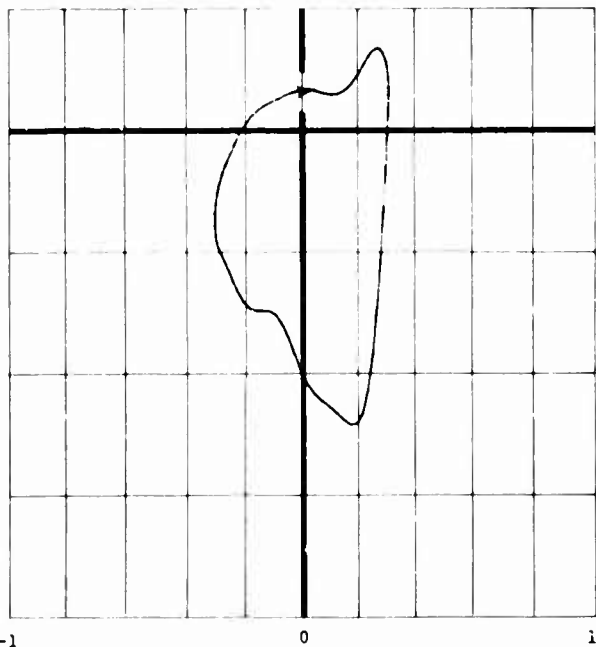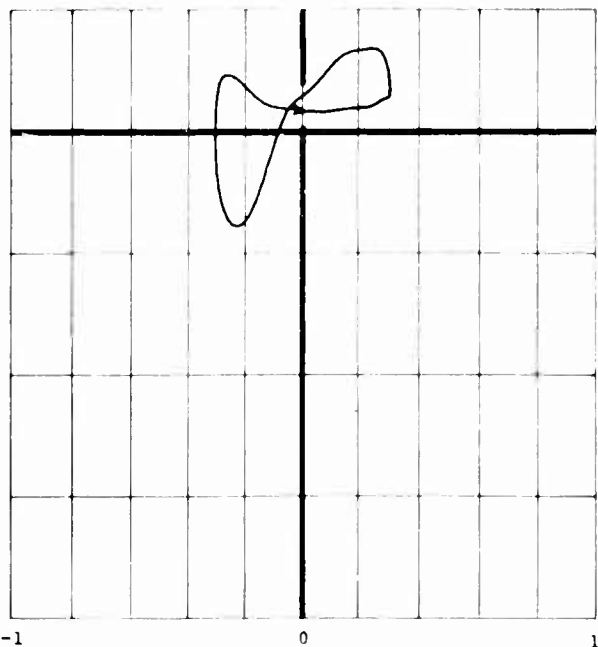
ITION (h)          TRANSLATION POSITION (h)          -1          TRANSLATION POSITION (h)

1.58
.306.

B.
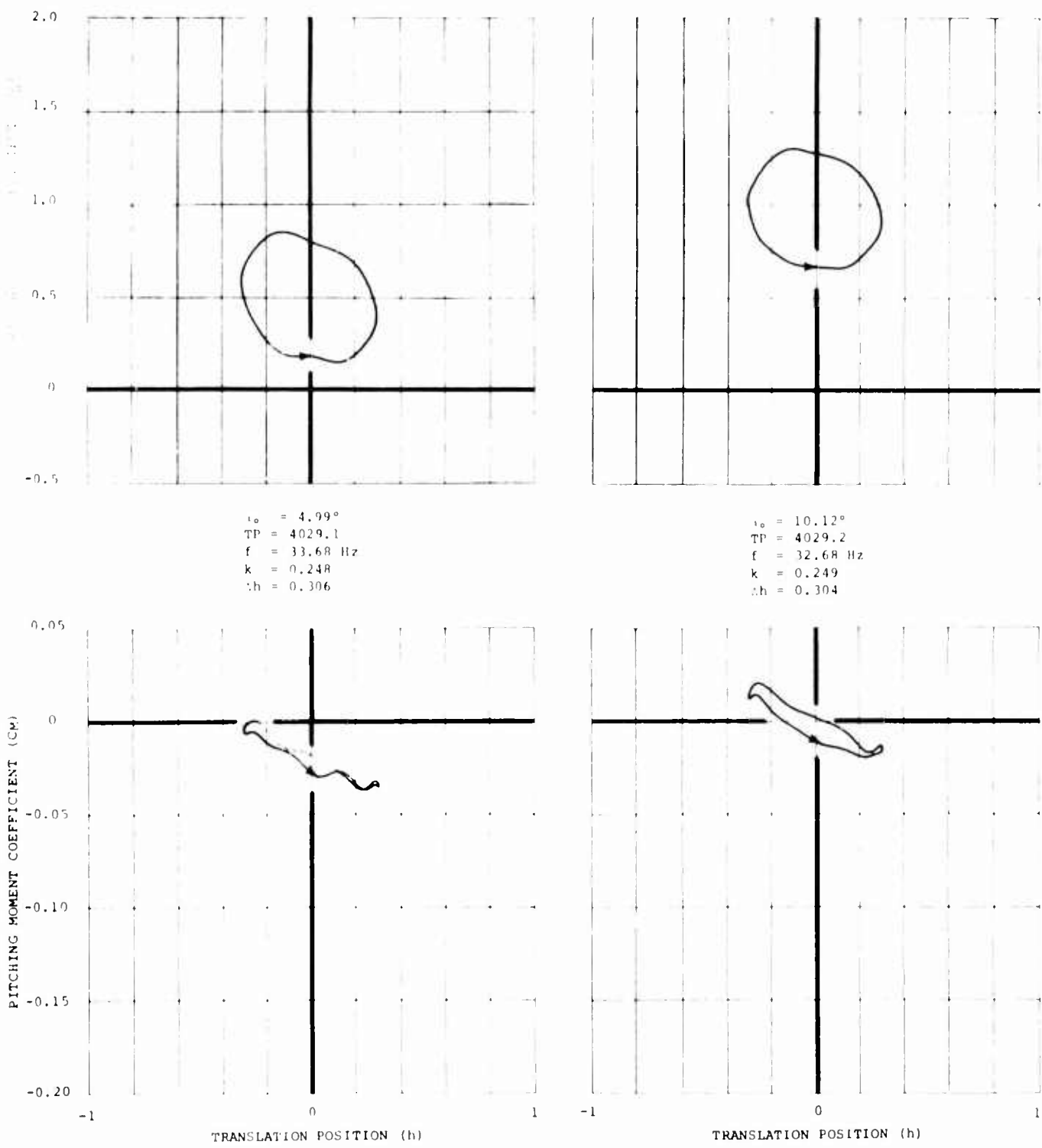
Figure 23. Dynamic $C_N$ and $C_M$ Versus h for Vertol 23010-1.58 Airfoil at M = 0.2, f = 33 Hertz, and $\Delta h$ = 0.306.

65

A.
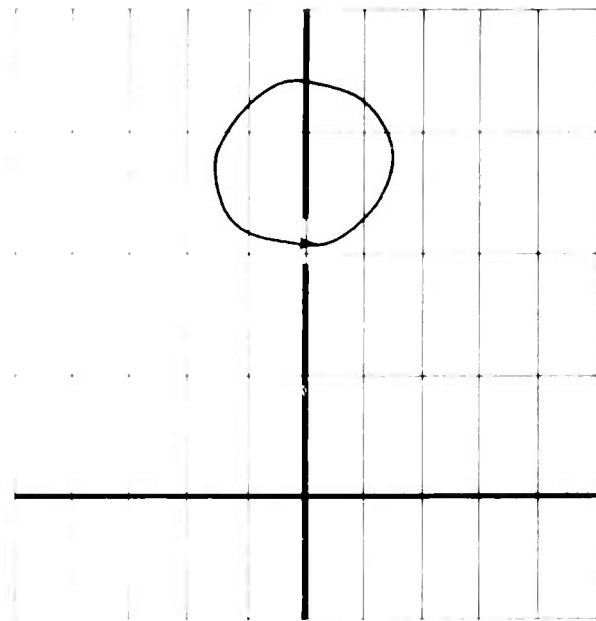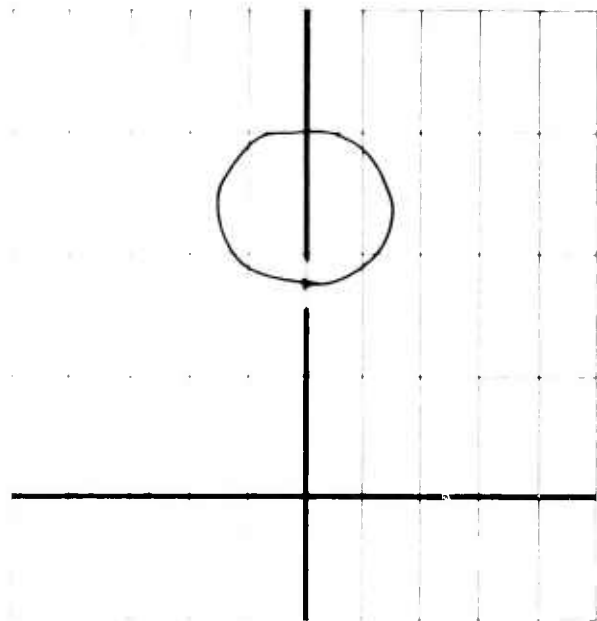
$a_0 = 12.61°$
TP = 4029.3
f = 32.79 Hz
k = 0.250
$\Delta h$ = 0.305

$a_0 = 15.10°$
TP = 4029.4
f = 32.68 Hz
k = 0.249
$\Delta h$ = 0.305

ION (h)          -1          0          1  -1          0          1

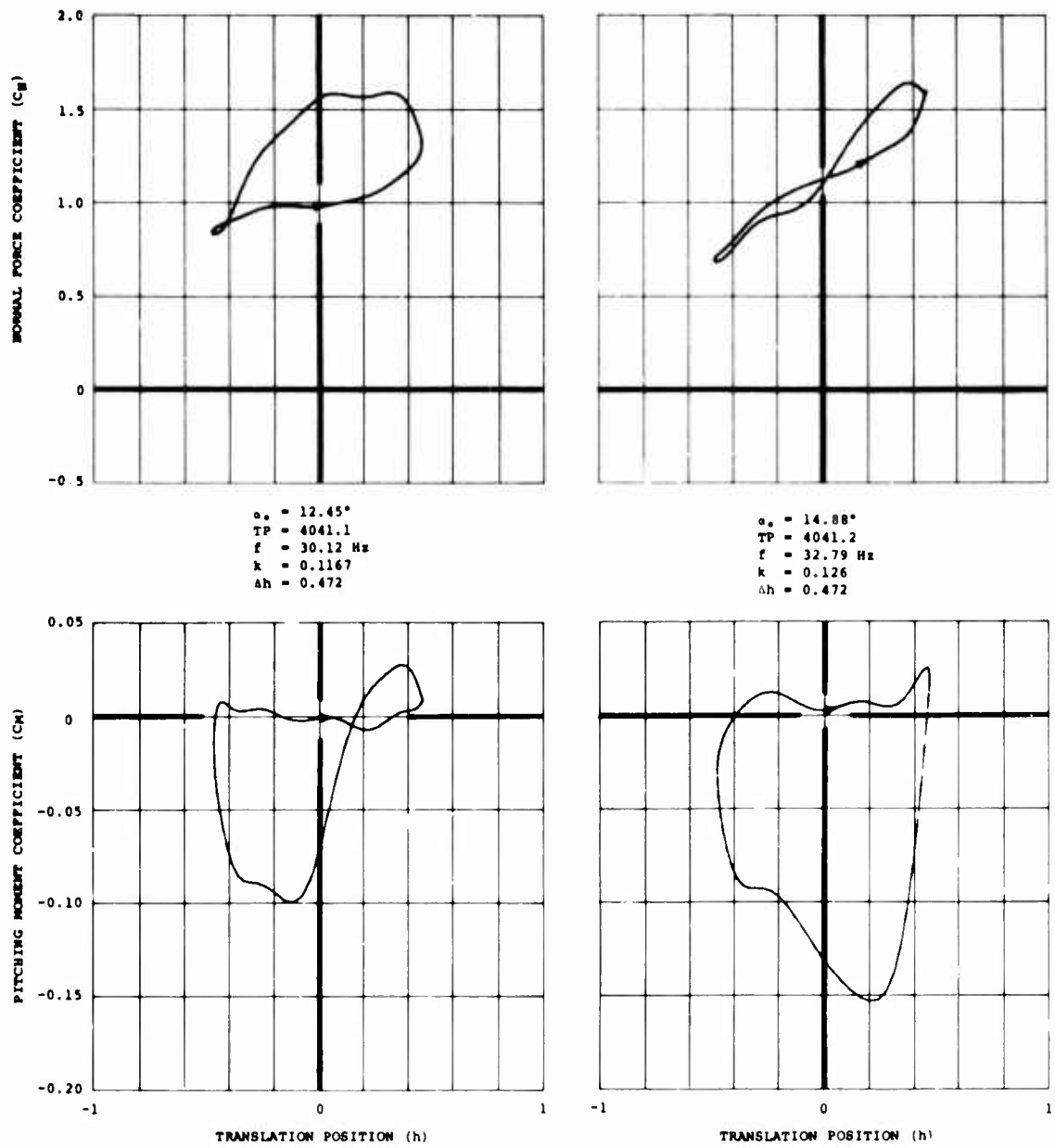TRANSLATION POSITION (h)          TRANSLATION POSITION (h)

$\beta$.
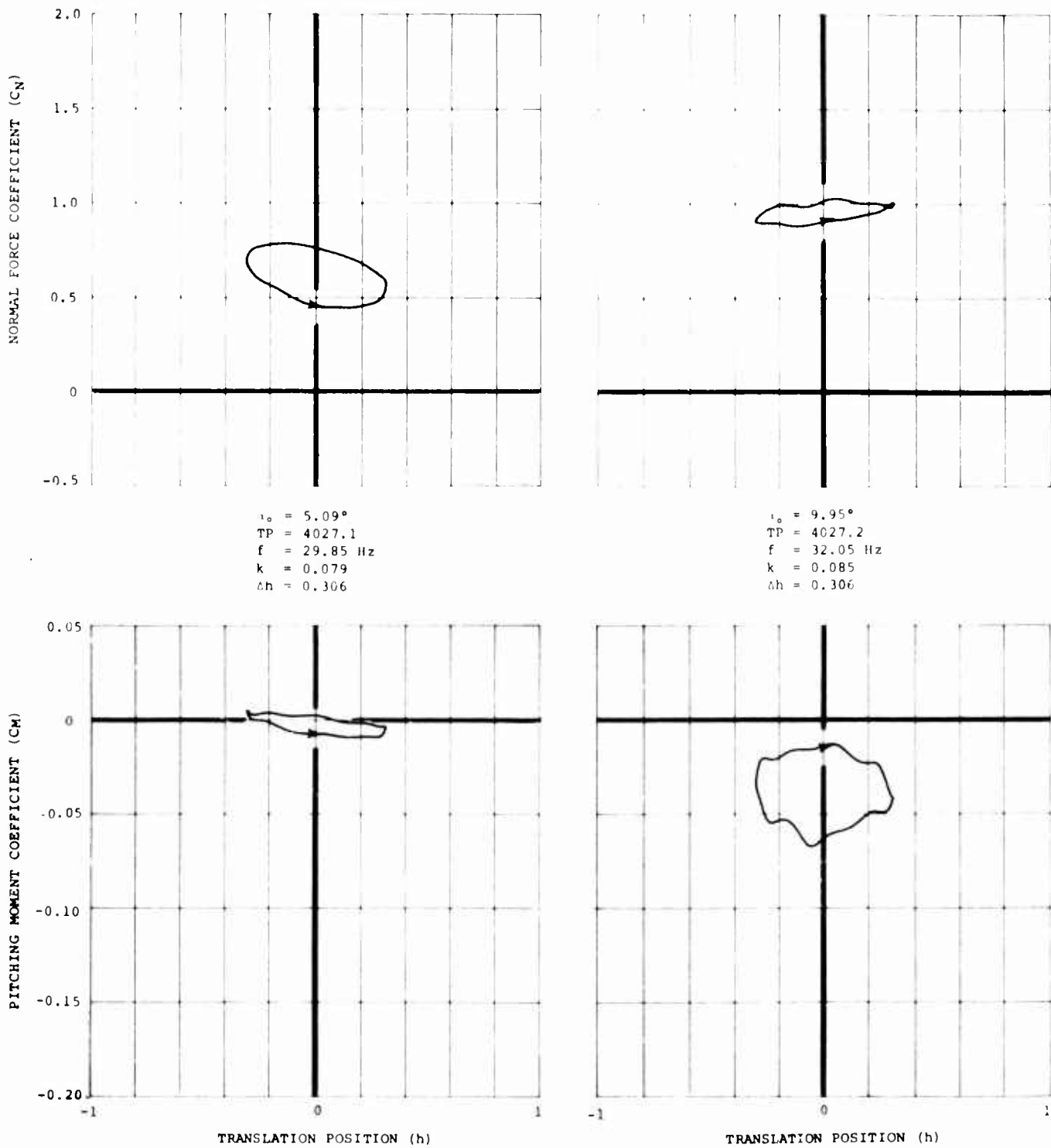
Figure 24. Dynamic $C_N$ and $C_M$ Versus h for Vertol 23010-1.58
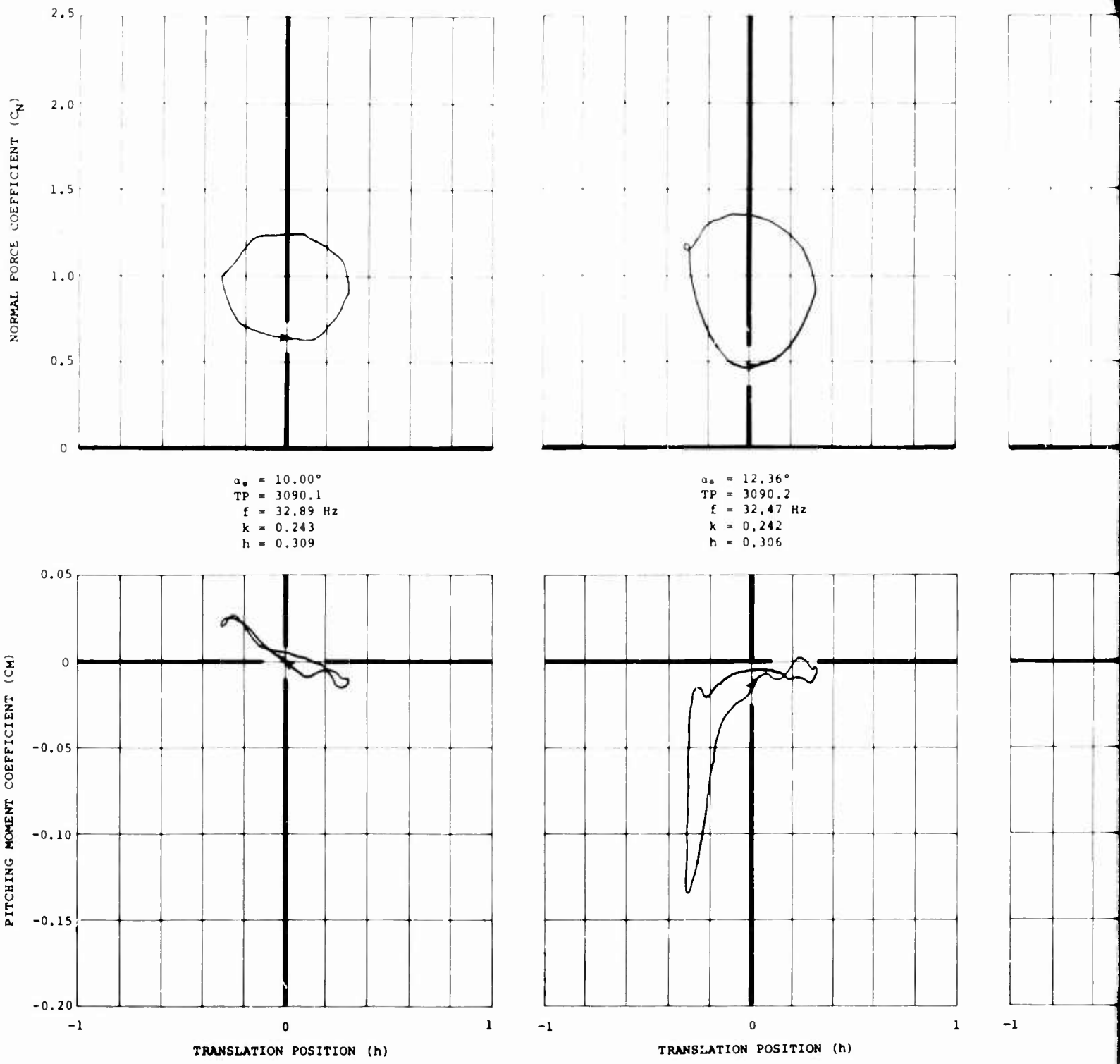Airfoil at M = 0.6, f = 33 Hertz, and $\Delta h$ = 0.306.

67
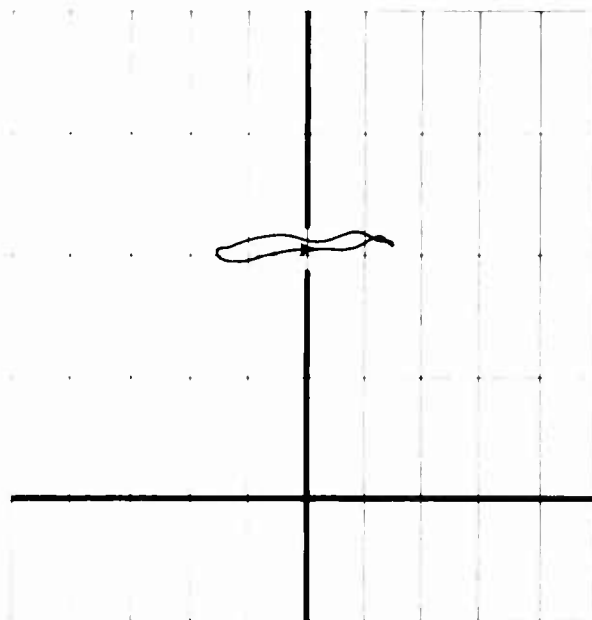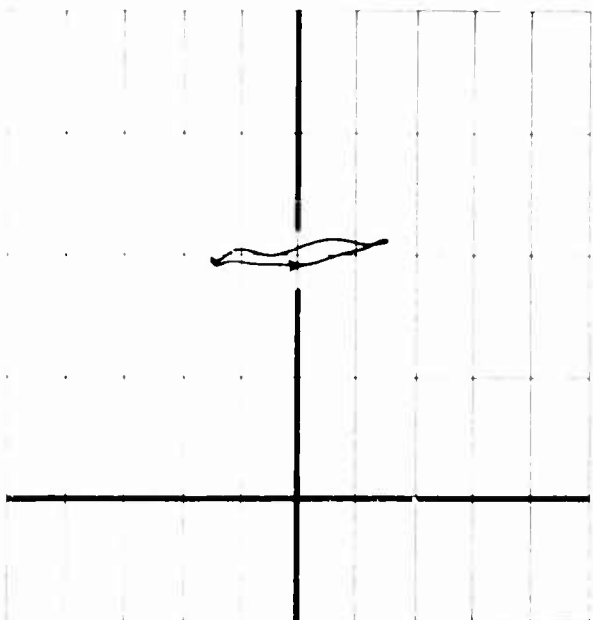
$\mathfrak{i}_o = 12.34°$
TP = 4027.3
f = 32.36 Hz
k = 0.086
$\Delta$h = 0.306

$\mathfrak{i}_o = 14.77°$
TP = 4027.4
f = 32.57 Hz
k = 0.087
$\Delta$h = 0.305

Hz

ITION (h)

TRANSLATION POSITION (h)

TRANSLATION POSITION (h)

B.

Figure 25. Dynamic $C_N$ and $C_M$ Versus h for Vertol 23010-1.58 Airfoil at M = 0.4, f = 33 Hertz, and $\Delta h = 0.472$.
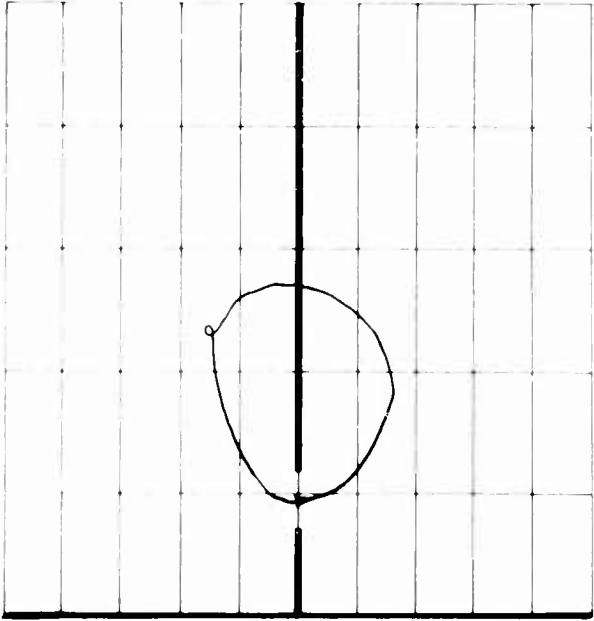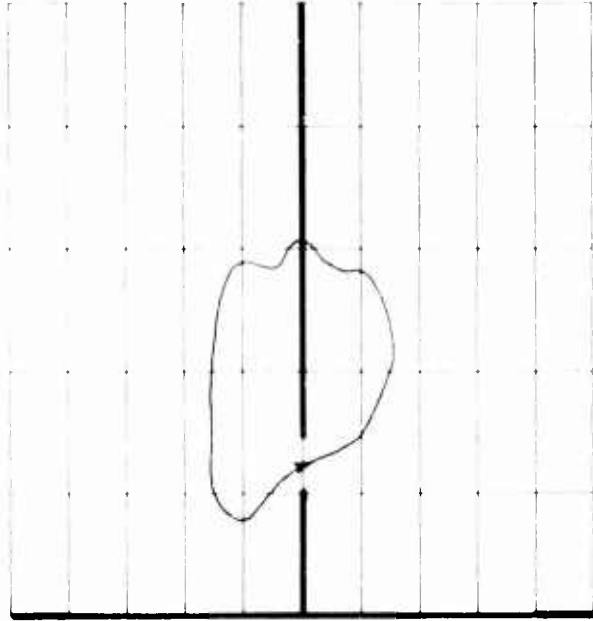
69

Figure 26. Dynamic $C_N$ and $C_M$ Versus h for NACA 0012 (Modified)
Airfoil at M = 0.2, f = 32 Hertz, and $\Delta h$ = 0.306.

71

A.

$\alpha_o = 12.36°$
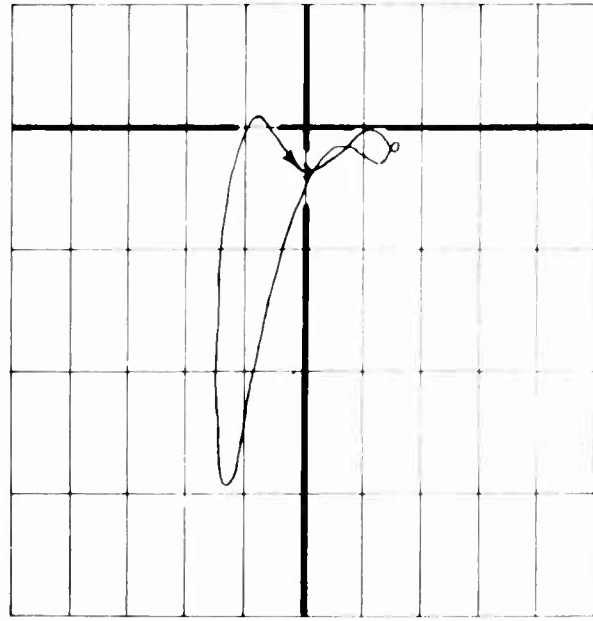TP = 3090.2
f = 32.47 Hz
k = 0.242
h = 0.306

$\alpha_o = 14.67°$
TP = 3090.3
f = 31.75 Hz
k = 0.237
h = 0.307

TRANSLATION POSITION (h)

TRANSLATION POSITION (h)

Versus h for NACA 0012 (Modified)
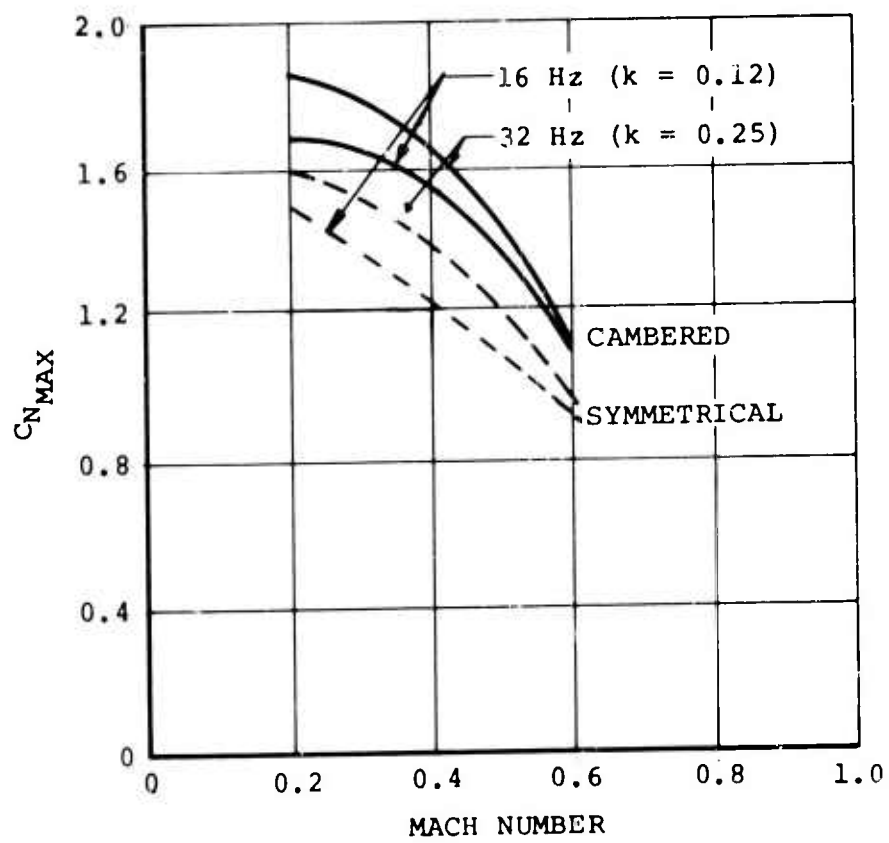2, f = 32 Hertz, and $\Delta h = 0.306$.

71

B.

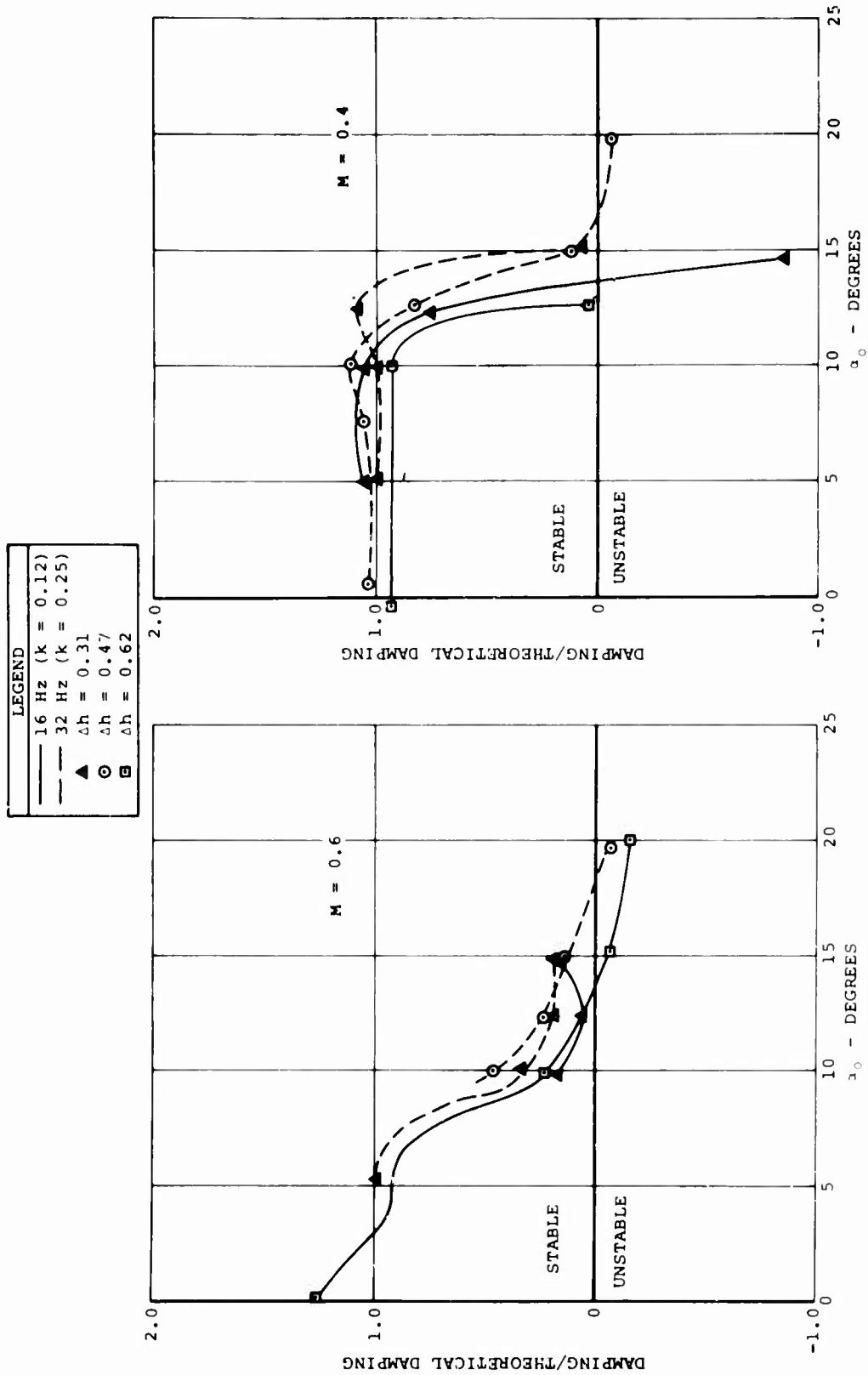Figure 27. Summary of Maximum Normal Force Attained During Translation Tests.

Figure 28. Summary of Damping Data in Vertical Translation for Vertol 23010-1.58 Airfoil.
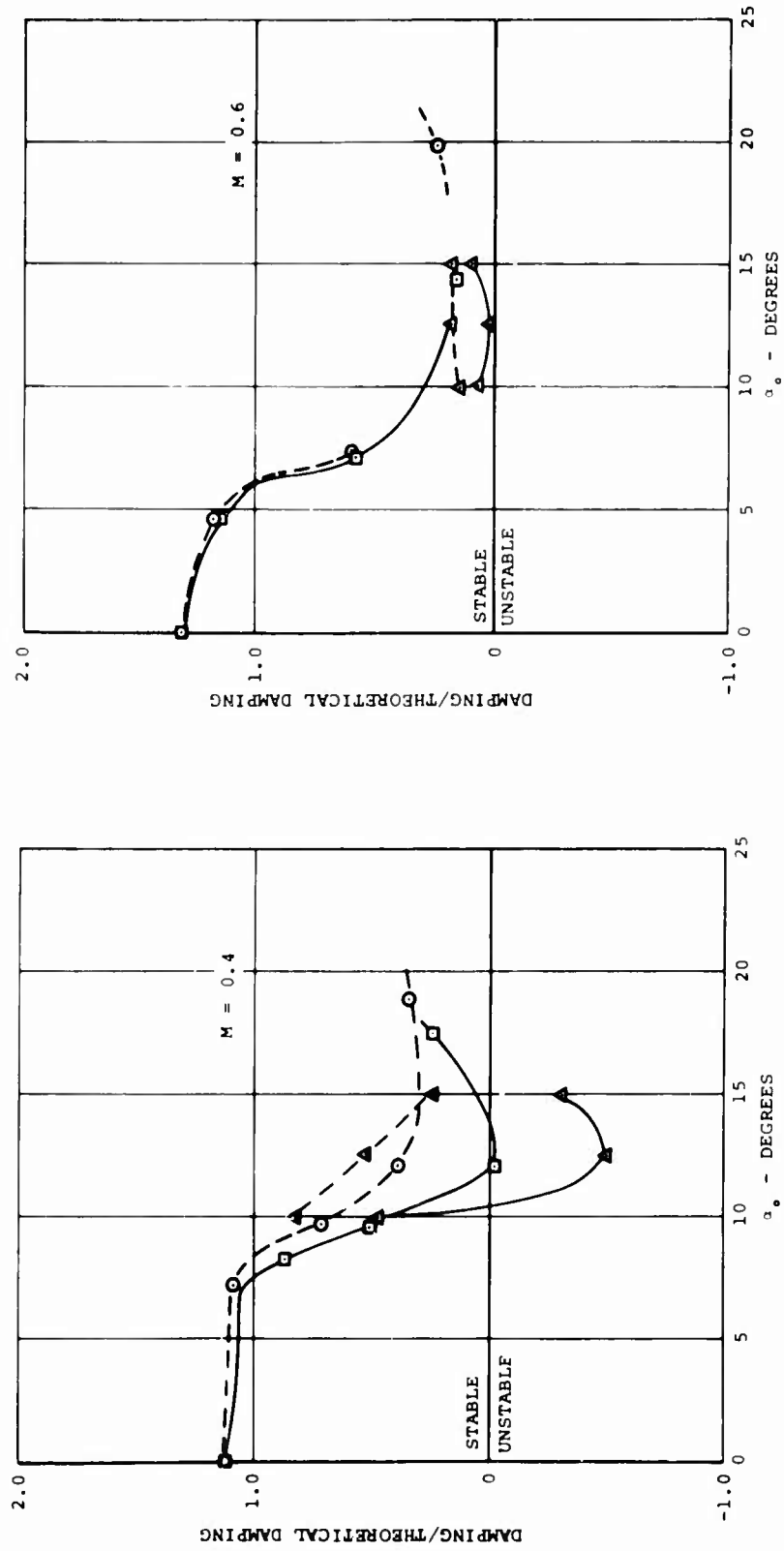
74

Figure 29. Summary of Damping Data in Vertical Translation for NACA 0012 (Modified) Airfoil.
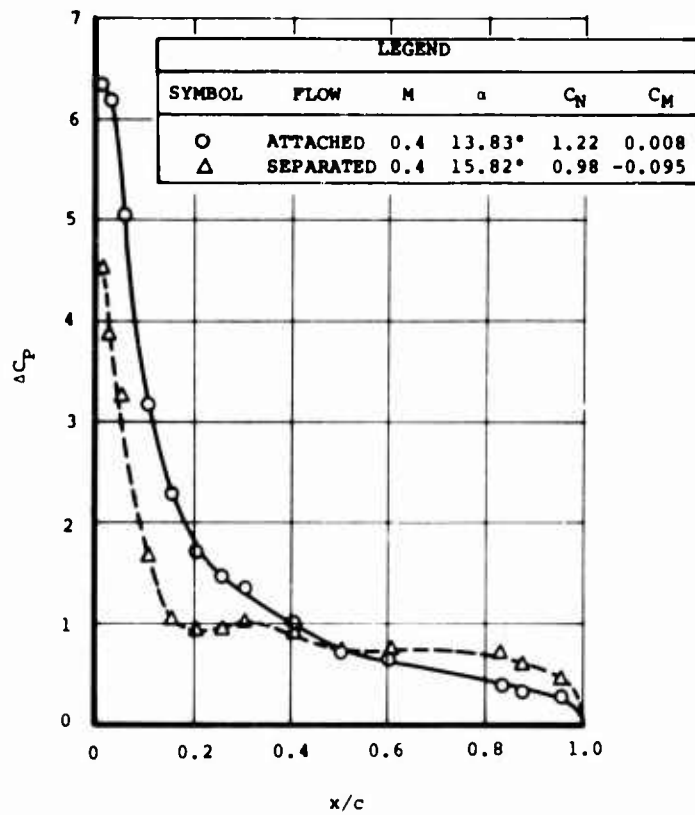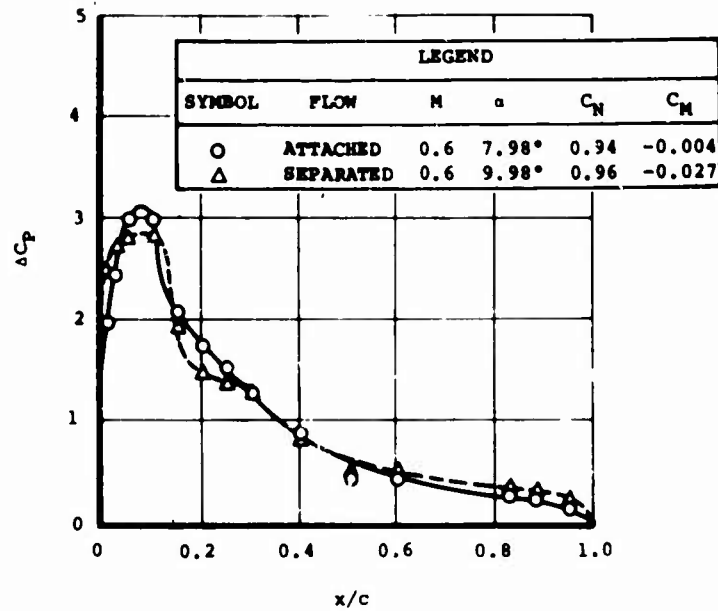
Figure 30. Effect of Mach Number on the Loading Distributions of the Vertol 23010-1.58 Airfoil at α's Near Stall.

NOTES   1.  TP = 1685.4
        2.  M  = 0.4
        3.  f  = 16.38 Hz (k = 0.061)
        4.  $\alpha_o$ = 12.22°
        5.  $\Delta\alpha$ = 4.83°

Figure 31.   Stall Time History of $C_N$, $C_M$, and $\Delta C_P$ for Vertol 23010-1.58 Airfoil in Pitch at $M = 0.4$, $f = 16.4$ Hertz, and $\alpha_o = 12.2°$.

77

Figure 32. Stall Time History of Chordwise Pressure for
Vertol 23010-1.58 Airfoil in Pitch at M = 0.4,
f = 16.4 Hertz, and $\alpha_\bullet$ = 12.2°.

78

Figure 33. Stall Time History of $C_N$, $C_M$, and $\Delta C_P$ for Vertol 23010-1.58 Airfoil in Pitch at $M = 0.4$, $f = 94.3$ Hertz, and $\alpha_o = 12.5°$.

79

Figure 34. Stall Time History of Chordwise Pressures for
Vertol 23010-1.58 Airfoil in Pitch at M = 0.4,
f = 94.3 Hertz, and $\alpha_o$ = 12.5°.

80

Figure 35.  Load Distributions on the Vertol 23010-1.58
Airfoil During a High-$\alpha$ Dynamic Stall at
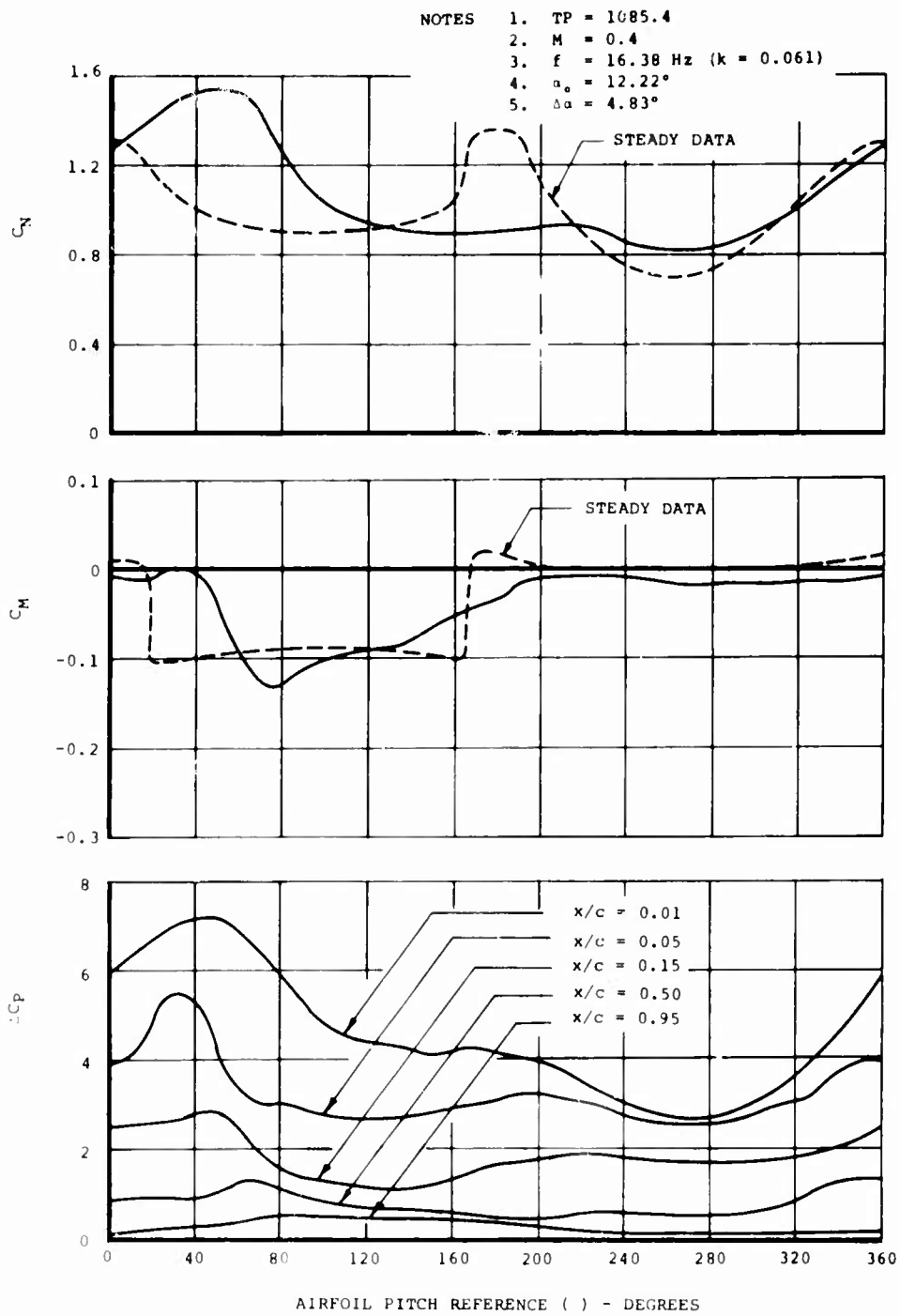$M = 0.2$, $f = 16$ Hertz, and $\Delta\alpha = 5°$.
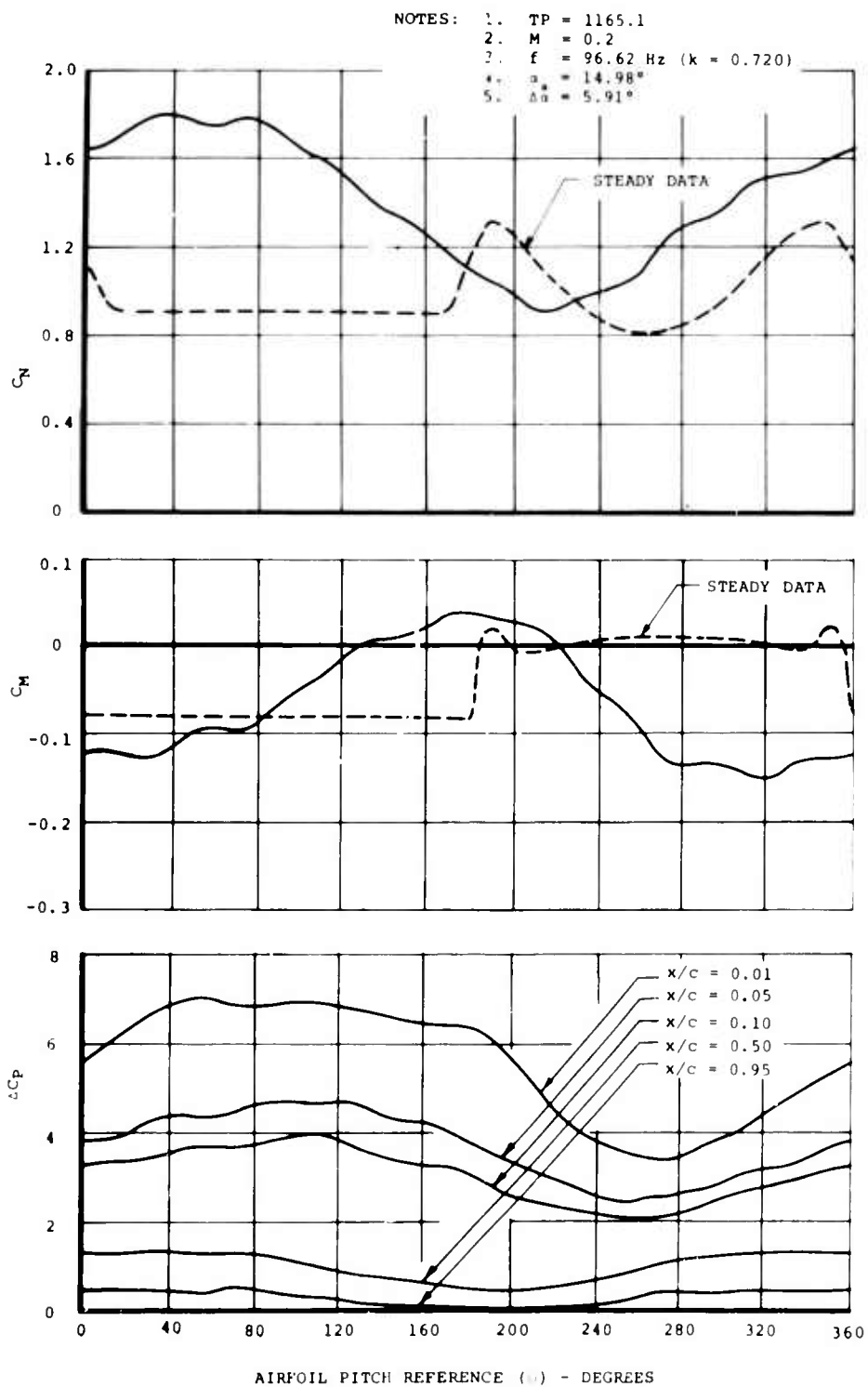
Figure 36. Stall Time History of $C_N$, $C_M$, and $\Delta C_P$ for Vertol 23010-1.58 Airfoil in Pitch at $M = 0.2$, $f = 96.6$ Hertz, and $\alpha_o = 15.0°$.
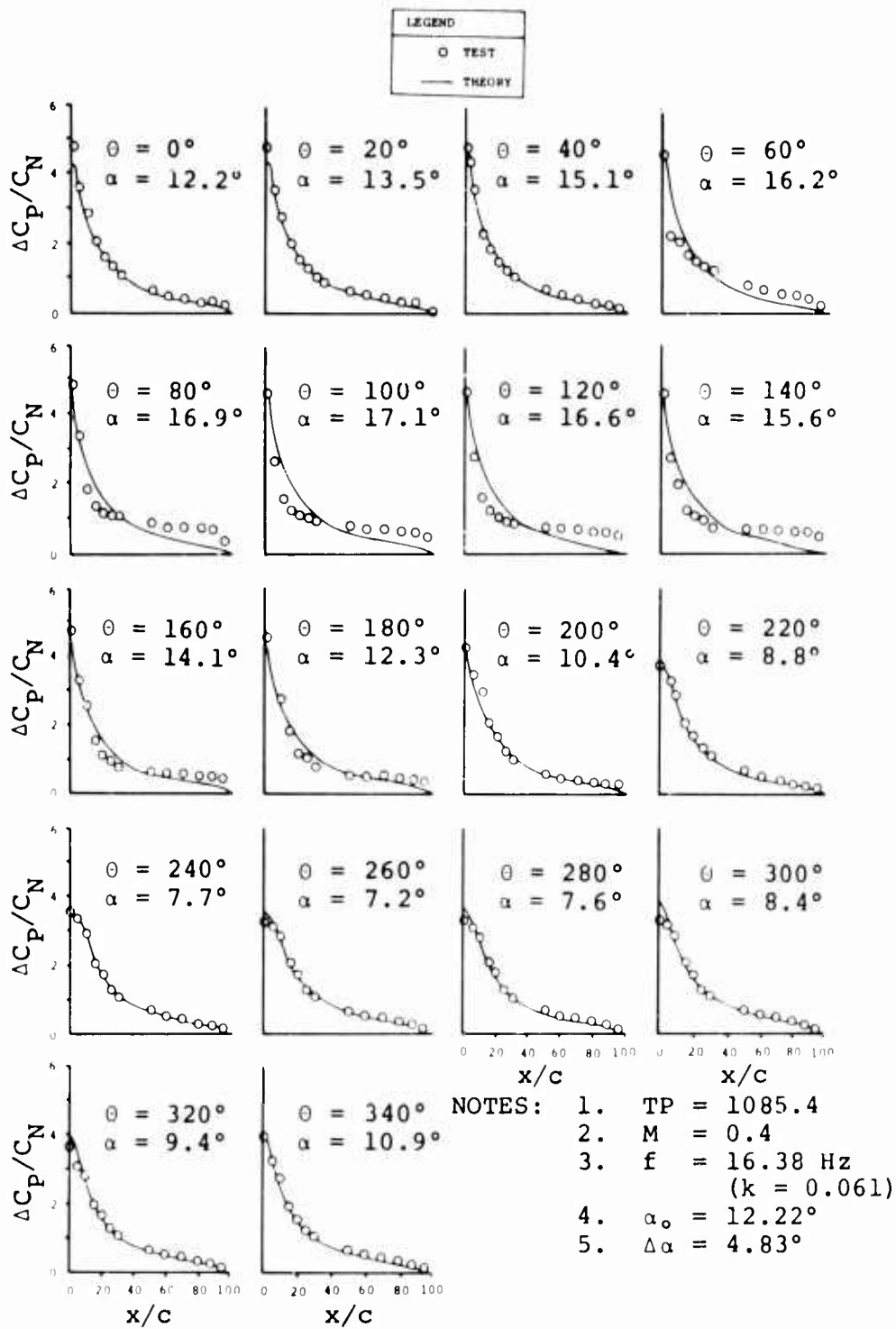
82

Figure 37. Stall Time History of Chordwise Pressures for
Vertol 23010-1.58 Airfoil in Pitch at M = 0.2,
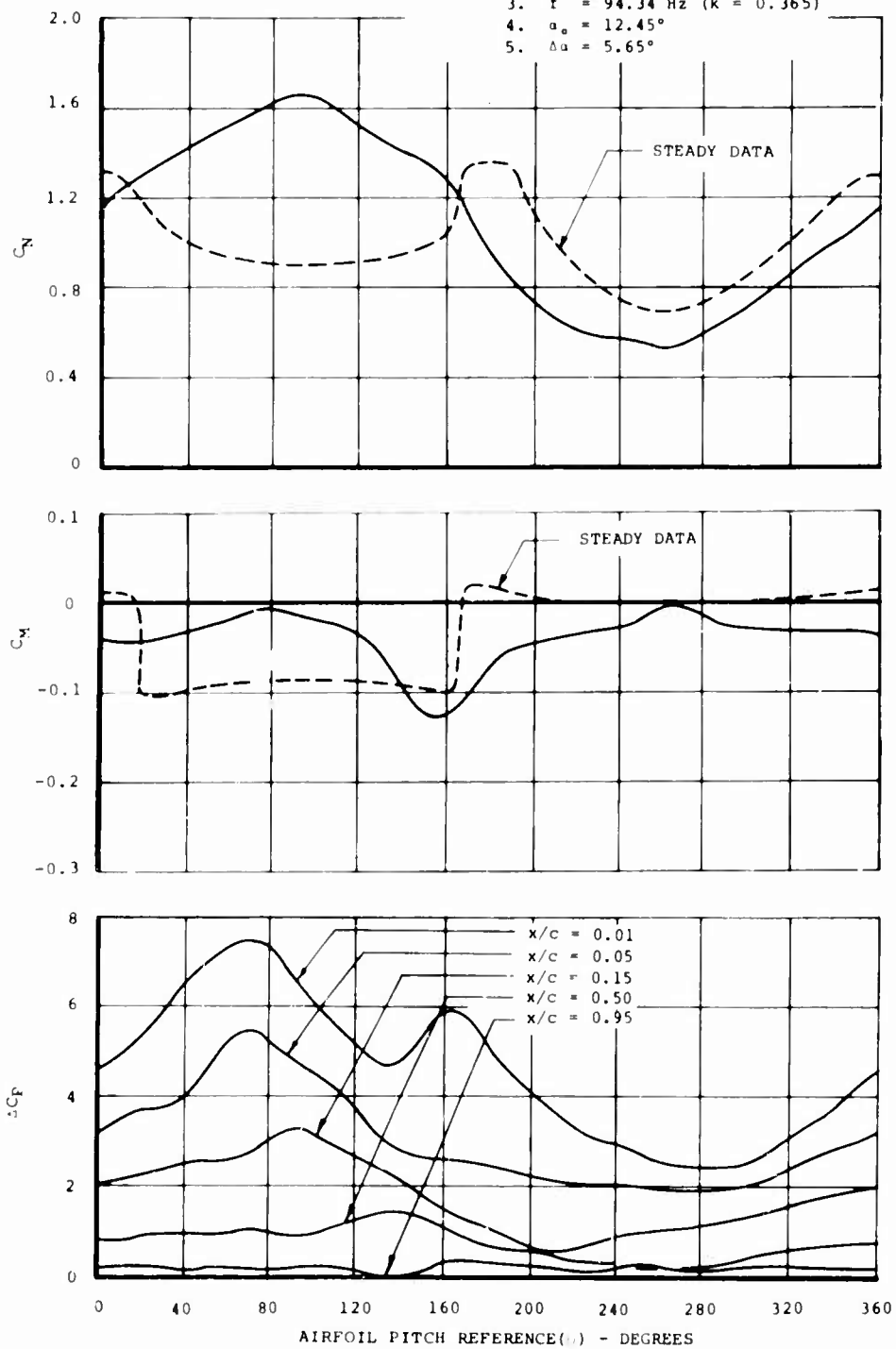f = 96.6 Hertz, and $\alpha_o$ = 15.0°.

83
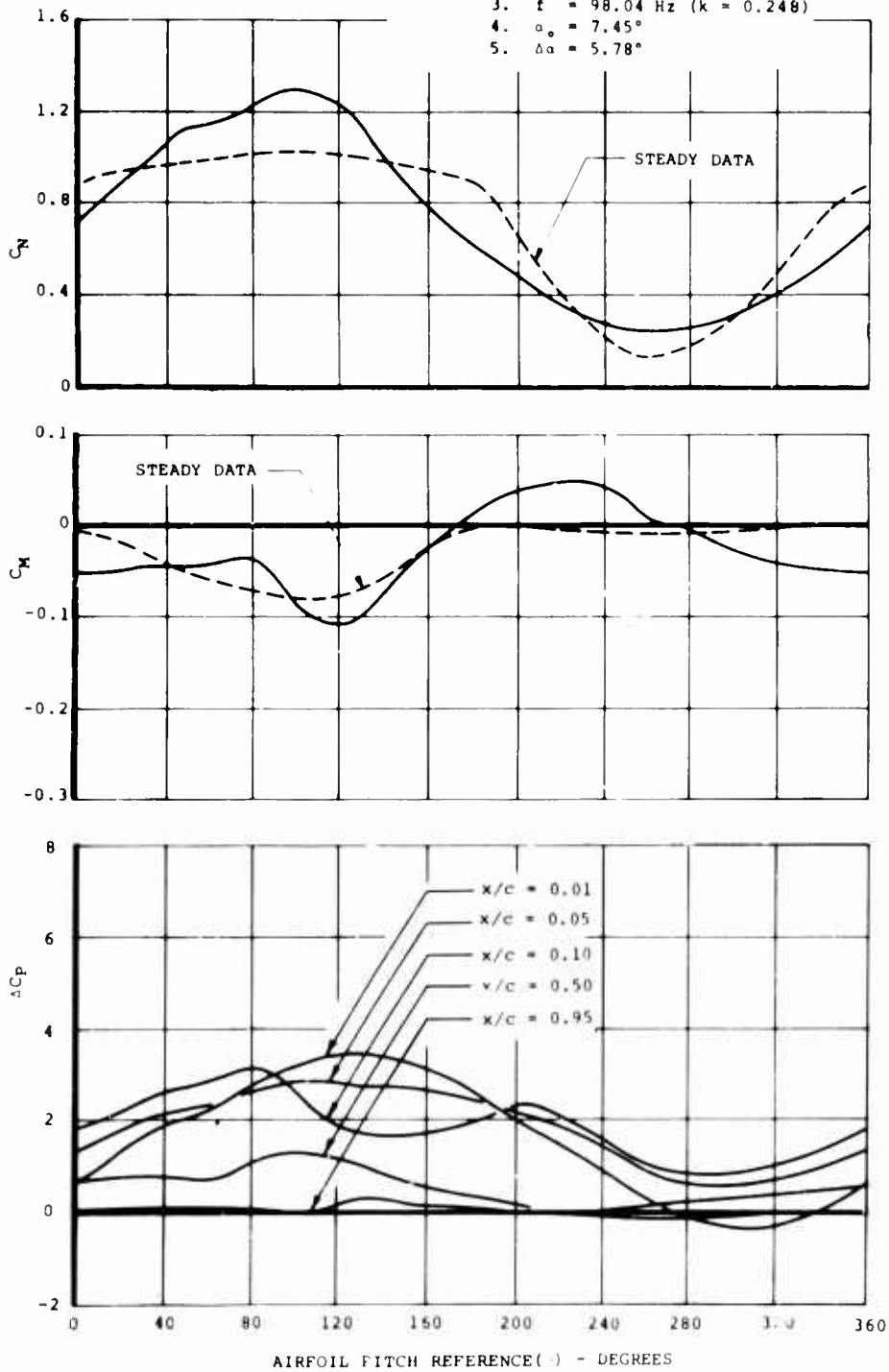
Figure 38. Stall Time History of $C_N$, $C_M$, and $\Delta C_p$ for Vertol 23010-1.58 Airfoil in Pitch at $M = 0.6$, $f = 98.0$ Hertz, and $\alpha_o = 7.5°$.
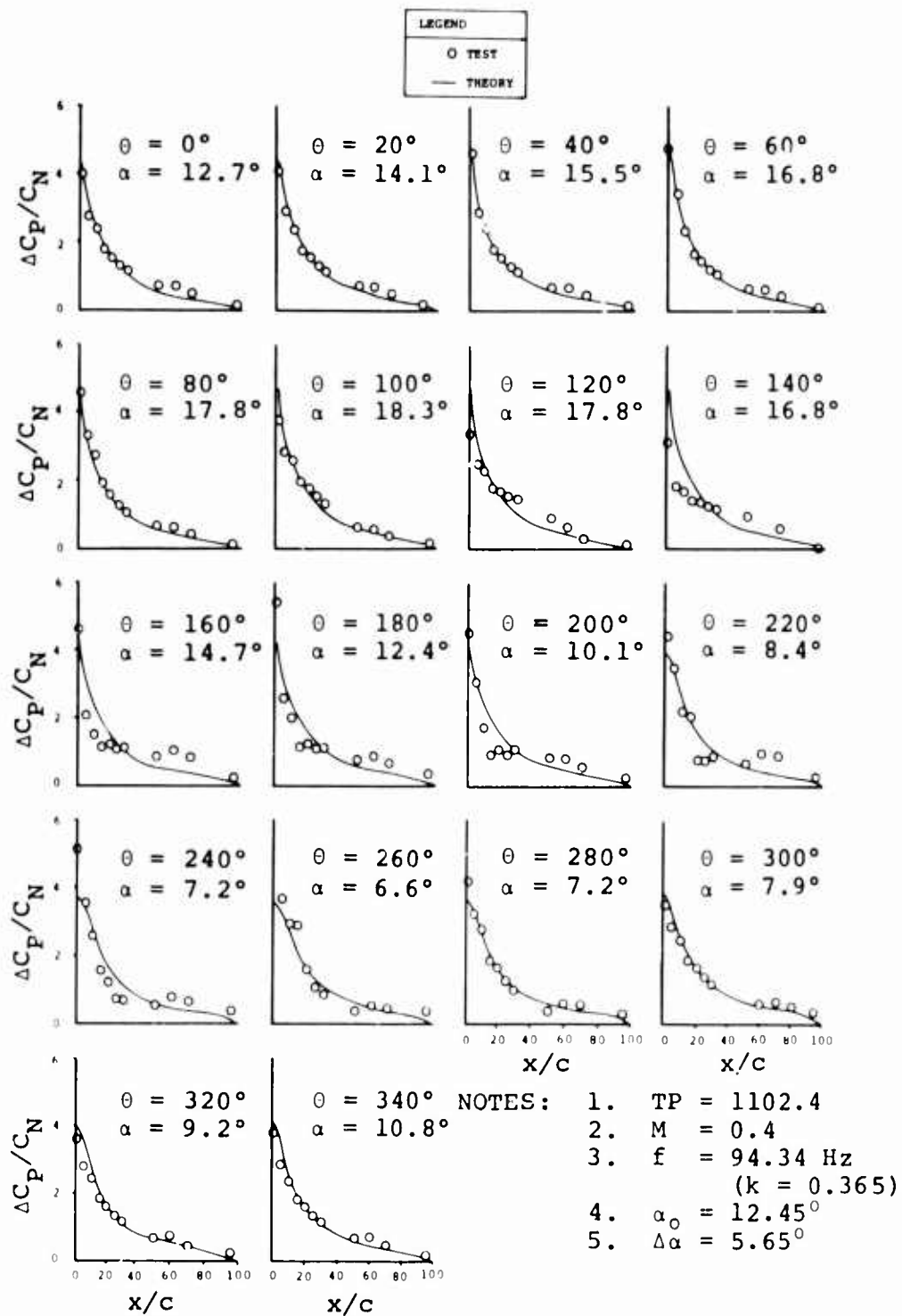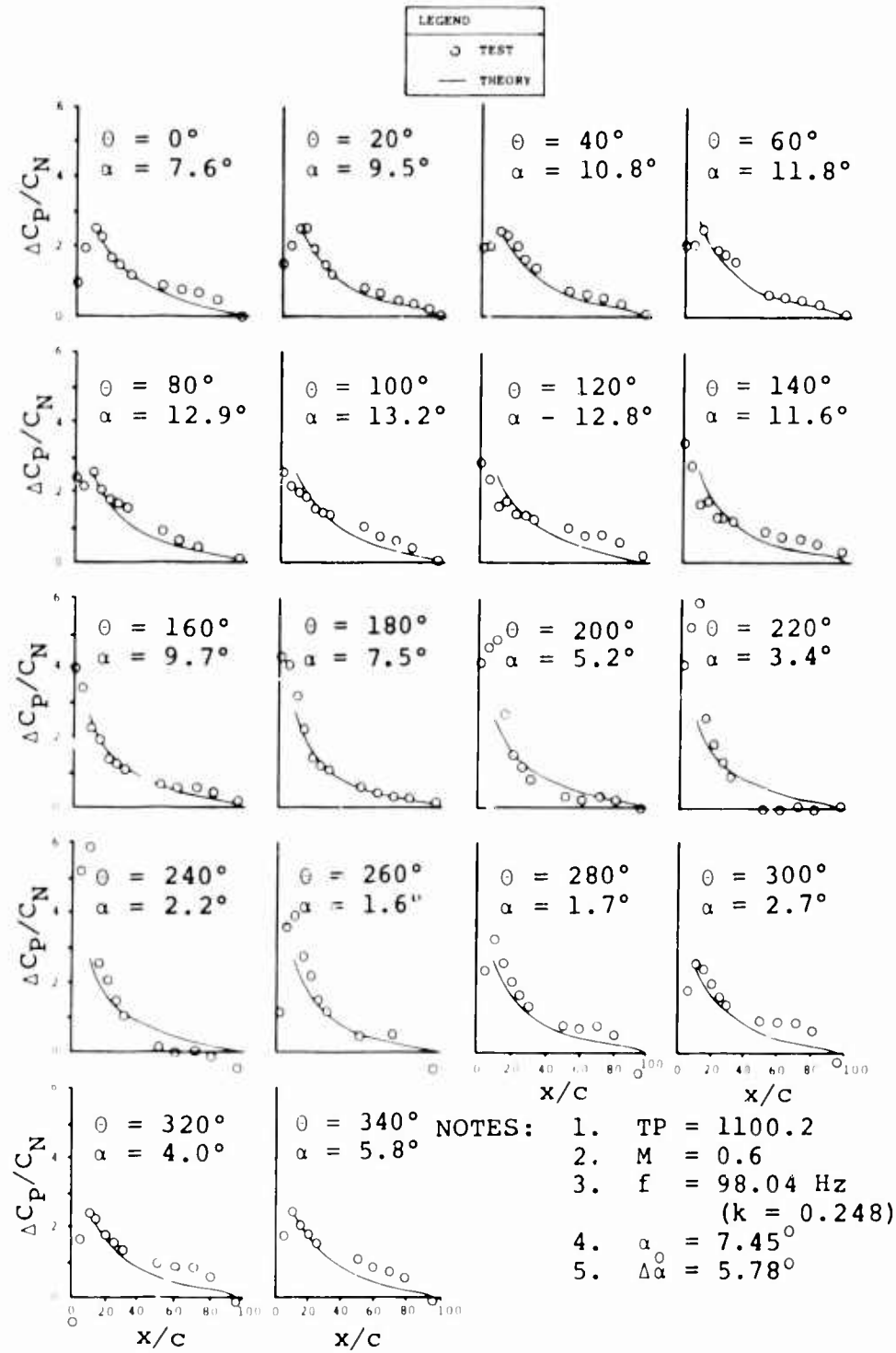
Figure 39.   Stall Time History of Chordwise Pressures for
Vertol 23010-1.58 Airfoil in Pitch at M = 0.6,
f = 98.0 Hertz, and $\alpha_o$ = 7.5°.
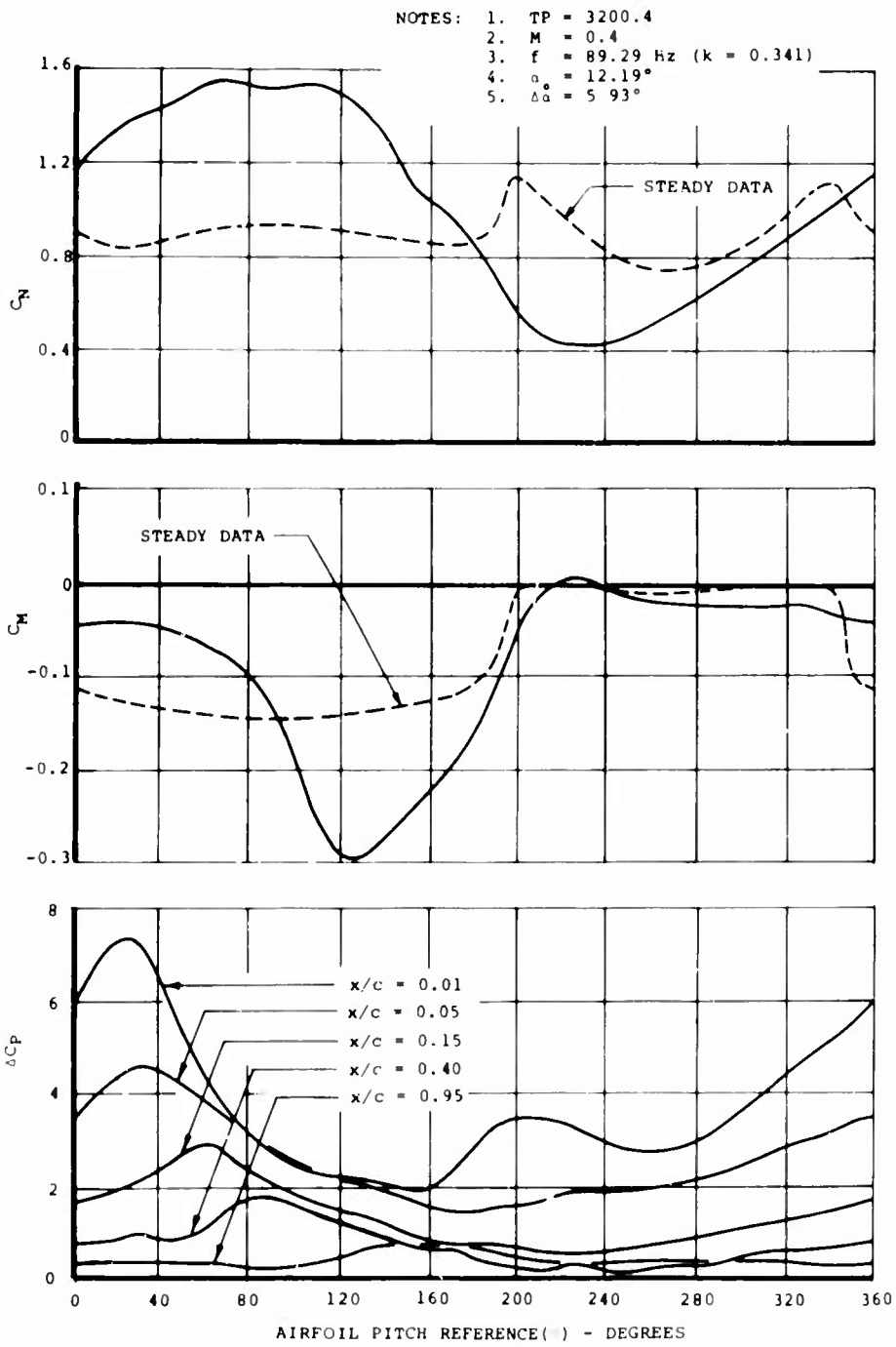
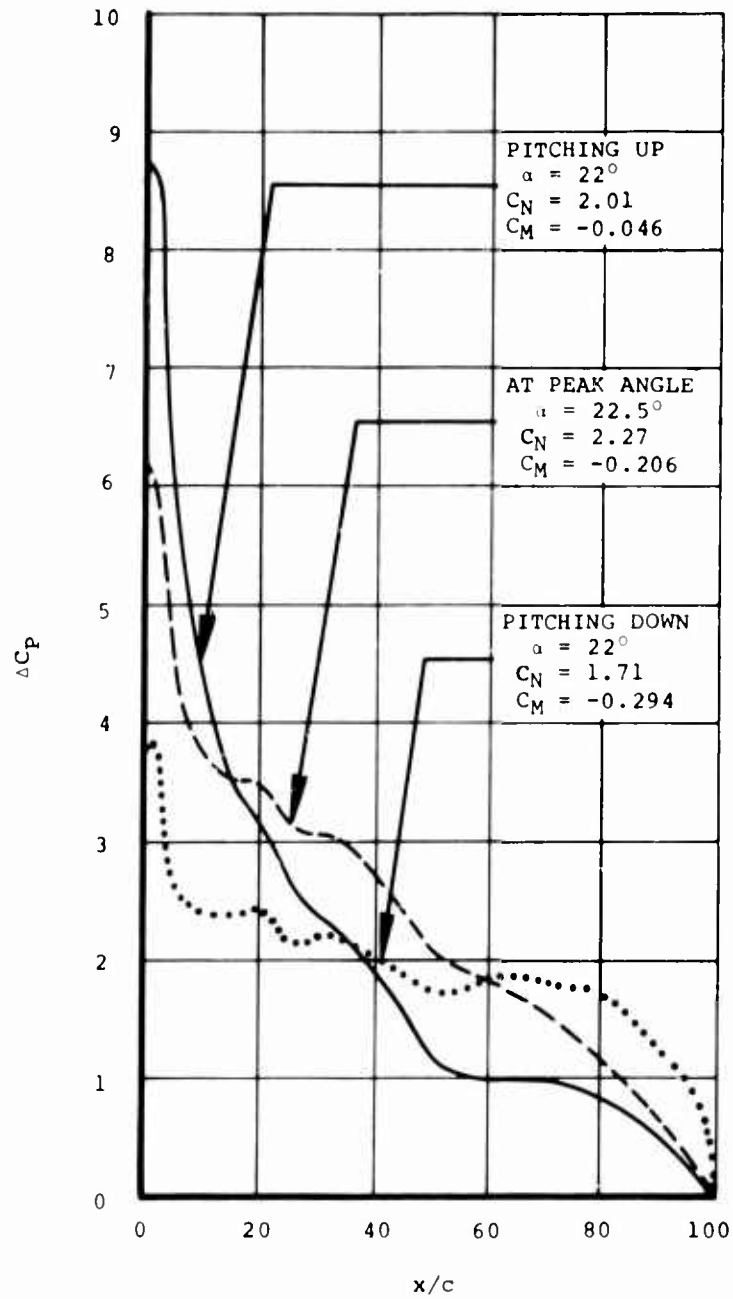Figure 40. Stall Time History of $C_N$, $C_M$, and $\Delta C_p$ for NACA 0012 (Modified) Airfoil in Pitch at $M = 0.4$, $f = 89.3$ Hertz, and $\alpha_o = 12.2°$.
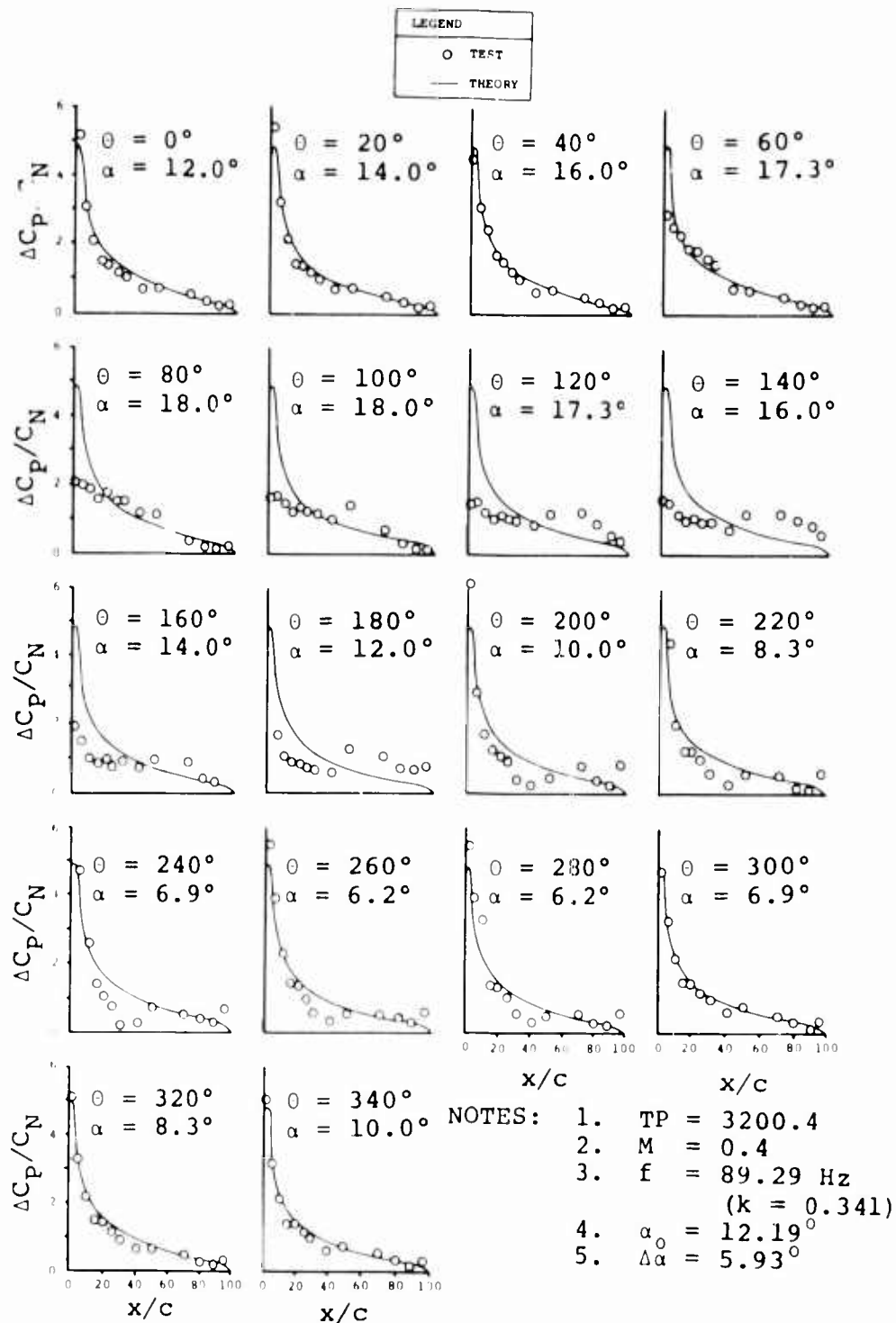
Figure 41. Stall Time History of Chordwise Pressures for NACA 0012 (Modified) Airfoil in Pitch at M = 0.4, f = 89.3 Hertz, and $\alpha_0 = 12$ .

87

NOTES: 1. TP = 4041.1
2. M = 0.4
3. f = 30.12 Hz (k = 0.116)
4. $\alpha_0$ = 12.45°
5. $\Delta$h = 0.47

STEADY DATA

STEADY DATA

x/c = 0.01
x/c = 0.05
x/c = 0.10
x/c = 0.50
x/c = 0.95

AIRFOIL PITCH REFERENCE ( ) - DEGREES
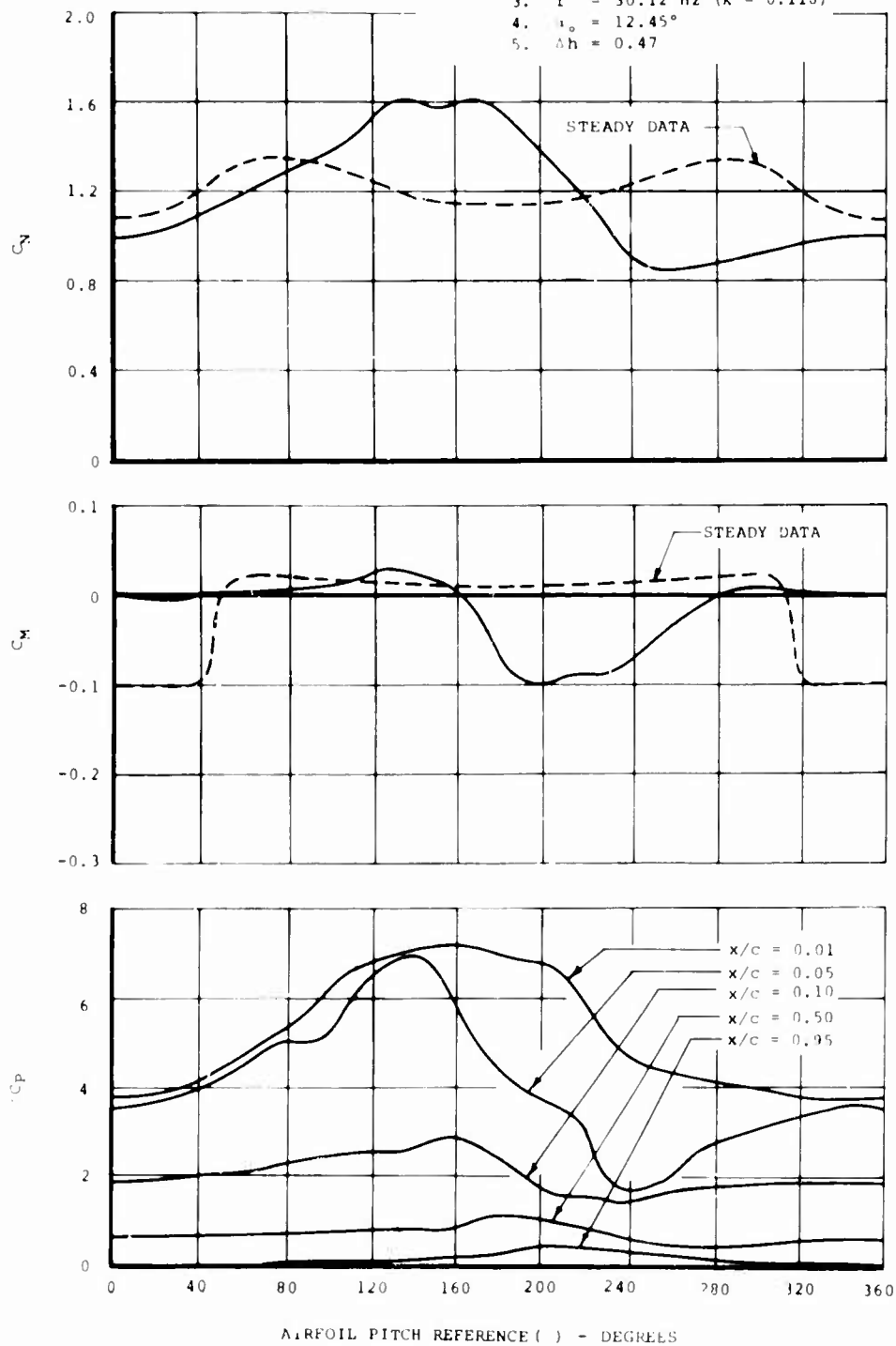
Figure 42.   Stall Time History of $C_N$, $C_M$, and $\Delta C_p$ for
Vertol 23010-1.58 Airfoil in Translation
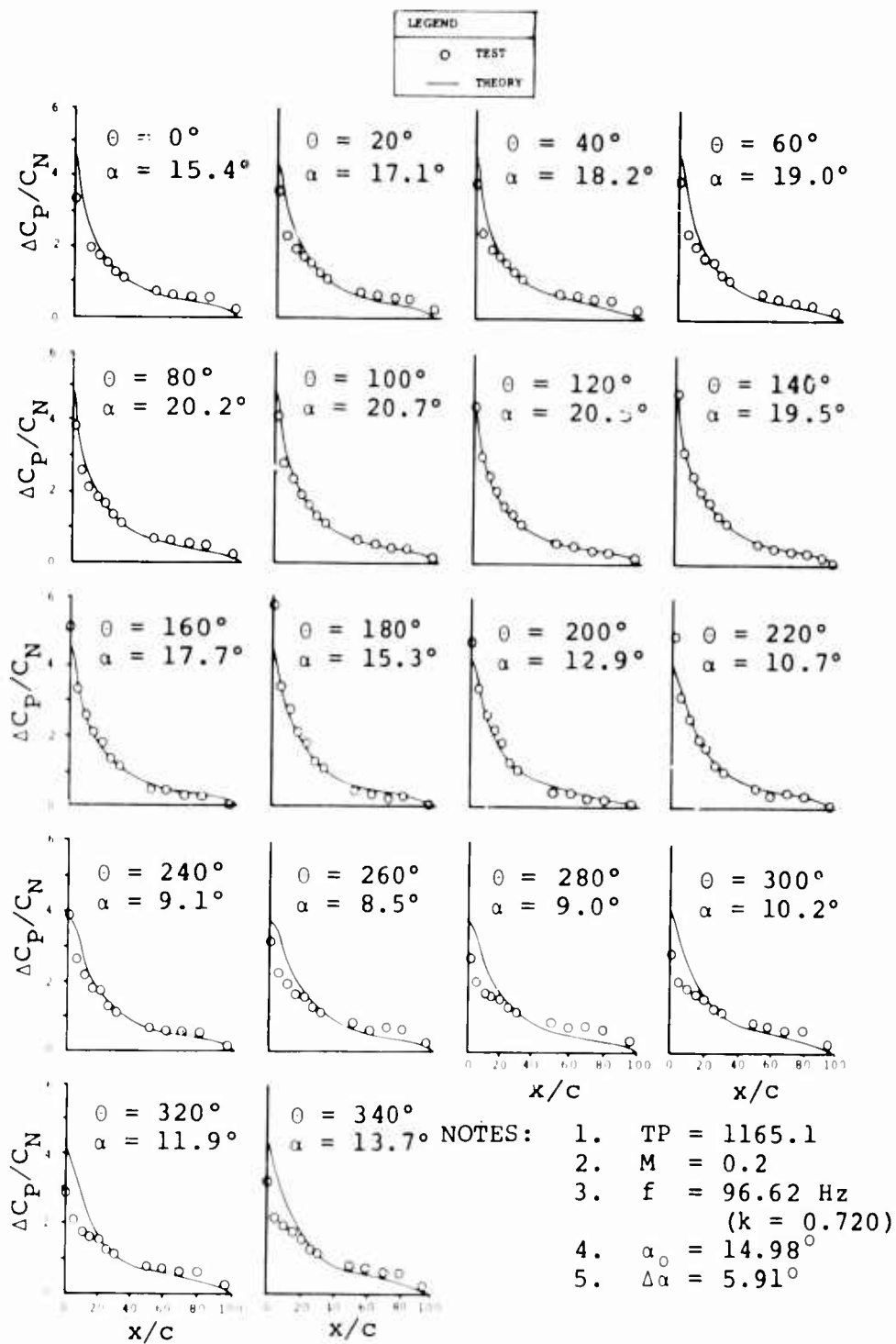at M = 0.4, f = 30.1 Hertz, and $\alpha_o$ = 12.5°.

88
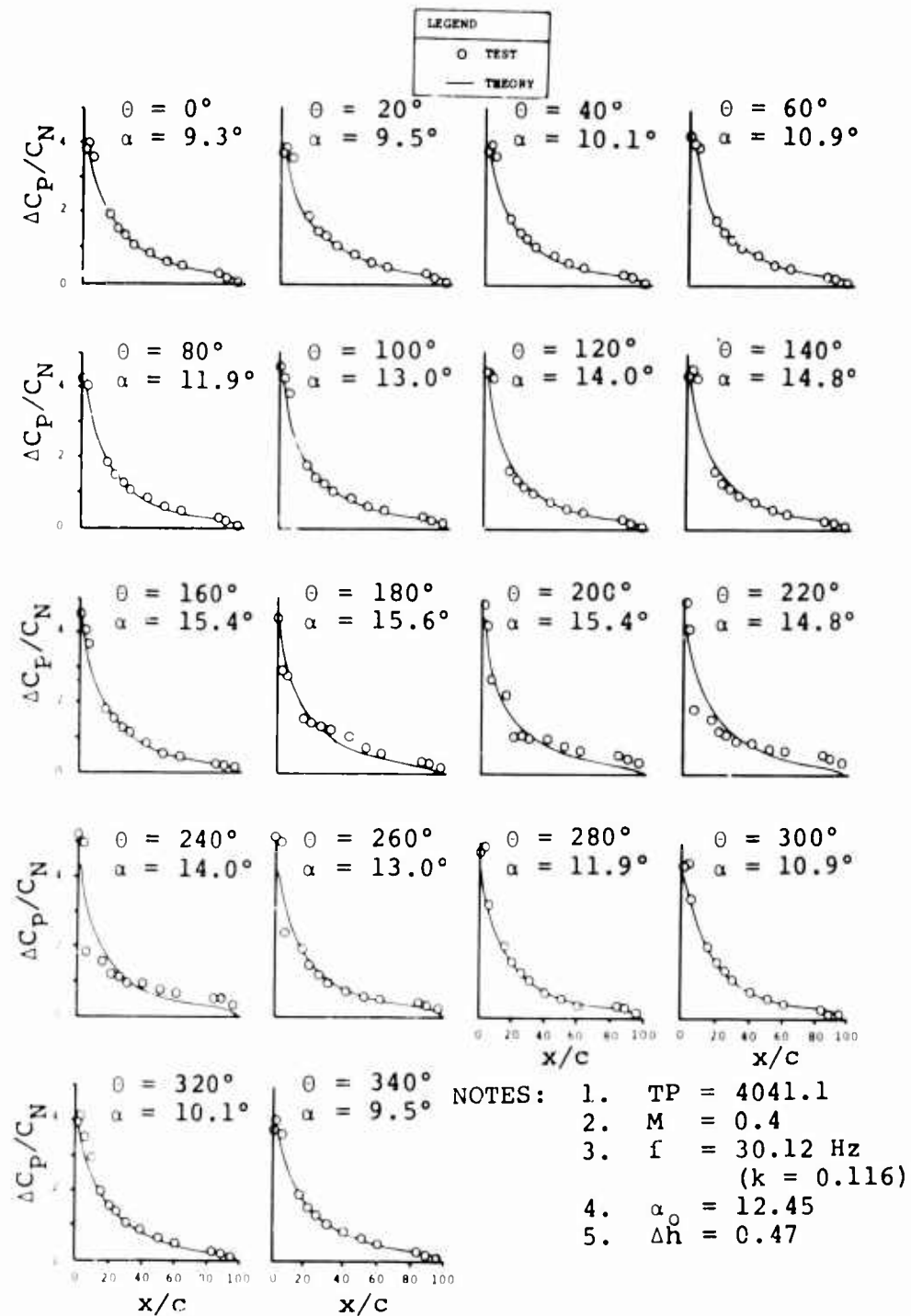
Figure 43.   Stall Time History of Chordwise Pressures for
             Vertol 23010-1.58 Airfoil in Translation at
             $M = 0.4$, $f = 30.1$ Hertz, and $\alpha_o = 12.5°$.

89
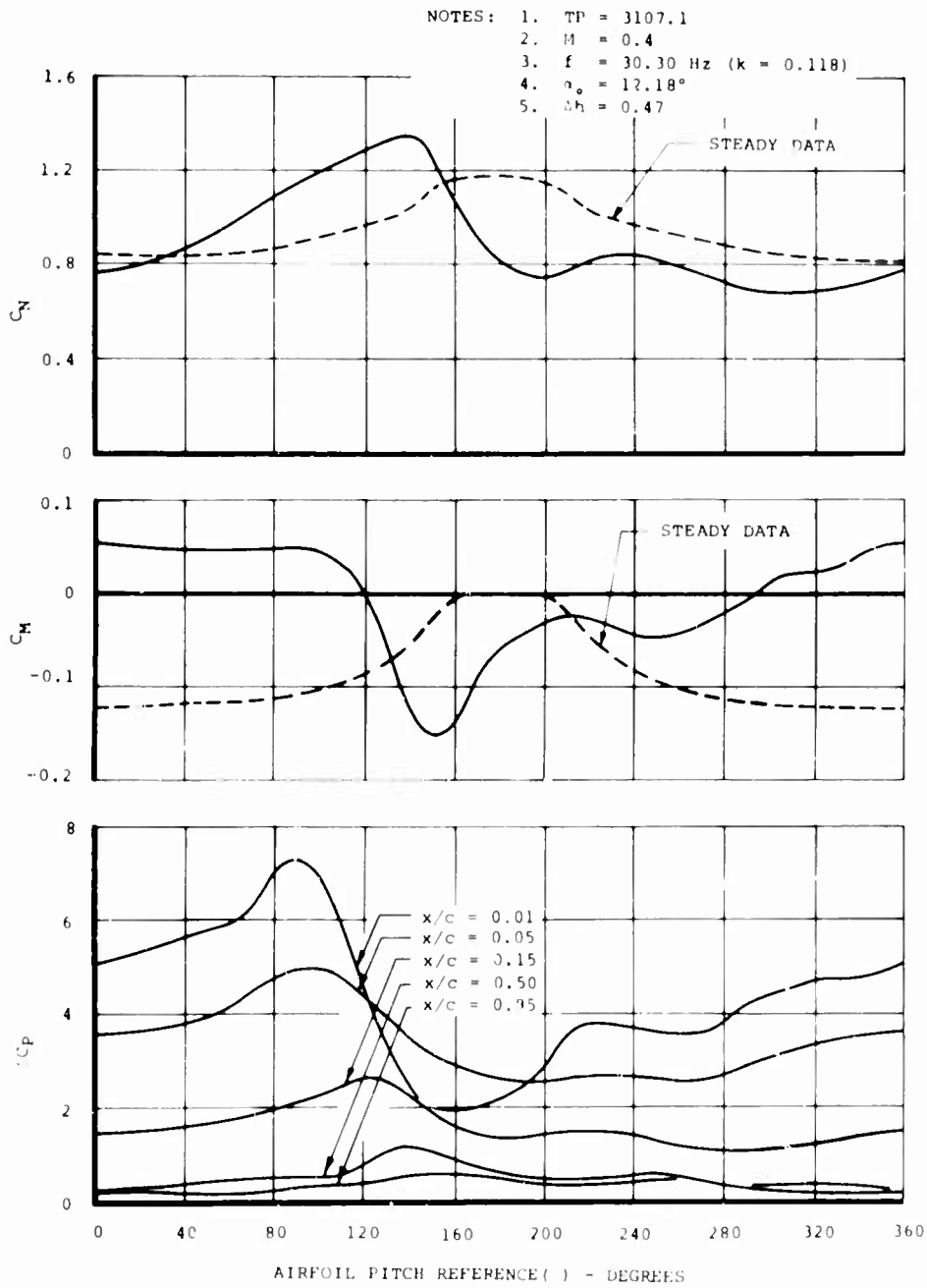
Figure 44. Stall Time History of $C_N$, $C_M$, and $\Delta C_p$ for NACA 0012 (Modified) Airfoil in Translation at M = 0.4, f = 30.3 Hertz, and $\alpha_o$ = 12.2°.
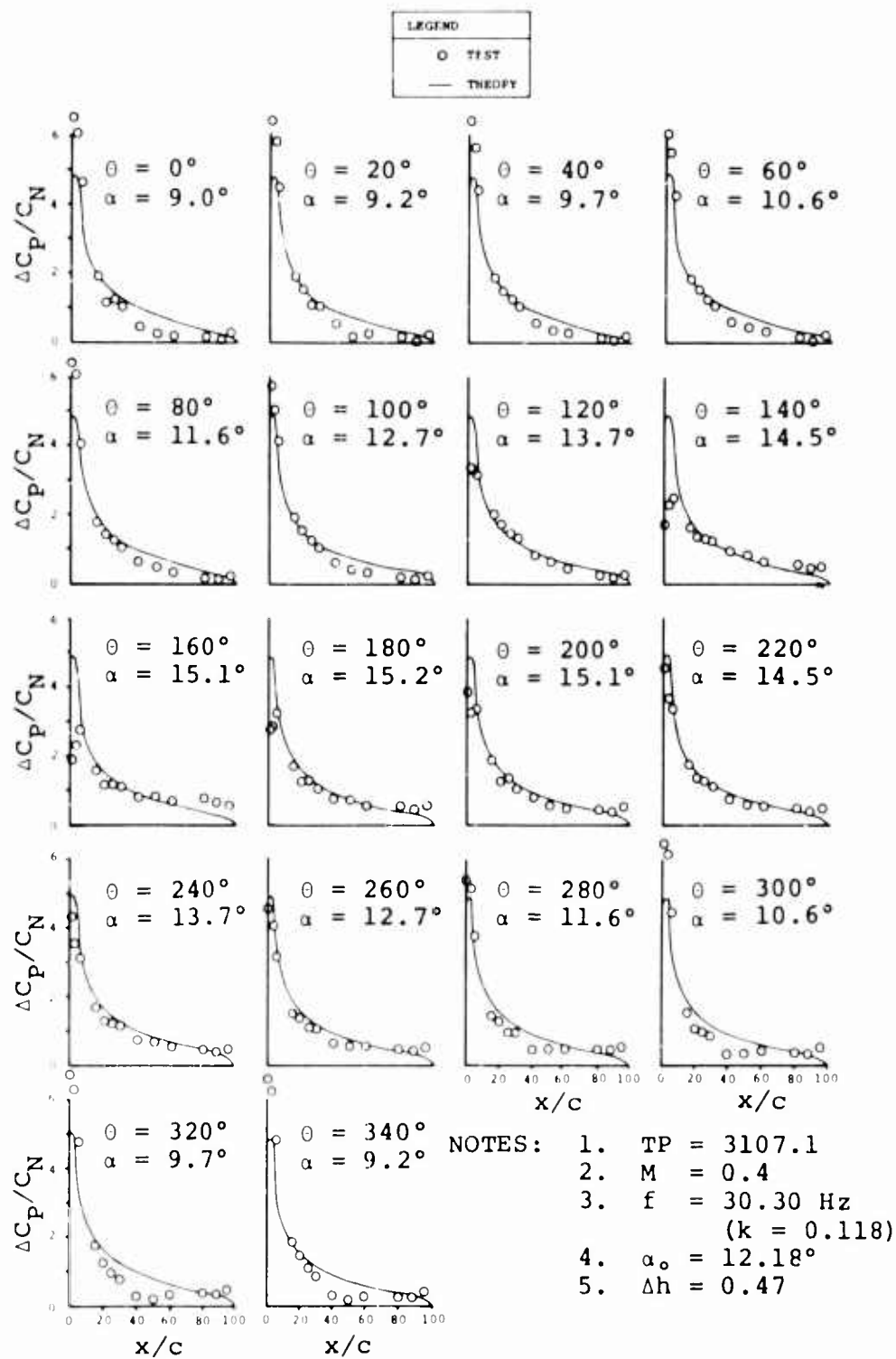
Figure 45. Stall Time History of Chordwise Pressures for
NACA 0012 (Modified) Airfoil in Translation at
M = 0.4, f = 30.3 Hertz, and $\alpha_o$ = 12.2°.
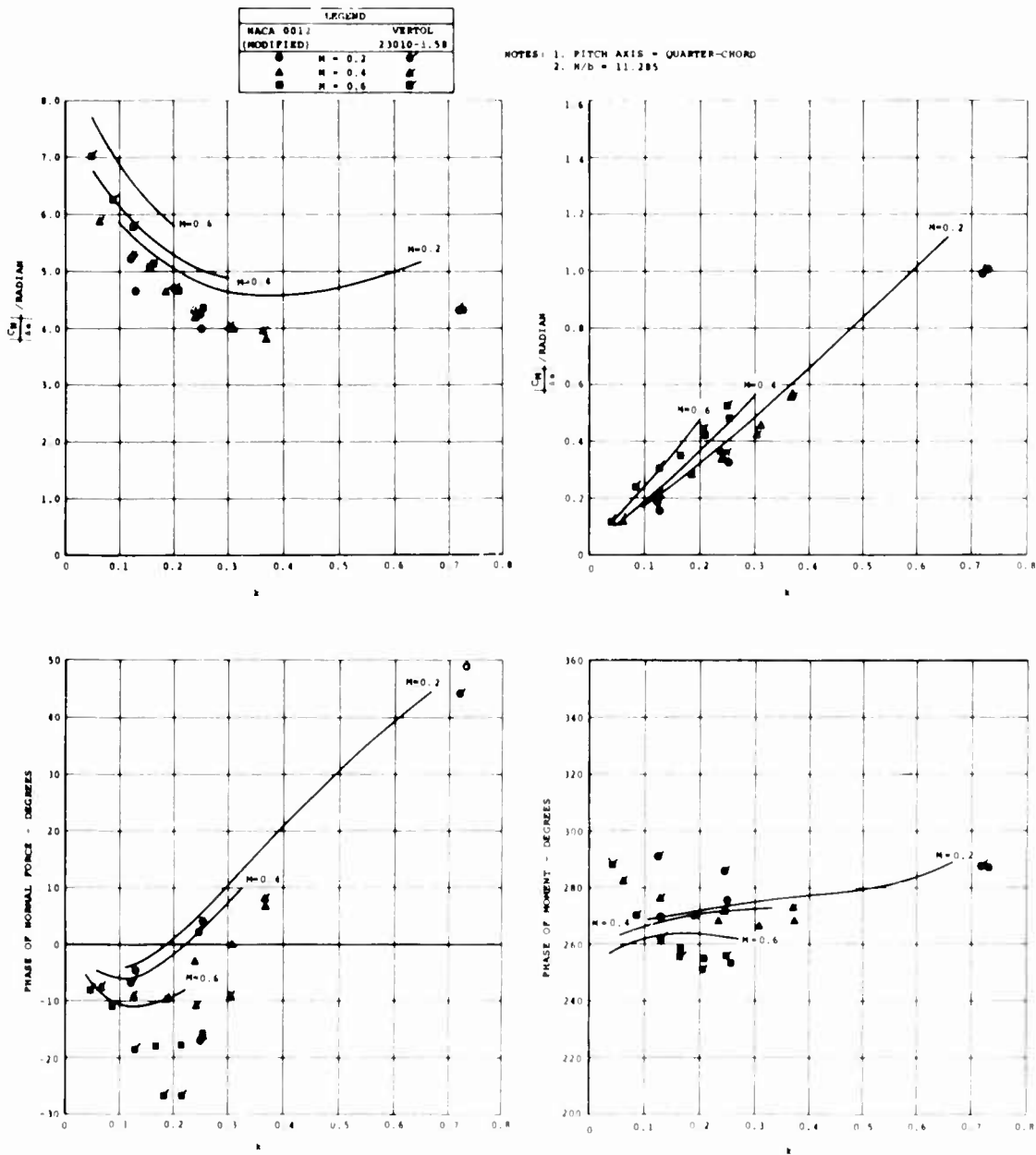
Figure 46.    Comparison of Pitch Oscillation Test Data
With Theory.

92
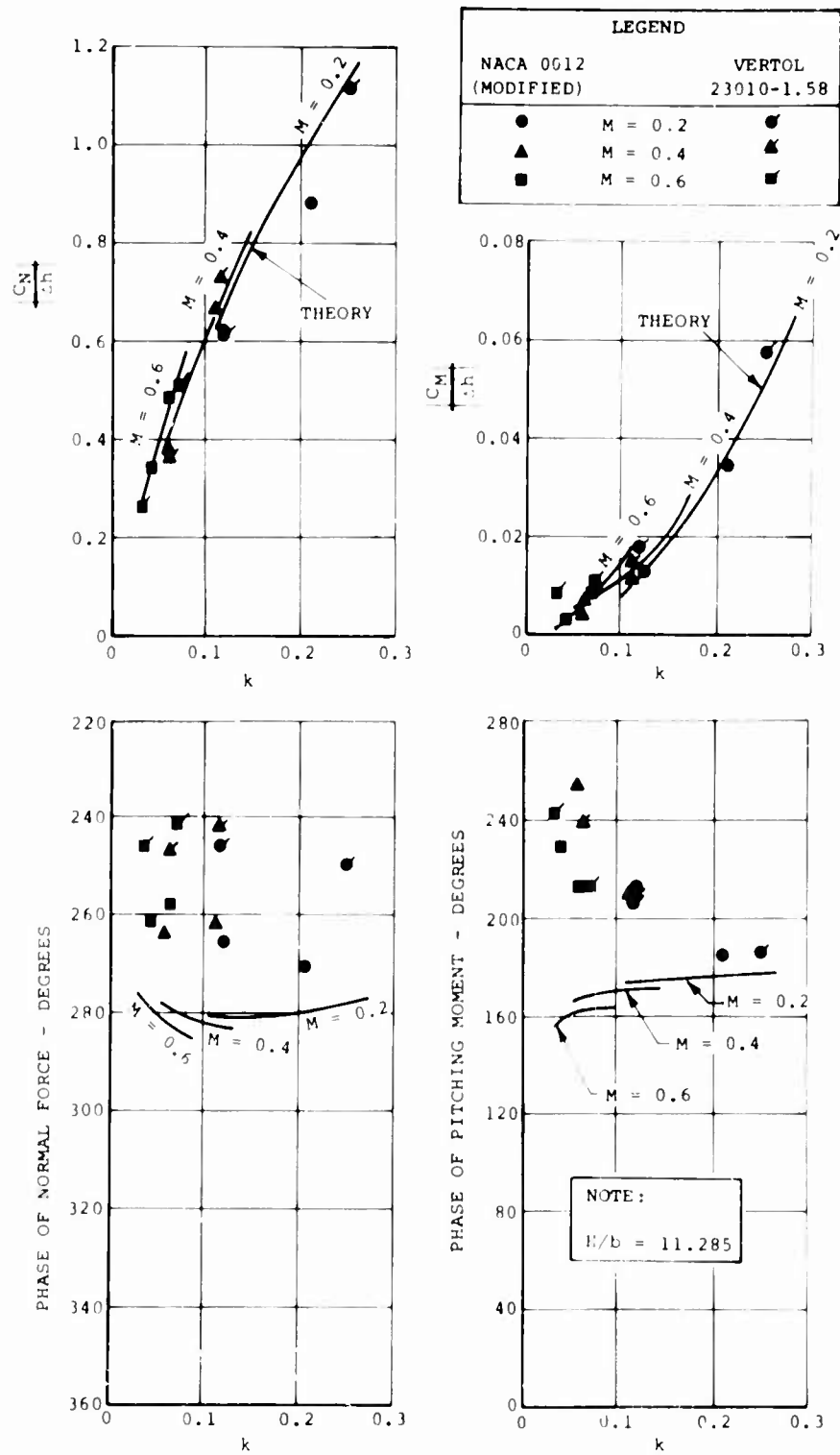
Figure 47.  Comparison of Translation With Theory.
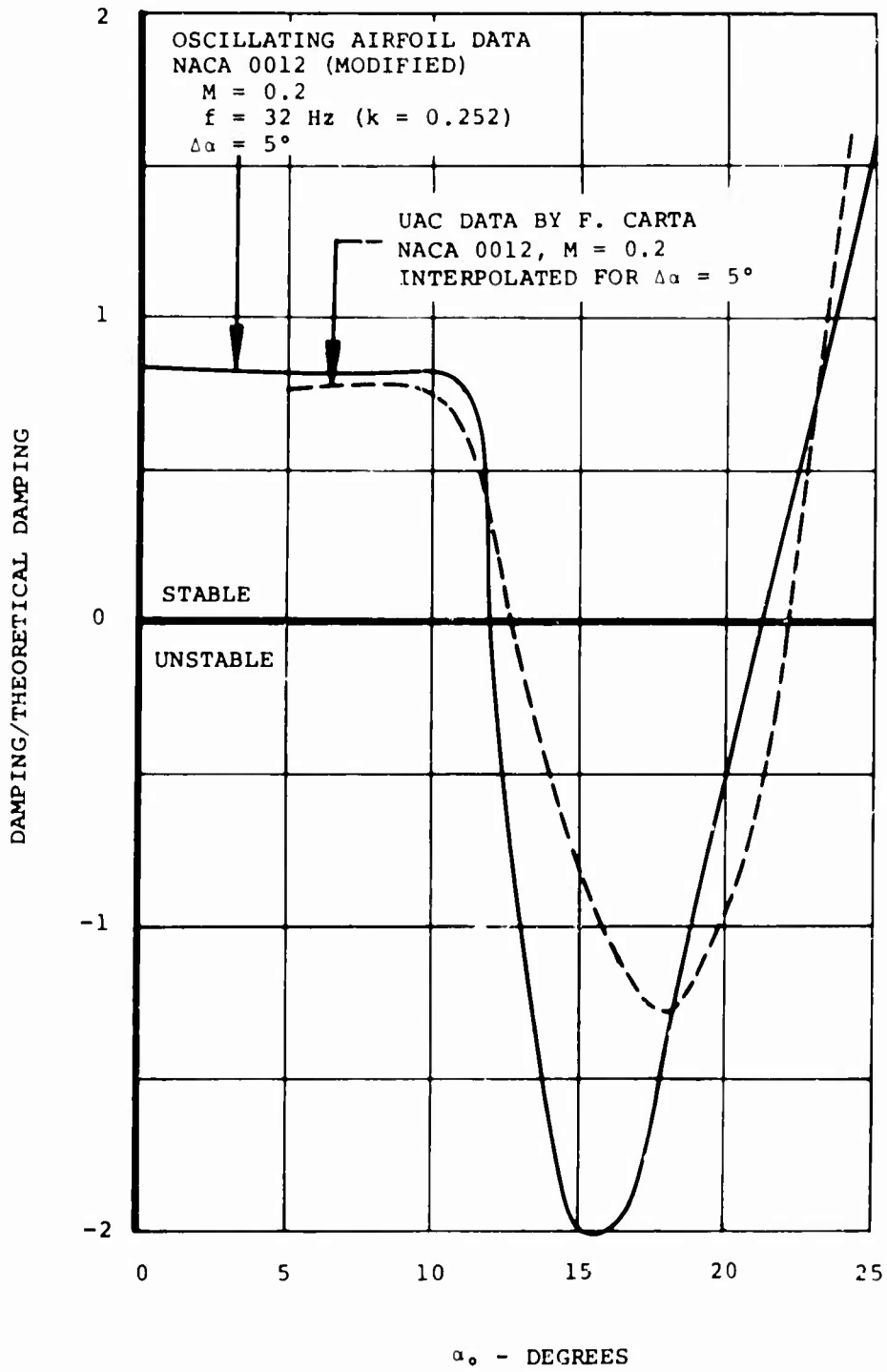
Figure 48.  Comparison of Damping with Data of Reference 4.

94
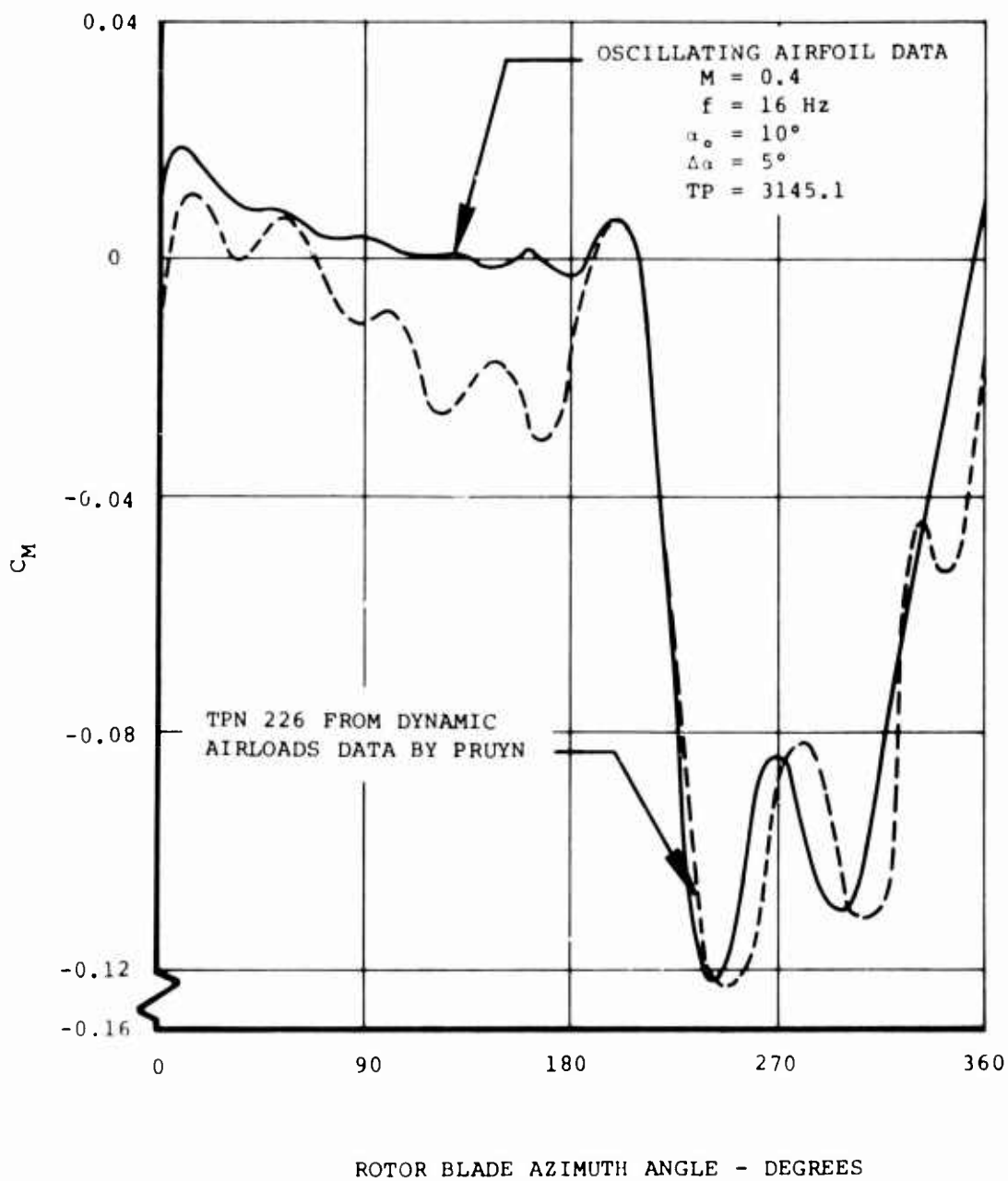
Figure 49.   Comparison of Rotor Flight Test Data
and Wind Tunnel Data.

95
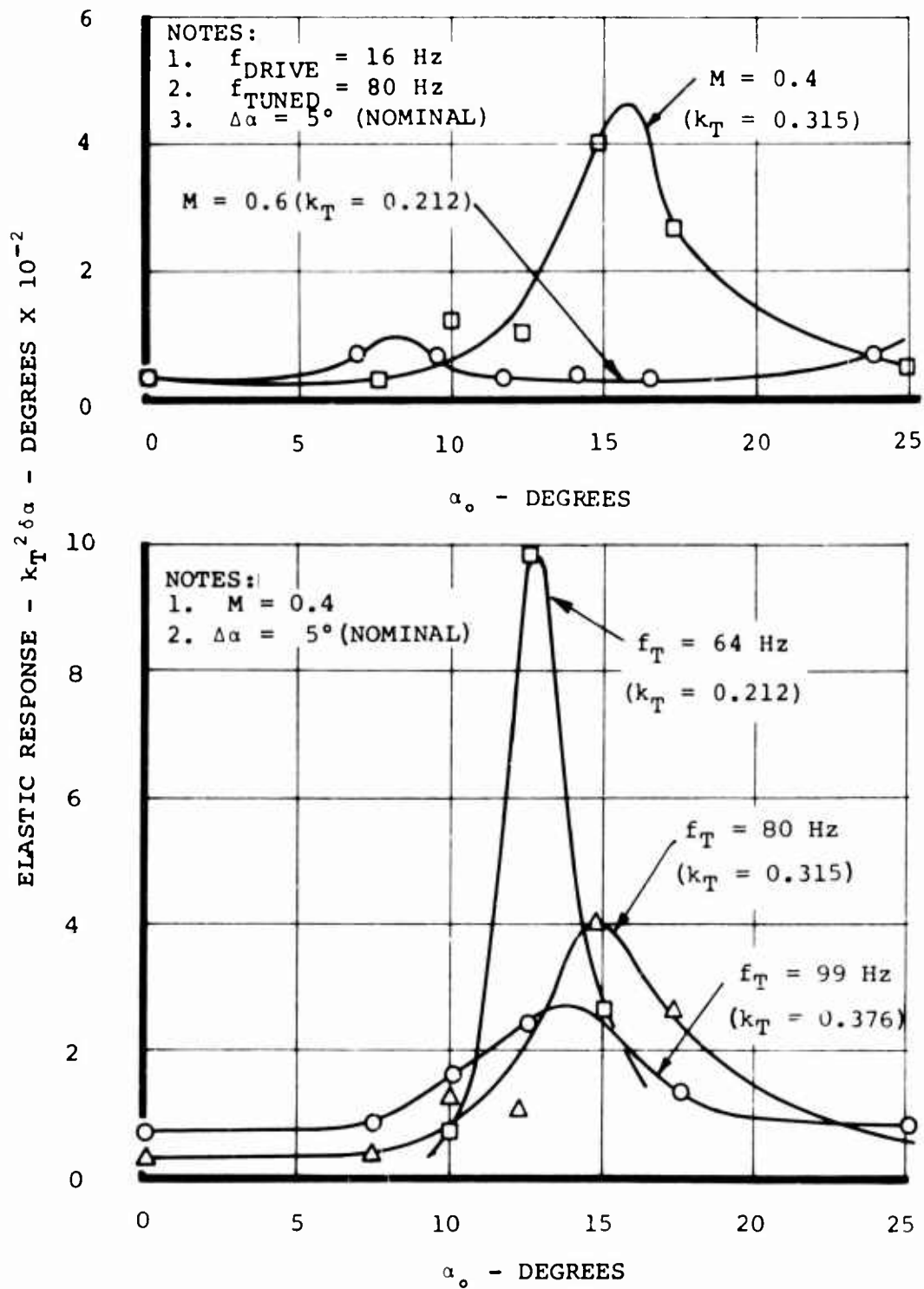
Figure 50. Effect of Mach Number and System Resonant Frequency on Elastic Pitch Response.

96
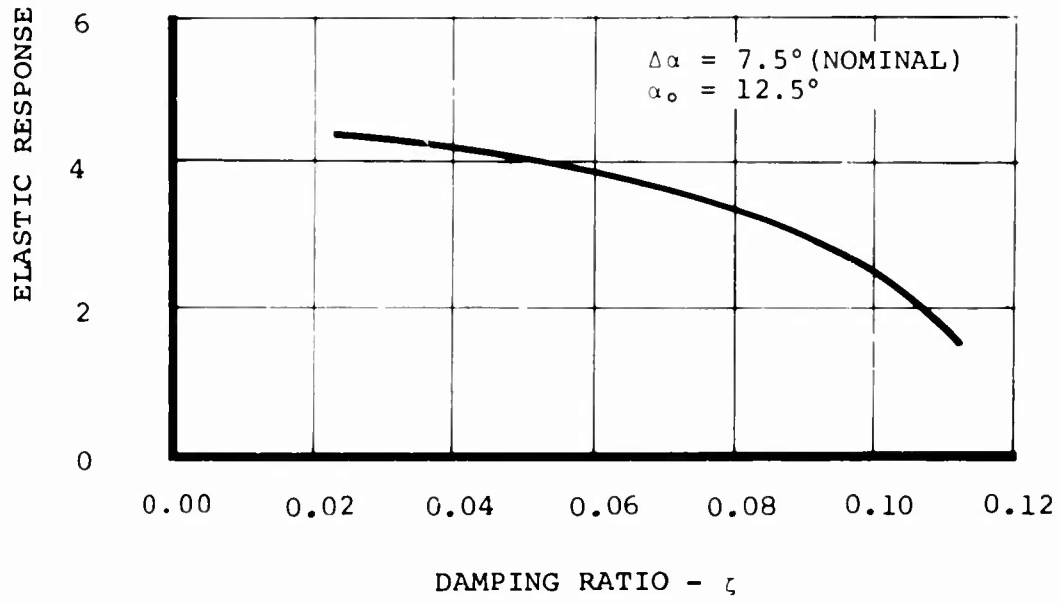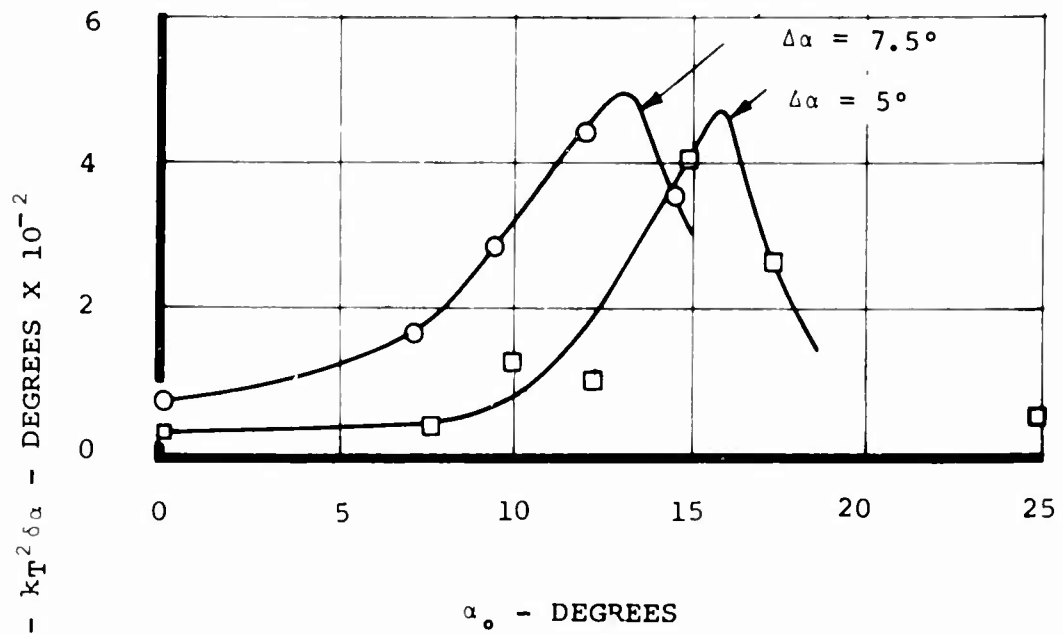
Figure 51.  Effect of Driving Amplitude and External
Damping on Elastic Pitch Response.

97

# LITERATURE CITED

1.  McCloud, John L., III, and McCullough, George B., WIND TUNNEL TEST OF A FULL-SCALE HELICOPTER ROTOR WITH SYMMETRICAL AND WITH CAMBERED BLADE SECTIONS AT ADVANCE RATIOS FROM 0.3 TO 0.4, NACA TN 4367, September 1958.

2.  Harris, Franklin D., and Pruyn, Richard R., BLADE STALL - HALF FACT, HALF FICTION, American Helicopter Society, Inc., 23rd Annual National Forum Proceedings, No. 101, May 1967.

3.  Halfman, Robert C., Johnson, H.C., and Haley, S.M., EVALUATION OF HIGH-ANGLE-OF-ATTACK AERODYNAMIC-DERIVATIVE DATA AND STALL-FLUTTER PREDICTION TECHNIQUES, Massachusetts Institute of Technology, TN 2533, National Advisory Committee for Aeronautics, Washington, D.C., November 1951.

4.  Carta, Franklin O., and Ham, Norman D., AN ANALYSIS OF THE STALL FLUTTER INSTABILITY OF HELICOPTER ROTOR BLADES, American Helicopter Society, Inc., 23rd Annual National Forum Proceedings, No. 130, May 1967.

5.  Carta, Franklin O., THE UNSTEADY NORMAL FORCE RESPONSE OF AN AIRFOIL IN A PERIODICALLY DISTORTED INLET FLOW INCLUDING STALLING EFFECTS, AIAA Paper No. 67-18, AIAA 5th Aerospace Sciences Meeting, New York, January 1967.

6.  Pruyn, Richard R., IN-FLIGHT MEASUREMENT OF ROTOR BLADE AIRLOADS, BENDING MOMENTS, AND MOTIONS, TOGETHER WITH ROTOR SHAFT LOADS AND FUSELAGE VIBRATION, ON A TANDEM ROTOR HELICOPTER, VOLUME III, DATA PROCESSING AND ANALYSIS SYSTEM, The Boeing Company, USAAVLABS Technical Report 67-9C, U.S. Army Aviation Materiel Laboratories, Fort Eustis, Virginia, November 1967.

7.  Rainey, Gerald A., MEASUREMENT OF AERODYNAMIC FORCES FOR VARIOUS MEAN ANGLES OF ATTACK ON AN AIRFOIL OSCILLATING IN PITCH AND ON TWO FINITE-SPAN WINGS OSCILLATING IN BENDING WITH EMPHASIS ON DAMPING IN THE STALL, Langley Aeronautical Laboratory, Technical Note 3643, National Advisory Committee for Aeronautics, Washington, D.C., May 1956.

8.  Riegels, C.E., AEROFOIL SECTIONS, Butterworth Publishing Company, London, England, 1964.

9.   Runyan, Harry L., and Watkins, Charles E., CONSIDERA-
     TIONS ON THE EFFECT OF WIND-TUNNEL WALLS ON OSCILLATING
     AIR FORCES FOR TWO-DIMENSIONAL SUBSONIC COMPRESSIBLE
     FLOW, Langley Aeronautical Laboratory, Technical Note
     2552, National Advisory Committee for Aeronautics,
     Washington, D.C., December 1951.

10.  Pruyn, Richard R., IN-FLIGHT MEASUREMENT OF ROTOR BLADE
     AIRLOADS, BENDING MOMENTS, AND MOTIONS, TOGETHER WITH
     ROTOR SHAFT LOADS AND FUSELAGE VIBRATION, ON A TANDEM
     ROTOR HELICOPTER, VOLUME V, INVESTIGATION  OF BLADE
     STALL CONDITIONS, The Boeing Company, USAAVLABS Technical
     Report 67-9E, U.S. Army Aviation Materiel Laboratories,
     Fort Eustis, Virginia.

11.  Davenport, F.J., A METHOD FOR COMPUTING AIRLOADS ON THIN
     WING SECTIONS EXECUTING ARBITRARY MOTIONS, The Boeing
     Company, D8-0905, October 1967.

12.  Thomas, Eugene, and Tarzanin, Frank, AEROELASTIC ROTOR
     ANALYSIS D94/95, The Boeing Company, D8-0614, May 1967.

13.  Kisielowski, E., GENERALIZED ROTOR PERFORMANCE, The
     Boeing Company, USAAVLABS Technical Report 66-83, U.S.
     Army Aviation Materiel Laboratories, Fort Eustis,
     Virginia, February 1967.

14.  Davenport, F.J., and Front, J.V., AIRFOIL SECTIONS FOR
     ROTOR BLADES - A RECONSIDERATION, American Helicopter
     Society, Inc., 22nd Annual Forum, 12 May 1966.

15.  Bisplinghoff, Raymond L., Ashley, Holt, and Halfman,
     Robert L., AEROELASTICITY, Addison-Wesley Publishing
     Company, Inc., Reading, Massachusetts, 1955.

16.  Runyan, Harry L., Woolston, Donald S., and Rainey, A.
     Gerald, THEORETICAL AND EXPERIMENTAL INVESTIGATION OF
     THE EFFECT OF TUNNEL WALLS ON THE FORCES ON AN OSCIL-
     LATING AIRFOIL IN TWO-DIMENSIONAL SUBSONIC COMPRESSIBLE
     FLOW, Langley Aeronautical Laboratory, TN 3416, National
     Advisory Committee for Aeronautics, Washington, D.C.,
     June 1955.

17.  MANUAL ON AEROELASTICITY, PART IV, North Atlantic Treaty
     Organization Advisory Group for Aeronautical Research
     and Development, NASA N63-17815, August 1965.

## SELECTED BIBLIOGRAPHY

Acum, W.E.A., THE COMPARISON OF THEORY AND EXPERIMENT FOR OS-
CILLATING WINGS, NPL Aeronautical Report 1005, March 1962,
AD288603.

Acum, W.E.A., and Garner, H.C., THE ESTIMATION OF OSCILLATORY
WING AND CONTROL DERIVATIVES, North Atlantic Treaty Organiza-
tion Advisory Group for Aeronautical Research and Development,
April 1961, AD275409.

Acum, W.E.A., THEORY OF LIFTING SURFACES OSCILLATING AT
GENERAL FREQUENCIES IN A STREAM OF HIGH SUBSONIC MACH NUMBER,
Aeronautical Research Council 17824, 1956.

Acum, W.E.A., WALL CORRECTIONS FOR WINGS OSCILLATING IN WIND
TUNNELS OF CLOSED RECTANGULAR SECTION, Aeronautical Research
Council R&M No. 3312, January 1958.

Allis, A.E., and Swihart, J.M., THE EFFECT OF BLADE-SECTION
CAMBER ON THE STALL FLUTTER CHARACTERISTICS OF THREE NACA
PROPELLERS AT ZERO ADVANCE, NACA RM L53B17, 1953.

Baker, J.E., and Brooks, G.W., AN EXPERIMENTAL INVESTIGATION
OF THE EFFECTS OF VARIOUS PARAMETERS INCLUDING TIP MACH NO.
IN THE FLUTTER OF SOME MODEL HELICOPTER ROTOR BLADES, NACA
TN 4005, 1958.

Barron, M., and George, T., A THEORETICAL APPROACH TO STALL
FLUTTER, Cornell Graduate School of Engineering, ASTIA,
August 1953, AD2115.

Beckman, P.A., and Martin, R.J., MEASUREMENTS OF OSCILLATORY
AERODYNAMIC INFLUENCE COEFFICIENTS, Stewart-Warner Corporation,
February 1957, AD135045.

Bergh, H., A NEW METHOD FOR MEASURING THE PRESSURE DISTRIBUTION
ON HARMONICALLY OSCILLATING WINGS OF ARBITRARY PLANFORM, ICAS
Paper 64-576, December 1964.

Biot and Boehnlein, AERODYNAMIC THEORY OF OSCILLATING WINGS
OF FINITE SPAN, Report No. 5, Guggenheim Aeronautical Labora-
tories, California Institute of Technology, October 1963.

Bollay, W., and Brown, C.D., SOME EXPERIMENTAL RESULTS ON WING
FLUTTER, Journal of the Aeronautical Sciences, No. 8, 1941.

Bratt, J.B., and Chinneck, A., MEASUREMENTS OF MID-CHORD
PITCHING MOMENT DERIVATIVES AT HIGH SPEEDS, Aeronautical
Research Council R&M 2680, 1947.

Bratt, J.B., Rayner, W.G., and Wight, K.D., MEASUREMENTS OF
THE DIRECT PITCHING MOMENT DERIVATIVES FOR TWO-DIMENSIONAL
FLOW AT SUBSONIC AND SUPERSONIC SPEEDS, AND FOR A WING OF
ASPECT RATIO 4 AT SUBSONIC SPEEDS, Aeronautical Research
Council 20, 714, 21 January 1959.

Bratt, J.B., and Scruton, C., MEASUREMENTS OF PITCHING MOMENT
DERIVATIVES FOR AN AIRFOIL OSCILLATION ABOUT THE HALF CHORD
AXIS, Aeronautical Research Council R&M 1921, November 1938.

Bratt, J.B., Wight, K.C., and Chinneck, A., FREE OSCILLATIONS
OF AN AEROFOIL ABOUT THE HALF-CHORD AXIS AT HIGH INCIDENCES
AND PITCHING MOMENT DERIVATIVES FOR DECAYING OSCILLATIONS,
Aeronautical Research Council R&M 2214, 1940.

Bratt, J.B., and Wight, K.C., THE EFFECT OF MEAN INCIDENCE,
AMPLITUDE OF OSCILLATION, PROFILE AND ASPECT RATIO ON PITCHING
MOMENT DERIVATIVES, Aeronautical Research Council R&M 2064,
June 1945.

Brown, R.H., and Sterne, L.H.G., THE ELIMINATION OF FLUTTER
FROM A PROPELLER, Aeronautical Research Council R&M 2047,
1943.

Buchan, A.L., Harris, K.D., and Somervail, P.M., THE MEASURE-
MENT OF THE DERIVATIVE ZW FOR AN OSCILLATING AEROFOIL,
Aeronautical Research Council C.P.52, June 1950.

Carpenter, P.J., and Jewel, J.W., Jr., A PRELIMINARY INVESTI-
GATION OF THE EFFECTS OF GUSTY AIR ON HELICOPTER BLADE BENDING
MOMENTS, NACA TN 3074, 1954.

Carpenter, P.J., and Powell, R.D., Jr., LOW TIP MACH NO. STALL
CHARACTERISTICS AND HIGH TIP MACH NO. COMPRESSIBILITY EFFECT
ON A HELICOPTER ROTOR WITH A NACA 0009 TIP AIRFOIL SECTION,
NACA TN 4355, 1958.

Clevenson, S.A., and Widmayer, E., EXPERIMENTAL MEASUREMENTS OF
FORCES AND MOMENTS ON A TWO-DIMENSIONAL OSCILLATING WING AT
SUBSONIC SPEEDS, NACA TN 3686, 1956.

Coleman, R.P., DAMPING FORMULAS AND EXPERIMENTAL VALUES OF
DAMPING IN FLUTTER MODELS, NACA TN 751, 1940.

Crim, A.D., and Gessow, L., A METHOD FOR STUDYING THE TRANSIENT
BLADE-FLAPPING BEHAVIOR OF LIFTING ROTORS AT EXTREME OPERATING
CONDITIONS, NACA TN 3366, November 1954.

Cunningham, H.J., ANALYSIS OF PURE-BENDING FLUTTER OF A
CANTILEVER SWEPT WING AND ITS RELATION TO BENDING-TORSION
FLUTTER, NACA TN 2461, September 1951.

101

Cunningham, Runyar, and Watkins, THEORETICAL INVESTIGATIONS OF SEVERAL TYPES OF SINGLE-DEGREE-OF-FREEDOM FLUTTER, Journal of the Aeronautical Sciences, No. 19, 1952.

Daughaday, H., DuWaldt, F., and Gates, C., INVESTIGATION OF HELICOPTER BLADE FLUTTER AND LOAD AMPLIFICATION PROBLEMS, Cornell Aeronautical Laboratory Report No. SB-862-S-4, August 1956, Journal of the American Helicopter Society, Vol. 2, No. 3, July 1957.

DeJager, THE AERODYNAMIC FORCES AND MOMENTS ON AN OSCILLATING AEROFOIL WITH CONTROL SURFACE BETWEEN TWO PARALLEL WALLS, Report F-140, Netherlands National Aero and Astronautical Research Institute, 1953.

Dietz, F., THE AIR FORCES OF THE HARMONICALLY VIBRATING WING IN COMPRESSIBLE MEDIUM AT SUBSONIC VELOCITY (PLANE PROBLEM), AAF, Air Mat. Com., Wright Field, Technical Intelligence Trans F-TS-506-RE, November 1946.

Drischer, H., MODERN UNSTEADY AEROFOIL THEORY, Translation Available as British Aeronautical Research Council Paper 11843, 1948.

Garner, H.C., MULTHOPP'S SUBSONIC LIFTING SURFACE THEORY OF WINGS IN SLOW PITCHING OSCILLATIONS, Aeronautical Research Council R&M 2885, 1952.

Greidanus, J.H., van de Vooren, A.I., and Bergh, H., EXPERIMENTAL DETERMINATIONS OF THE AERODYNAMIC COEFFICIENTS OF AN OSCILLATING WING IN INCOMPRESSIBLE TWO-DIMENSIONAL FLOW, Parts I, II, III, and IV, Reports F. 101, F. 102, F. 103, and F. 104, Netherlands National Aero and Astronautical Research Institute, 1952.

Guyett, P.R., and Curran, J.K., AERODYNAMIC DERIVATIVE MEASUREMENTS ON A RECTANGULAR WING OF ASPECT RATIO 3.3, Aeronautical Research Council R&M 3171, 1958.

Haley, S.M., Halfman, R.L., and Johnson, H.C., EVALUATION OF HIGH ANGLES OF ATTACK, AERODYNAMIC DERIVATIVE DATA AND STALL FLUTTER PREDICTION TECHNIQUES, NACA TN 2533, 1951.

Halfman, Robert L., EXPERIMENTAL AERODYNAMIC DERIVATIVES OF A SINUSOIDALLY OSCILLATING AIRFOIL IN TWO-DIMENSIONAL FLOW, Massachusetts Institute of Technology, NACA Report 1108 (Formerly NACA TN 2465), November 1951.

Jones, J., THE INFLUENCE OF THE WAKE ON THE FLUTTER AND VIBRATION OF ROTOR BLADES, British Aeronautical Research Council Report No. 18, January 1956.

102

Jones, J.P., DETERMINATION OF THE FORCES MOMENTS ON AN AIRFOIL OSCILLATING THROUGH THE STALL, University of Southampton Annual Technical Report No. 1, A.A.S.U. 252, January 1964, AD447110.

Jones, W.P., AEROFOIL OSCILLATIONS AT HIGH MEAN INCIDENCES, Aeronautical Research Council R&M 2654, 1948.

Jones, W.P., WIND TUNNEL INTERFERENCE EFFECTS ON MEASUREMENTS OF AERODYNAMIC COEFFICIENTS FOR OSCILLATING AIRFOILS, Aeronautical Research Council R&M 2786, 1950, AD223688.

Jones, W.P., WIND TUNNEL WALL INTERFERENCE EFFECTS ON OSCILLATING AIRFOILS IN SUBSONIC FLOW, Aeronautical Research Council R&M 2943, 1953.

Ladeson, C.L., and Lindsey, W.F., INVESTIGATION OF UNSTEADY FLOW PAST FOUR NACA 6 PERCENT THICK AIRFOIL SECTIONS, Astrophysical Journal, April 1965, AD102205.

Laidlaw, W.R., THEORETICAL AND EXPERIMENTAL PRESSURE DISTRIBUTIONS ON LOW ASPECT RATIO WINGS OSCILLATING IN INCOMPRESSIBLE FLOW, Aeroelastic and Structures Research Laboratory, Massachusetts Institute of Technology, Technical Report 51-2, September 1954.

Laidlaw, W.R., and Halfman, R.L., EXPERIMENTAL PRESSURE DISTRIBUTIONS ON OSCILLATING LOW ASPECT RATIO WINGS, Journal of the Aeronautical Sciences, Vol. 23, No. 2, February 1956.

Lawrence, H.R., and Gerber, E.H., THE AERODYNAMIC FORCES ON LOW ASPECT RATIO WINGS OSCILLATING IN AN INCOMPRESSIBLE FLOW, Journal of the Aeronautical Sciences, Vol. 19, No. 11, November 1952.

Leehey, P., THE HILBERT PROBLEM FOR AN AIRFOIL IN UNSTEADY FLOW, David W. Taylor Model Basin, Washington, D.C., January 1957, AD124295.

LeRoy, H.L., and Scheiman, J., QUALITATIVE EVALUATION OF EFFECTS OF HELICOPTER ROTOR BLADE TIP VORTEX ON BLADE AIRLOADS, NASA TN D-1637, May 1963.

Mazelsky, B., DETERMINATION OF INDICIAL LIFT AND MOMENT OF A TWO-DIMENSIONAL PITCHING AIRFOIL AT SUBSONIC MACH NUMBERS FROM OSCILLATING COEFFICIENTS WITH NUMERICAL CALCULATIONS FOR M = 0.7, NACA TN 2613, 1952.

Mendelson, A., AERODYNAMIC HYSTERESIS AS A FACTOR IN CRITICAL FLUTTER SPEED OF COMPRESSOR BLADES AT STALLING CONDITIONS, Journal of the Aeronautical Sciences, No. 16, 1949.

Mendelson, A., EFFECT OF CENTRIFUGAL FORCE ON FLUTTER OF UNIFORM CANTILEVER BEAM AT SUBSONIC SPEEDS WITH APPLICATION TO COMPRESSOR AND TURBINE BLADES, NACA TN 1893, 1949.

Miller, R.H., UNSTEADY AIR LOADS ON HELICOPTER ROTOR BLADES, Journal of the Royal Aeronautical Society, April 1964.

Miller, R.H., ON THE COMPUTATION OF AIRLOADS ACTING ON ROTOR BLADES IN FORWARD FLIGHT, Journal of the American Helicopter Society, Vol. 7, No. 2, April 1962.

Minhinnick, I.T., AN INVESTIGATION OF THE FLUTTER SPEED OF AN AIRSCREW BLADE TAKING INTO ACCOUNT THE CHORDWISE FLEXIBILITY AND THE TWIST OF THE BLADE, Aeronautical Research Council R&M 2073, 1943.

Molyneux, W.G., AN APPROXIMATE THEORETICAL APPROACH FOR THE DETERMINATION OF OSCILLATORY AERODYNAMIC COEFFICIENTS FOR A HELICOPTER ROTOR IN FORWARD FLIGHT, The Aeronautical Quarterly, Vol. 13, February-November 1962.

Molyneux, W.G., TECHNIQUES FOR THE MEASUREMENT OF THE AERO-DYNAMIC FORCES ON OSCILLATING AIRFOILS, TN STR161, Royal Aircraft Establishment, Farnborough, England, June 1955, AD72545.

Molyneux, W.G., and Ruddlesden, F., A TECHNIQUE FOR THE MEASUREMENT OF PRESSURE DISTRIBUTION ON OSCILLATING AEROFOILS, WITH RESULTS FOR A RECTANGULAR WING OF ASPECT RATIO 3.3, Aeronautical Research Council C.P. 233, 1955.

Moore, F.K., LIFT HYSTERESIS AT STALL AS AN UNSTEADY BOUNDARY-LAYER PHENOMENON, Lewis Flight Propulsion Laboratories, Cleveland, Ohio, November 1955, AD77939.

Moss, G.F., LOW-SPEED WIND-TUNNEL MEASUREMENTS OF LONGITUDINAL OSCILLATORY DERIVATIVES ON THREE WING PLANFORMS, Aeronautical Research Council R&M 3009, 1952.

Piziali, R.A., TABLES OF TWO-DIMENSIONAL OSCILLATING AIRFOIL COEFFICIENTS FOR ROTARY WINGS, TRECOM TR-64-53, U.S. Army Transportation Research Command, Fort Eustis, Virginia, October 1964, AD610029.

Polyakhov, N.N., THEORY OF A WING OF FINITE SPAN, OSCILLATING HARMONIOUSLY, Foreign Technical Division, Air Force Systems Command, Wright-Patterson Air Force Base, Ohio, AD610292.

Rainey, A.G., MEASUREMENT OF AERODYNAMIC FORCES FOR VARIOUS MEAN ANGLES OF ATTACK ON AN AIRFOIL OSCILLATING IN PITCH AND ON TWO FINITE-SPAN WINGS OSCILLATING IN BENDING WITH EMPHASIS ON DAMPING IN THE STALL, NACA Report No. 1305, 1957.

Rainey, A.G., PRELIMINARY STUDY OF SOME FACTORS WHICH AFFECT
THE STALL-FLUTTER CHARACTERISTICS OF THIN WINGS, NACA TN 3622,
1956.

Randall, D.G., FORCES ON AEROFOILS WITH BOTH INCIDENCE AND FOR-
WARD SPEED VARYING, Royal Aircraft Establishment, Farnborough,
England, May 1964, AD447747.

Lessing, H.C., Troutman, J.L., and Menees, G.P., EXPERIMENTAL
DETERMINATION OF THE PRESSURE DISTRIBUTION ON A RECTANGULAR
WING OSCILLATING IN THE FIRST BENDING MODE FOR MACH NUMBERS
FROM 0.24 TO 1.30, NASA Technical Note D-344, December 1960.

Reid, E.G., EXPERIMENTS ON THE LIFT OF AIRFOILS IN NON-UNIFORM
MOTION, Stanford University Report, 23 July 1942.

Reid, E.G., and Vincenti, W., AN EXPERIMENTAL DETERMINATION OF
THE LIFT OF AN OSCILLATING AIRFOIL, Journal of Aeronautical
Sciences, Vol. 8, No. 1, November 1940.

Reissner, E., WIND TUNNEL CORRECTIONS FOR THE TWO-DIMENSIONAL
THEORY OF OSCILLATING AIRFOILS, Report No. SB-318-S-3,
Cornell Aeronautical Laboratories, Inc., 22 April 1947.

Reissner, E., and Stevens, J., EFFECT OF FINITE SPAN ON THE
AIRLOAD DISTRIBUTIONS FOR OSCILLATING WINGS, VOLUME II,
METHODS OF CALCULATION AND EXAMPLES OF APPLICATION, NACA TN
1195, 1947.

Richardson, J.R., A METHOD FOR CALCULATING THE LIFTING FORCES
ON WINGS (UNSTEADY SUBSONIC LIFTING SURFACE THEORY), Aero-
nautical Research Council R&M 3157, 1955.

Rodden, W.P., Farkas, E.F., Malcom, H., and Koliszewski, A.M.,
AERODYNAMIC INFLUENCE COEFFICIENTS FROM INCOMPRESSIBLE STRIP
THEORY:  ANALYTICAL DEVELOPMENT AND COMPUTATIONAL PROCEDURE,
Aerospace Corporation, Los Angeles, California, January 1966,
AD438171.

Rodden, W.P., and Revell, J.D., THE STATUS OF UNSTEADY AERO-
DYNAMIC INFLUENCE COEFFICIENTS, Aerospace Corporation, Los
Angeles, California, November 1961, AD272908.

Rott, N., OSCILLATING AIRFOILS AT MACH NUMBER ONE, Journal of
the Aeronautical Sciences, No. 16, 1949.

Runyan, H.L., and Watkins, C.E., CONSIDERATIONS ON THE EFFECT
OF WIND-TUNNEL WALLS ON OSCILLATING AIR FORCES FOR TWO-
DIMENSIONAL SUBSONIC COMPRESSIBLE FLOW, NACA TN 2552, December
1951.

Runyan, H.L., and Woolston, D.S., APPRAISAL OF METHODS OF FLUTTER ANALYSIS BASED ON CHOSEN MODES BY COMPARISON WITH EXPERIMENT FOR CASES OF LARGE MASS COUPLING, NACA TN 1902, 1942.

Runyan, H.L., Woolston, D.S., and Rainey, A.G., THEORETICAL AND EXPERIMENTAL INVESTIGATION OF THE EFFECT OF TUNNEL WALLS ON THE FORCES ON AN OSCILLATING AIRFOIL IN TWO-DIMENSIONAL SUBSONIC COMPRESSIBLE FLOW, NACA TN 3416, June 1955.

Schnittger, J.R., SINGLE DEGREE OF FREEDOM FLUTTER OF COMPRESSOR BLADES IN SEPARATED FLOW, Journal of the Aeronautical Sciences, January 1954.

Shulman, Y., STABILITY OF A FLEXIBLE HELICOPTER ROTOR BLADE IN FORWARD FLIGHT, Journal of the Aeronautical Sciences, Vol. 7, July 1956.

Silverstein, A., and Joyner, U.T., EXPERIMENTAL VERIFICATION OF THE THEORY OF OSCILLATING AIRFOILS, NACA Report No. 673, 1939.

Smilg, B., THE INSTABILITY OF PITCHING OSCILLATIONS OF AN AIRFOIL IN SUBSONIC INCOMPRESSIBLE POTENTIAL FLOW, Journal of Aeronautical Sciences, No. 16, November 1949.

Smith, F.E., and Sevick, M., AN INVESTIGATION OF THE FORCES ON AN AIRFOIL OSCILLATING IN PITCH ABOUT THE QUARTER CHORD, N64-21587, Ordnance Research Laboratory, Pennsylvania State University, University Park, Pennsylvania, 1964, AD438890.

Spielberg, I.N., THE TWO-DIMENSIONAL INCOMPRESSIBLE AERODYNAMIC COEFFICIENTS FOR OSCILLATORY CHANGES IN AIRFOIL CAMBER, Journal of the Aeronautical Sciences, No. 20, 1953.

Steiner, R.W., EXPERIMENTAL STUDY OF THE UNSTEADY FLOW CHARACTERISTICS OF STALLED AIRFOILS, Air Force Institute of Technology, Wright-Patterson Air Force Base, Ohio, August 1956, AD106313.

Theodorsen, T., and Garrick, I.E., NONSTATIONARY FLOW ABOUT A WING-AILERON-TAB COMBINATION INCLUDING AERODYNAMIC BALANCE, NACA Report 736, 1941.

Timman, R., THE AERODYNAMIC FORCES ON AN OSCILLATING AEROFOIL BETWEEN TWO PARALLEL WALLS, Appl. Sci. Res., (The Hague), Vol. A3, No. 1, 1951.

Timman, R., and van de Vooren, A.I., FLUTTER OF A HELICOPTER ROTOR ROTATING IN ITS OWN WAKE, Journal of the Aeronautical Sciences, Vol. 24, No. 9, September 1957.

Timman, R., van de Vooren, A.I., and Greidanus, J.H., AERO-
DYNAMIC COEFFICIENTS OF AN OSCILLATING AIRFOIL IN TWO-
DIMENSIONAL SUBSONIC FLOW, Journal of the Aeronautical
Sciences, No. 21, 1954.

Van de Vooren, A.I., UNSTEADY AIRFOIL THEORY, Advances In
Applied Mechanics, Vol. V, Academic Press, Inc., New York,
1958.

Victory, M., FLUTTER AT HIGH INCIDENCE, Aeronautical Research
Council R&M 2947, 1943.

Watkins, C.E., Woolston, D.S., and Cunningham, A SYSTEMATIC
KERNEL FUNCTION PROCEDURE FOR DETERMINING AERODYNAMIC FORCES
ON OSCILLATING OR STEADY FINITE WINGS AT SUBSONIC SPEEDS,
NASA TR R-48, 1959.

Watkins, C.E., Runyan, H.L., and Woolston, D.S., ON THE KERNEL
FUNCTION OF THE INTEGRAL EQUATION RELATING THE LIFT AND DOWN-
WARD DISTRIBUTIONS OF OSCILLATING FINITE WINGS IN SUBSONIC
FLOW, NACA TN 3131, January 1954.

Widmayer, E., Clevenson, S.A., and Leadbetter, S.A., SOME
MEASUREMENTS OF AERODYNAMIC FORCES AND MOMENTS AT SUBSONIC
SPEEDS ON A RECTANGULAR WING OF ASPECT RATIO 2 OSCILLATING
ABOUT THE MIDCHORD, NACA TN 4240, May 1958.

Wight, K.C., A REVIEW OF SLOTTED-WALL WIND-TUNNEL INTERFERENCE
EFFECTS ON OSCILLATING MODELS IN SUBSONIC AND TRANSONIC FLOWS,
NPL Aeronautical Report 1074, Aeronautical Research Council
25, 1938.

Woolston, D.S., and Runyan, H.L., SOME CONSIDERATIONS ON THE
AIR FORCES ON A WING OSCILLATING BETWEEN TWO WALLS FOR SUBSONIC
COMPRESSIBLE FLOW, Journal of the Aeronautical Sciences, Vol.
22, No. 1, January 1955.

Wyss, J.A., and Monfort, J.C., EFFECTS OF AIRFOIL PROFILE ON
THE TWO-DIMENSIONAL FLUTTER DERIVATIVES FOR WINGS OSCILLATING
IN PITCH AT HIGH SUBSONIC MACH NUMBERS, NACA R&M A54C24, 1954.

Young, M.I., A THEORY OF ROTOR BLADE MOTION STABILITY IN
POWERED FLIGHT, Journal of the American Helicopter Society,
Vol. 9, No. 3, July 1964.

Young, M.I., and Ham, N.D., ON THE STALL FLUTTER OF ROTOR AND
PROPELLER BLADES, presented at the Symposium on Aeroelastic
and Acoustic Problems of V/STOL Aircraft, University of
Southampton, England, September 1965.

## APPENDIX I
## DERIVATION OF THEORETICAL DAMPING

In order to nondimensionalize the cycle damping parameter, the corresponding value for the incompressible case will be derived using the Theodorsen[15] formulation for normal force and moment:

$$L = L_1 + L_2 + L_3 \tag{12}$$

where $L_1$ is circulatory origin, acting at quarter-chord

$L_2$ is noncirculatory origin, acting at mid-chord

$L_3$ is noncirculatory origin, acting at three-quarter-chord

$$L_1 = 2\pi\rho VbC(K) \; [\dot{h} + V\alpha + b(1/2-e) \; \dot{\alpha}] \tag{13}$$

$$L_2 = \pi\rho b^2 (\ddot{h} - be\ddot{\alpha}) \tag{14}$$

$$L_3 = \pi\rho b^2 V\dot{\alpha} \; . \tag{15}$$

The equations can be reduced to coefficient form by dividing by $1/2\rho V^2(2b)$ (1) with V assumed to be a constant.

$$C_{L_1} = 2\pi \; C(k) \left[ \frac{\dot{h}}{V} - \alpha + b \; (1/2-e) \; \frac{\dot{\alpha}}{V} \right] \tag{16}$$

$$C_{L_2} = \pi \left[ \frac{b\ddot{h}}{V^2} - \frac{b^2 e\ddot{\alpha}}{V^2} \right] \tag{17}$$

$$C_{L_3} = \frac{\pi b\dot{\alpha}}{V} \; . \tag{18}$$

Similarly, the pitching moment can be written as follows:

$$M = (1/2 + e) \; bL_1 + ebL_2 - (1/2-e) \; bL_3 - \frac{\rho\pi b^4 \ddot{\alpha}}{8} \; . \tag{19}$$

108

Converting to coefficient form by dividing by $1/2 \rho V^2 (2b)(1)(2b)$ yields

$$C_M = 1/2(1/2 + e) \; C_{L_1} + \frac{e}{2} \; C_{L_2} - 1/2(1/2-e) \; C_{L_3} - \frac{\pi b^2 \ddot{\alpha}}{16V^2} \; . \qquad (20)$$

## PITCHING OSCILLATION

Damping per cycle in pitch can be defined as

$$- \frac{1}{2f\pi^2 (\Delta\alpha)^2} \oint C_M \; d\alpha = - \frac{1}{2f\pi^2 (\Delta\alpha)^2} \int_o^{2\pi} C_M \; (\theta) \; \frac{d\alpha}{d\theta} \; d\alpha. \qquad (21)$$

If we assume sinusoidal pitching about the quarter-chord, the following relations apply:

$$\alpha = \Delta\alpha \; \sin \theta \qquad (22)$$

$$e = -1/2 \qquad (23)$$

$$h = -\frac{b}{2} \; \Delta\alpha \; \sin \theta \; . \qquad (24)$$

Differentiating and substituting into the $C_M$ equation, we obtain a simplified expression:

$$C_M = \Delta\alpha \left[ \frac{\pi k^2}{16} \; \sin \theta - \frac{\pi k}{2} \; \cos \theta \right] \; . \qquad (25)$$

By substituting into the damping equation and integrating, we obtain

$$\text{Damping} = - \frac{k}{4f} \; . \qquad (26)$$

## VERTICAL TRANSLATION

In vertical translation, average cycle damping can be defined as

$$- \frac{1}{2f\pi^2 f (\Delta h)^2} \; C_N \; dh. \qquad (27)$$

Substituting $C_N$ from the expression derived earlier and assuming sinusoidal motion, theoretical damping can be expressed as follows:

$$\text{Damping} = \frac{C(k) k}{f} \; . \qquad (28)$$

109

# APPENDIX II
## WIND TUNNEL WALL CORRECTIONS

Wind tunnel boundary corrections were developed by using a computer program provided by NASA (based on the formulation in References 9 and 16) to calculate $C_N$, $C_M$, and phase for an airfoil oscillating in a wind tunnel. The data tables in Reference 17 were then used for comparative free-air values. The theoretical values were based on compressible thin-airfoil theory. The method of images was used to simulate the walls.

The magnitude ratios of $C_N$ and $C_M$ in free air to the values in a tunnel, as well as phase differences, are shown in Figures 52 and 53 for pitching and plunging motions. The corrections on magnitude are largest at low values of k and high Mach number. The corrections are all less than 10 percent except for the pitching moment in translation, where corrections up to 25 percent apply at small k. The values of $C_M$ for that condition, however, are in the 0.002 range and are therefore close to the experimental resolution threshold. This makes the correction meaningless. Phase differences between test and theory are less than 10 degrees, except for translation where the correction is 15 degrees.

The corrections calculated here were found to be small in comparison with the large charges in both magnitude and phase due to stall; therefore, they have not been included in the wind tunnel results.

110
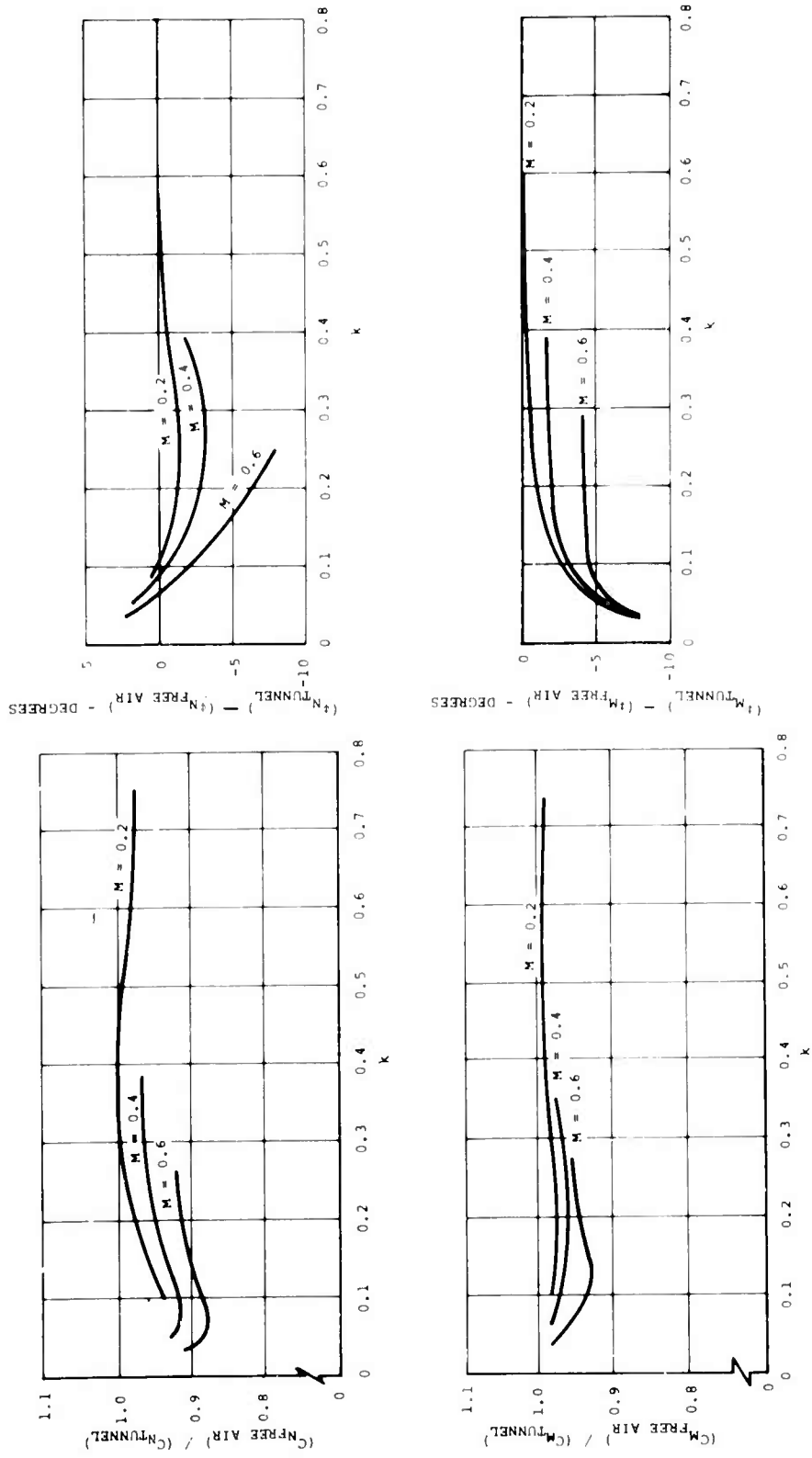
Figure 52. Wind Tunnel Wall Corrections for Pitching Oscillation.
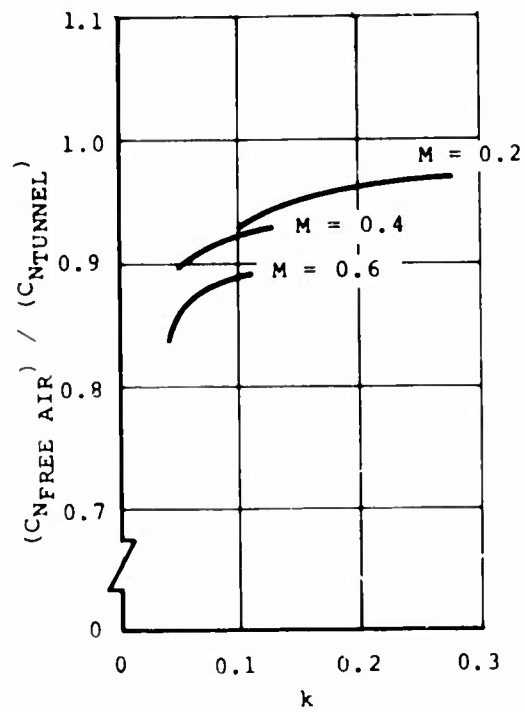
111
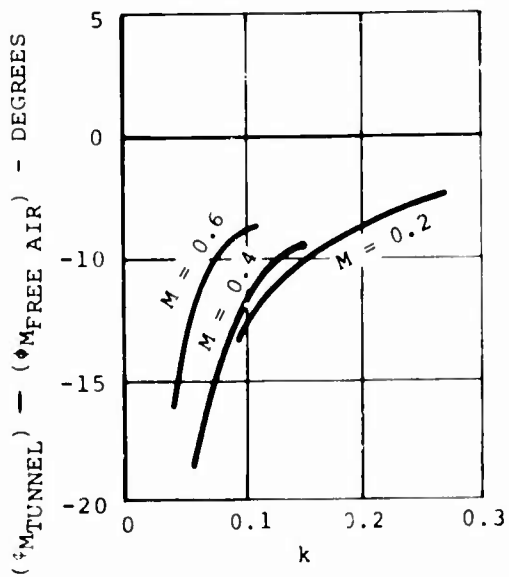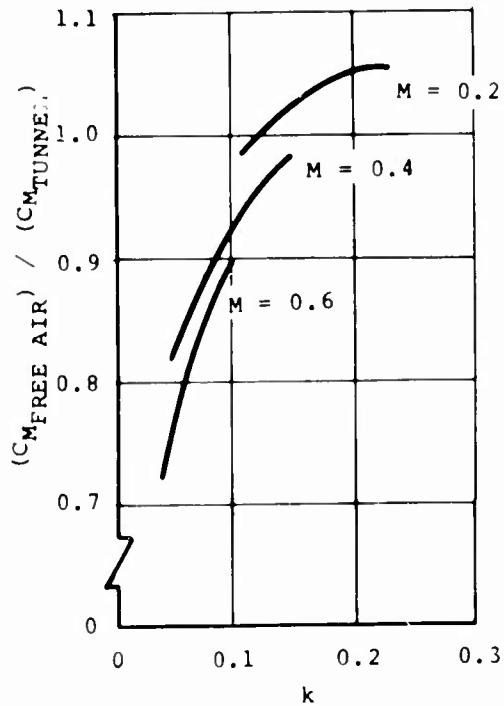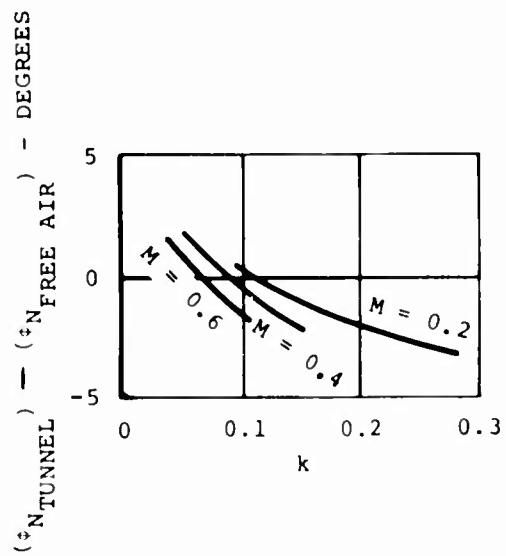
Figure 53. Wind Tunnel Wall Corrections for
Vertical Translation.

# APPENDIX III
## STATIC (NONOSCILLATORY) TESTS

Each airfoil was tested under steady-$\alpha$ condition over the entire range of $\alpha$'s and M's for which dynamic data were obtained.

Figures 54 through 56 show static $C_N$ and $C_M$ variations with $\alpha$ for both airfoils. The lines faired through the test points on the $C_N$ plots are drawn to show an abrupt drop at $\alpha_{STALL}$ for M = 0.2 and 0.4 to conform to the trends of the dynamic data and to other Boeing experience with the same airfoil sections.

The increased values of $C_{N_{MAX}}$ and $\alpha_{STALL}$ shown by the cambered section at M = 0.2 and 0.4 are consistent with results reported elsewhere, such as Reference 13. At M = 0.6, the $C_N$ curves of both airfoils are dominated by strong compressibility effects over which camber appears to have little influence.

Both profiles show small values of pitching moment about the quarter-chord at $\alpha$'s below those for stall. The data for M = 0.2 show considerable irregularity in the form of the curves. This is due to the low dynamic pressure and the _ ulting low transducer signal level. The $C_M$'s shown for the 0012 airfoil at M = 0.2 and 0.4 near zero lift are slightly negative, although zero would have been expected because of symmetry. The deviation is attributed to a zero drift of the transducers. Note, however, that the stall phenomena of principal interest in this test program generally involve $C_M$'s which are orders of magnitude larger. Consequently, the discrepancy is unimportant. Steady-flow drag data for the 23010-1.58 airfoil are shown in Figure 55. No drag data were measured for the NACA 0012 airfoil.

The static characteristics of the 23010-1.58 airfoil with 3-degree trailing-edge reflex are shown in Figure 57 for M = 0.4. There is no perceptible difference in the $C_N$ data. The low $-\alpha$ $C_M$ data are shifted from a slightly negative value to a consistent zero level. While the change is within the range of the drift mentioned above, it also agrees with previous results such as those reported by Davenport[14].
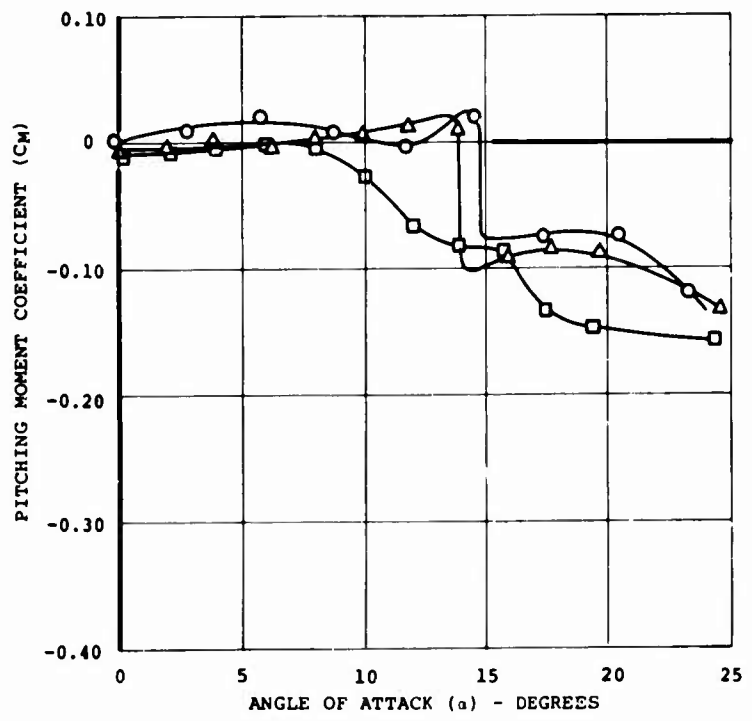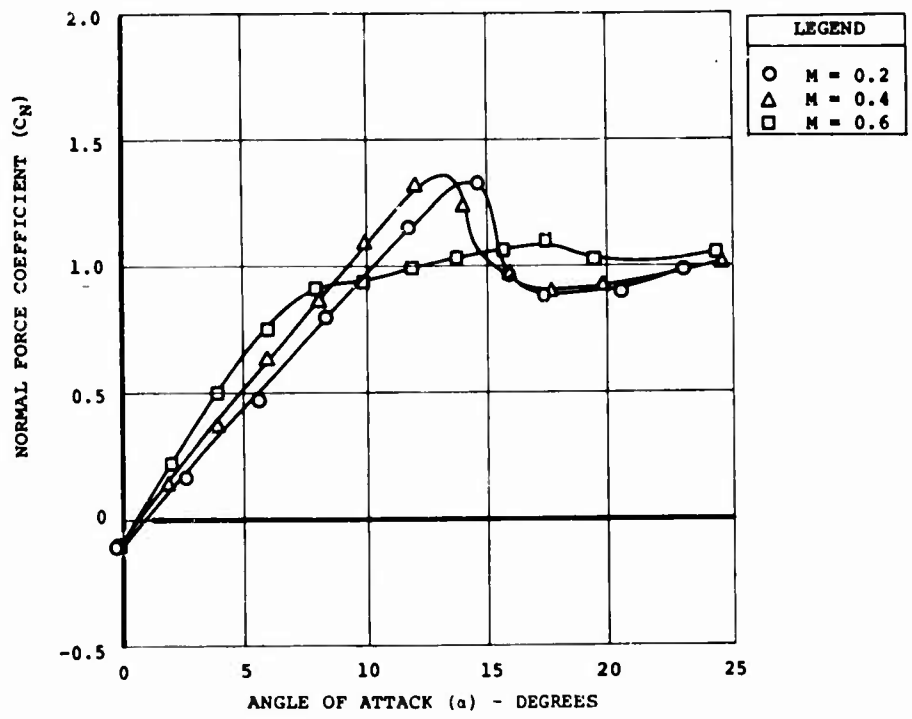
113

Figure 54.  Static $C_N$ and $C_M$ Characteristics for the Vertol 23010-1.58 Airfoil.
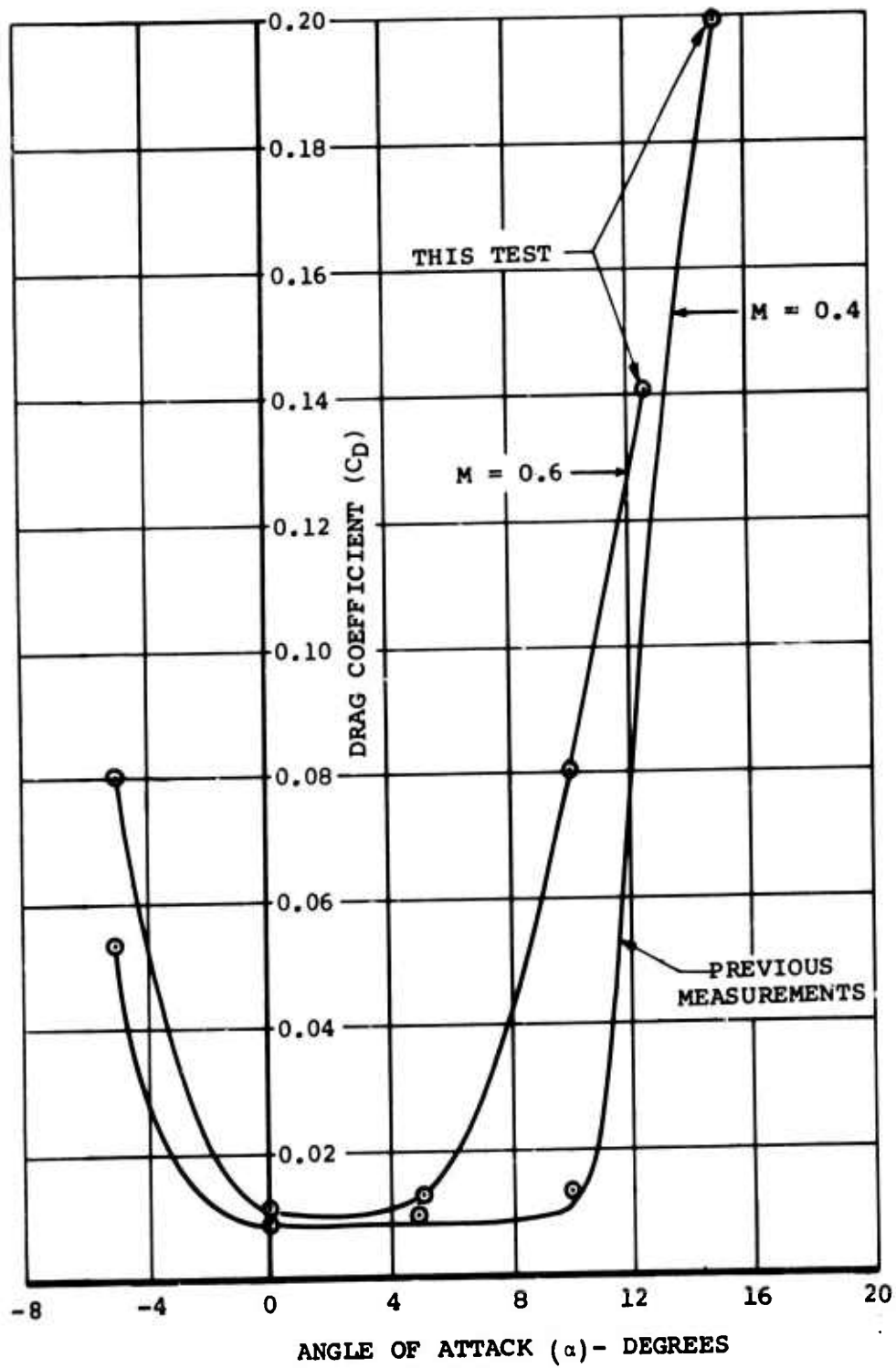
114

Figure 55.  Steady Drag Data for Vertol 23010-1.58
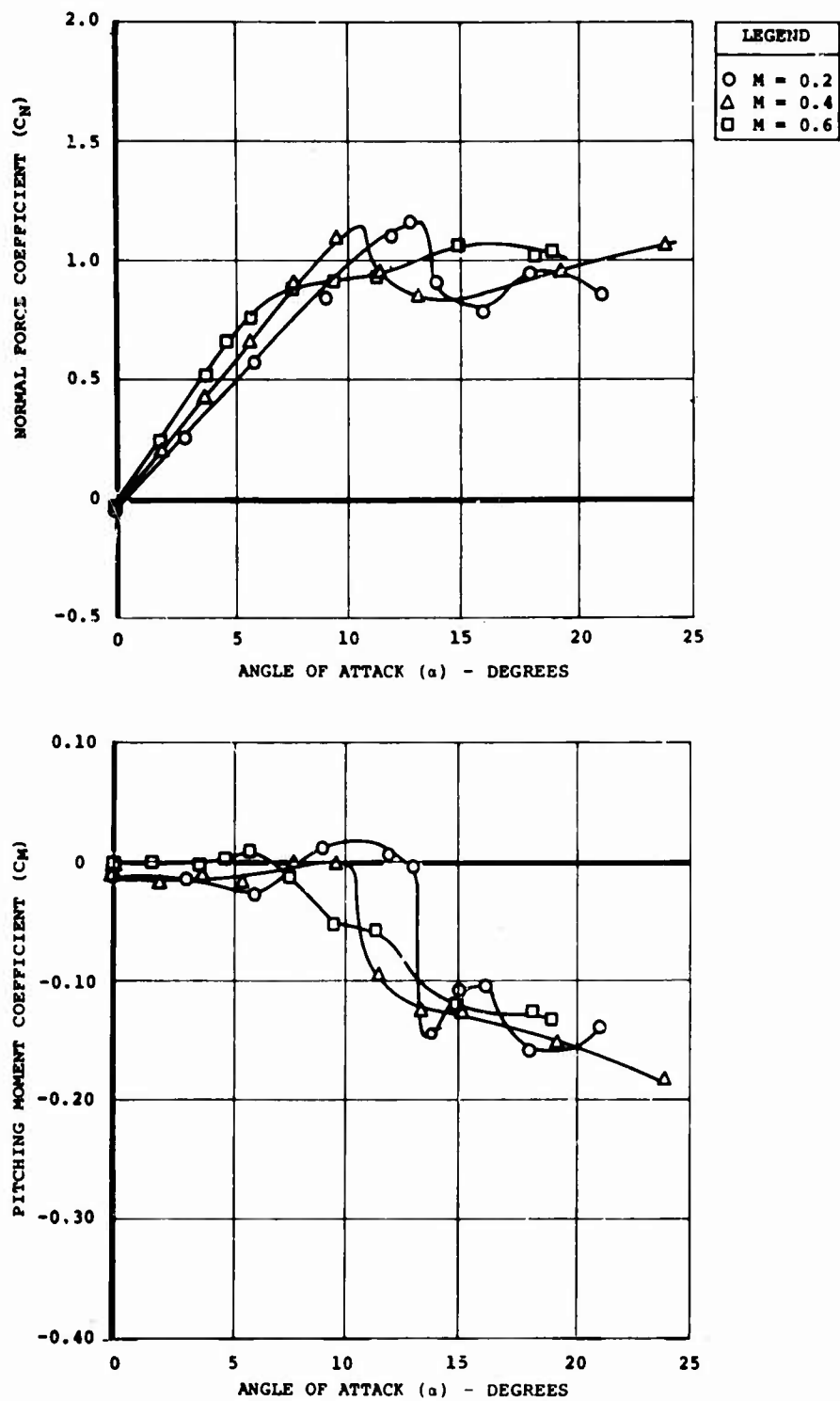Airfoil From Wake Traverse Measurements.

Figure 56.  Static $C_N$ and $C_M$ Characteristics for the NACA 0012 (Modified) Airfoil.
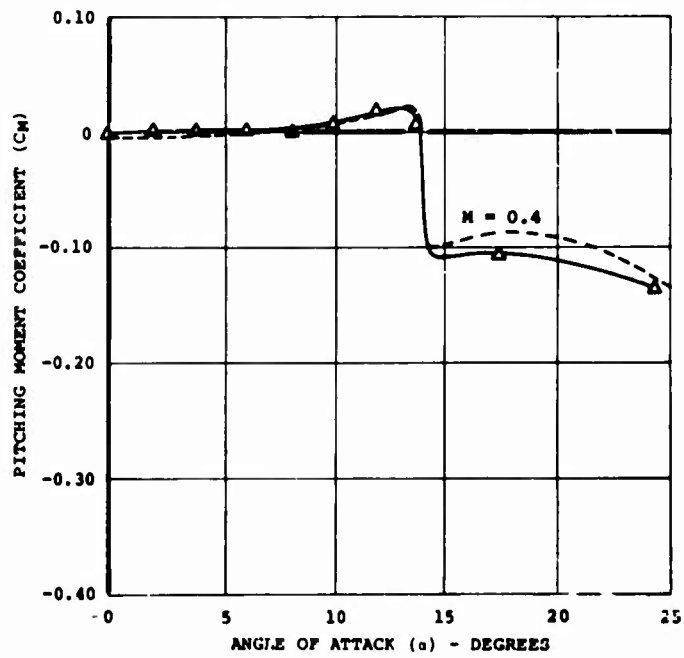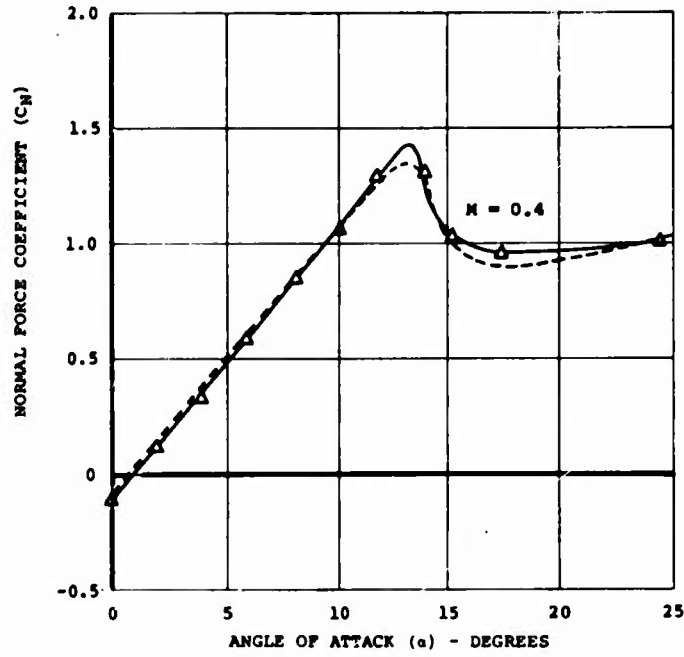
116

Figure 57. Static $C_N$ and $C_M$ Characteristics for the Vertol 23010-1.58 (Reflex) Airfoil.

117

## APPENDIX IV
## DISCUSSION OF INSTANTANEOUS WORK

The instantaneous work function $\delta W$ is shown in Figures 58 through 60 for the Vertol 23010-1.58 airfoil as a function of $\alpha$. Positive $\delta W$ indicates work done on the airfoil by the tunnel flow and can lead to instability if the system is free to respond. It is important to note that the area inside the $\delta W$-$\alpha$ curve is not the integrated work function $\Delta W$ (or damping) shown on the output listings. The $\delta W$ function must be integrated with respect to time rather than to $\alpha$ to obtain $\Delta W$. The incremental work function does, however, show the amount of work input or output at each angle of attack during a cycle of oscillation. Since all data have been averaged over five cycles or more, the instantaneous work function presented here represents an averaged value.

Figure 58 shows the effect of increases in $\alpha_0$ on the $\delta W$ function. Since the 7.3- and 9.6-degree $\alpha_0$ data do not stall during the cycle, the loop is small, with a somewhat larger area below the ordinate indicating stability. At $\alpha_0 = 12.2$ degrees, the airfoil stalls at 15 degrees, causing a nose-down pitching moment. Since $\alpha$ is still increasing up to 17.5 degrees, $\delta W$ is negative. When $d\alpha/dt$ changes sign at 17.5 degrees, $\delta W$ becomes positive since $C_M$ and $d\alpha/dt$ are now both negative. This is the condition when aerodynamic forces can drive the airfoil.

At $\alpha_0$ of 14.9 and 17.5 degrees, the negative $\delta W$ is increased in $\alpha$ duration and in magnitude, since the $\delta W$ break still occurs at 15 degrees. This shows that, for a constant frequency, the $\delta W$ and therefore the $C_M$ break (since $d\alpha/dt$ does not change rapidly at 15 degrees) are independent of $\alpha_0$ to a first-order approximation. The final loop on Figure 58 at $\alpha_0 = 24.6$ degrees shows work input on the negative $d\alpha/dt$ portion and work output during the positive portion of the cycle. The net integrated value of work per cycle ($\Delta W$ or damping) is shown to be stable for this case in Figure 17.

Figure 59 shows the effect of frequency on $\delta W$. Ths positive increment due to stall is seen to be largest when the stall occurs at the top of the $\alpha$ excursion. This occurs at 49 Hertz for this $\alpha_0$ (12.5 degrees).

The effect of a decrease in Mach number from 0.4 to 0.2 is shown in Figure 60 for two frequencies, 16 and 96 Hertz, for $\alpha_0$ near stall.

The sudden increase in $\delta W$ seen earlier does not occur until approximately 22.5 degrees for low frequencies, as seen from the first two loops in Figure 60. At the next higher $\alpha_0$ of 24.6 degrees, the airfoil is fully stalled over the whole cycle. For

118

the high-frequency oscillation, $\delta W$ is mostly negative over the whole cycle at $\alpha_0$ of 15 and 17.5 degrees. At 24.6 degrees, both negative and positive values are present. The net integrated $\Delta W$ is unstable as shown in Figure 16. Figure 61 shows the effect of Mach 0.6 for 16 and 96 Hertz. For the low-frequency oscillation, the $\delta W$ values are negative below an $\alpha_0$ of 7.5 degrees for both positive and negative pitch rates.

Above 7.5 degrees, the loop is essentially symmetrical about the ordinate axis and therefore indicates that the cycle damping is neutral or positive. For high-frequency oscillation, $\delta W$ is negative over three-quarters of the cycle, with the only positive inputs occurring between maximum and mean $\alpha$ on the pitch-down.

Figure 62 shows $\delta W$ for the symmetrical airfoil. $\alpha_0$ is increased from 9.9 to 14.7 degrees in the top sequence. Stall occurs 2.5 degrees earlier for the symmetrical airfoil than for the cambered airfoil in Figure 54. The three figures on the bottom show $\delta W$ characteristics for a sequence of increasing frequency at constant $\alpha_0$. The data at 97 Hertz are more unstable than the corresponding cambered airfoil data in Figure 59.

From these incremental work plots, it can be seen that the damping per cycle can be a very misleading parameter, since the instantaneous work or force inputs can be much larger than the cycle average. The damping per cycle can, however, be used to predict the limit oscillation when such an oscillation is established.
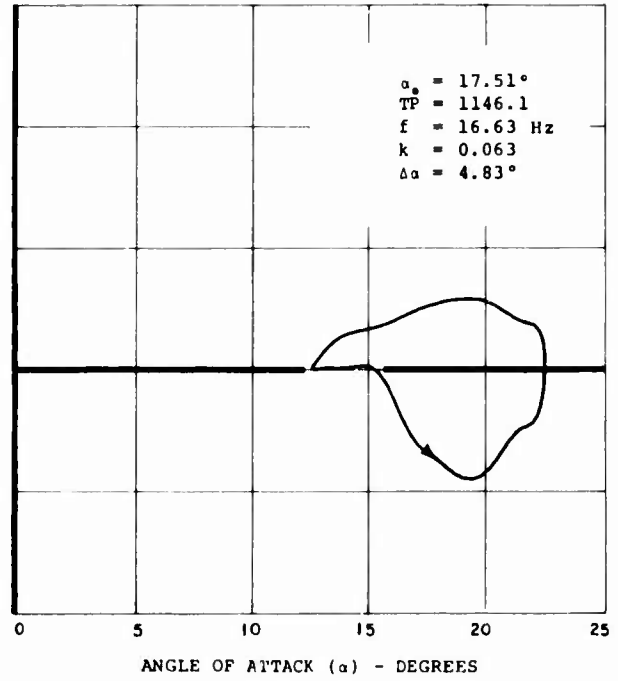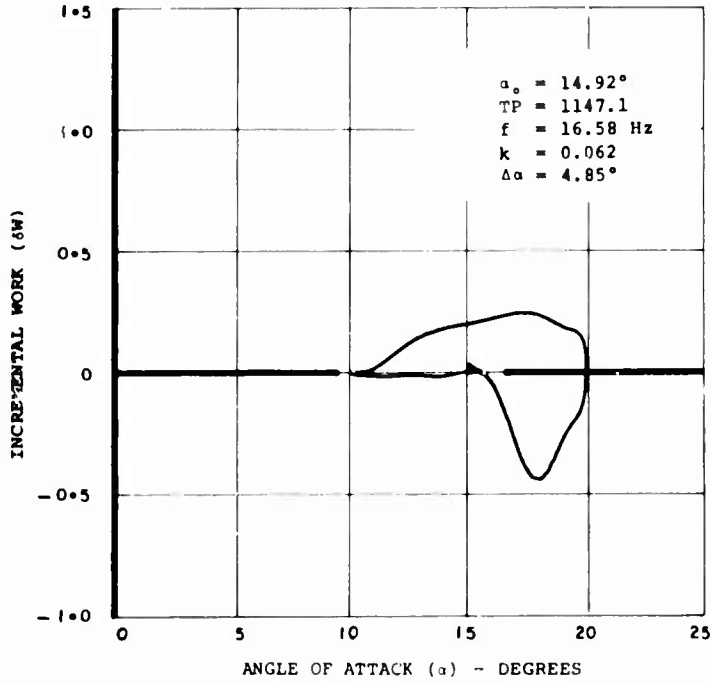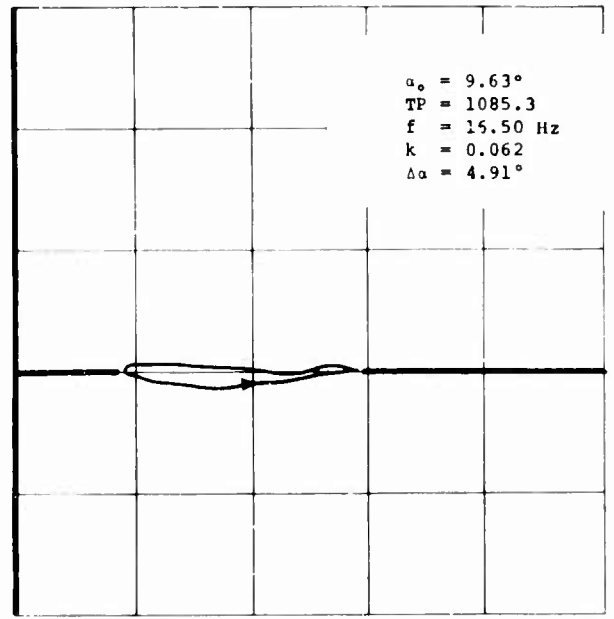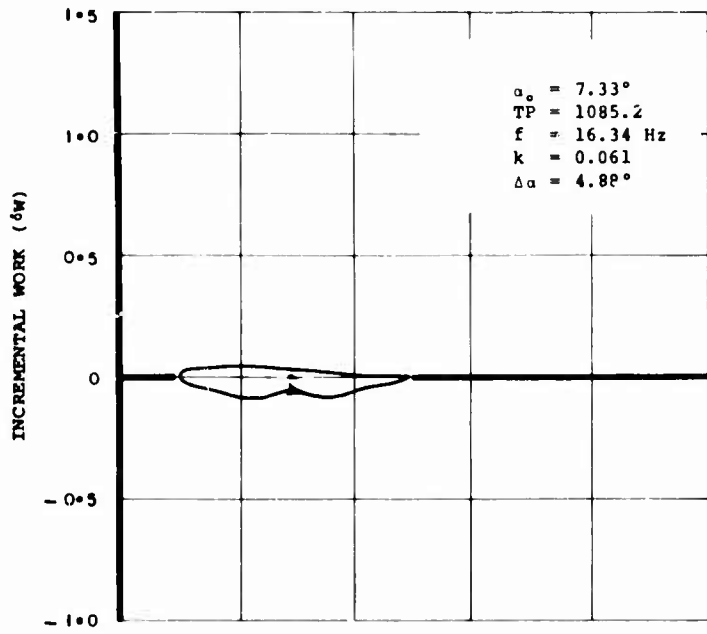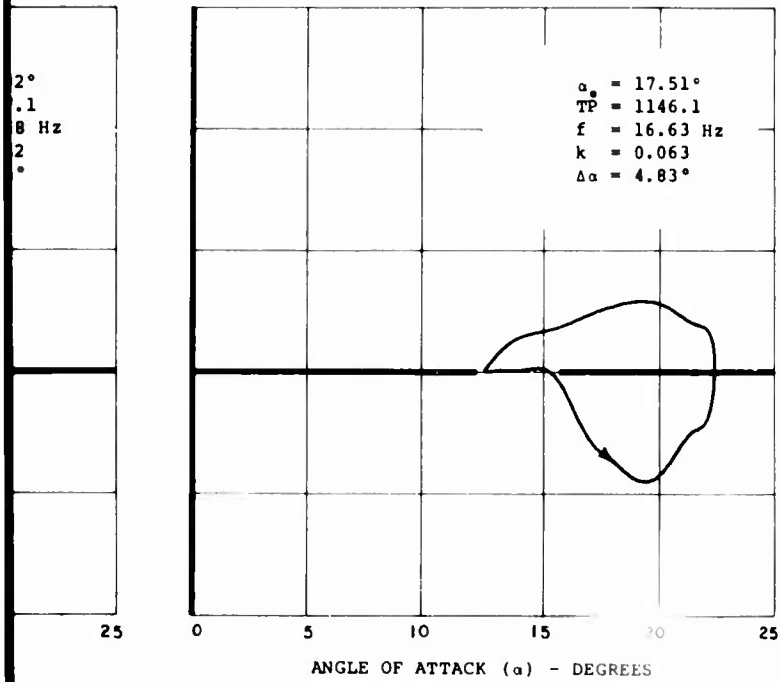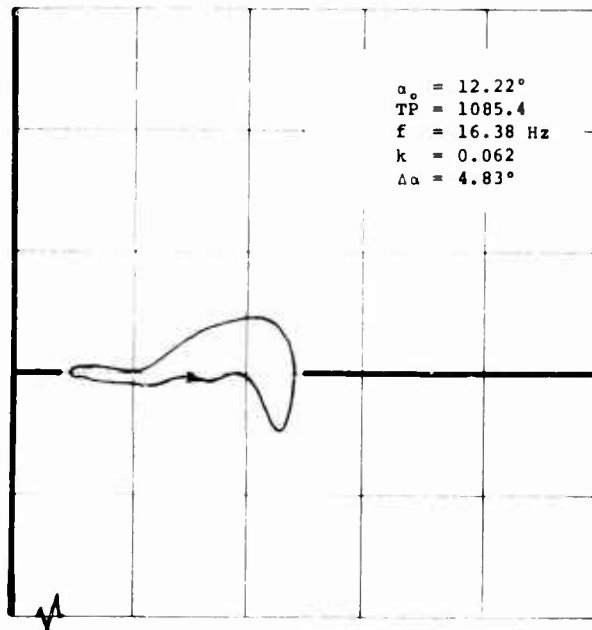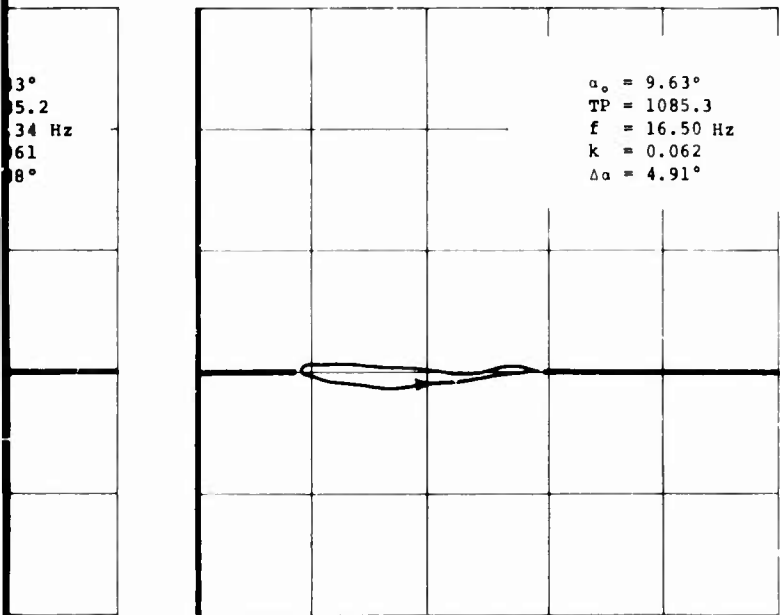
Figure 58.    Variation of Incremental Work With Mean Angle
of Attack for M = 0.4, f = 16 Hertz, and $\Delta\alpha$ = 5°.

121

Partial plot data, left top:

3°
5.2
34 Hz
61
8°

$\alpha_o$ = 9.63°
TP = 1085.3
f = 16.50 Hz
k = 0.062
$\Delta\alpha$ = 4.91°

$\alpha_o$ = 12.22°
TP = 1085.4
f = 16.38 Hz
k = 0.062
$\Delta\alpha$ = 4.83°

2°
.1
8 Hz
2
°

$\alpha_o$ = 17.51°
TP = 1146.1
f = 16.63 Hz
k = 0.063
$\Delta\alpha$ = 4.83°

$\alpha_o$ = 24.57°
TP = 1146.2
f = 16.41 Hz
k = 0.062
$\Delta\alpha$ = 4.86°

ANGLE OF ATTACK ($\alpha$) - DEGREES

ANGLE OF ATTACK ($\alpha$) - DEGREES
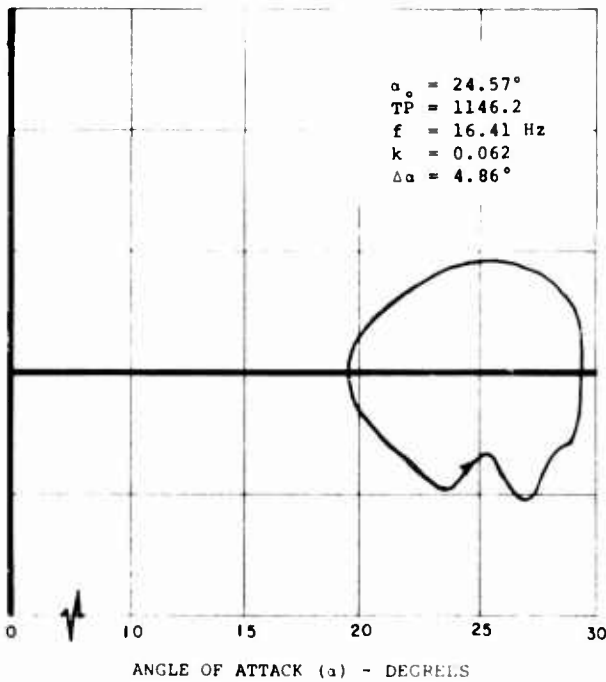
ntal Work With Mean Angle
4, f = 16 Hertz, and $\Delta\alpha$ = 5°.

B.
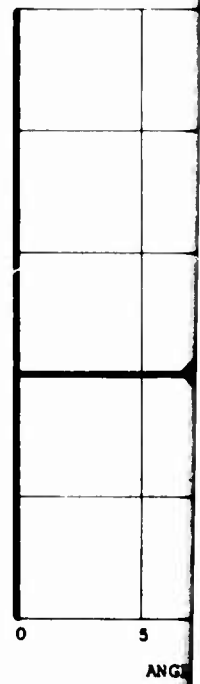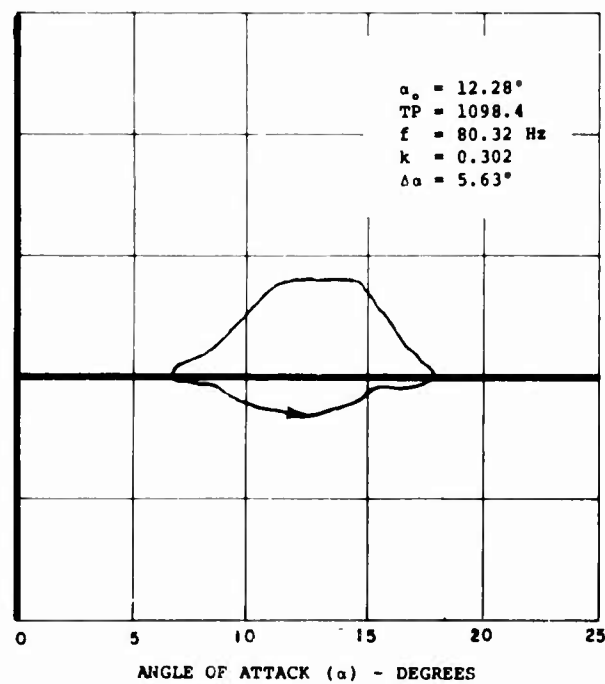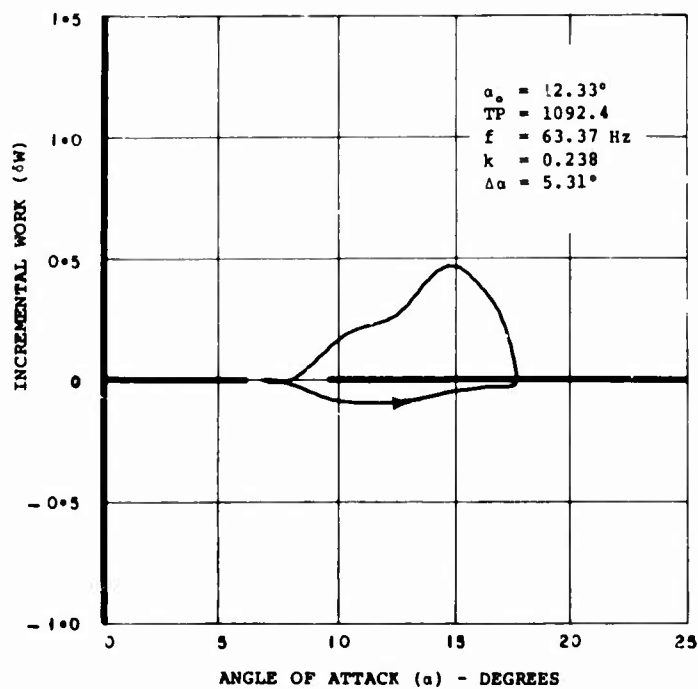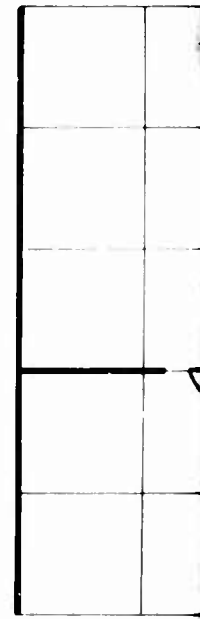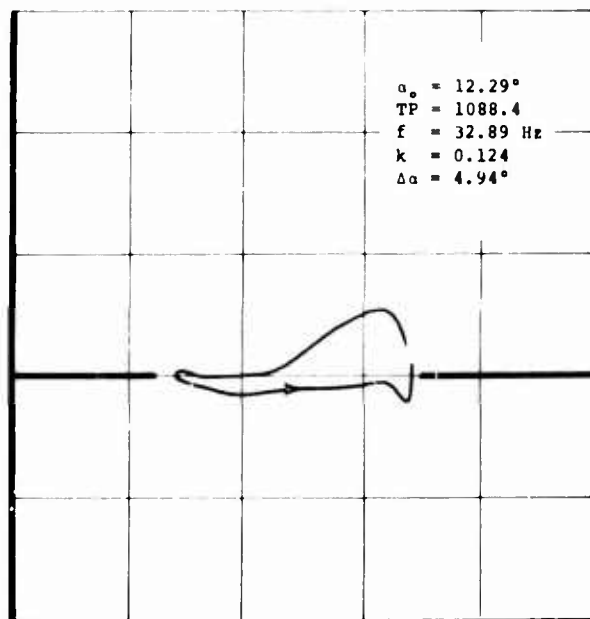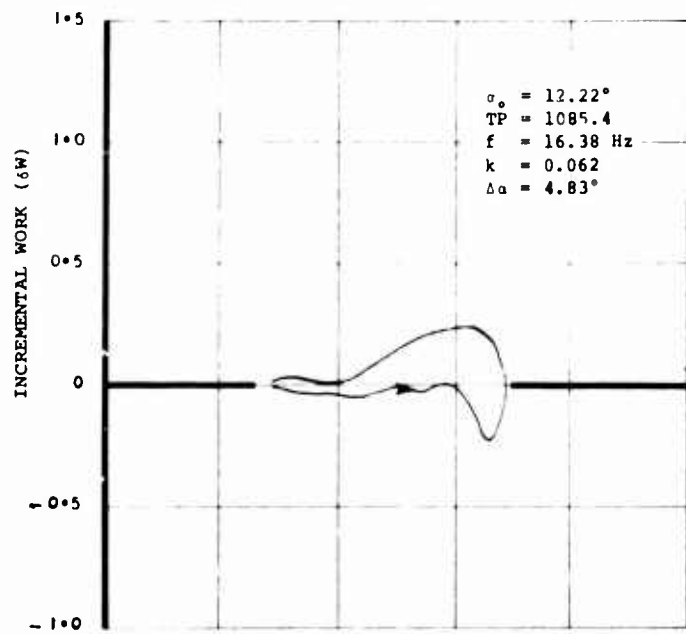
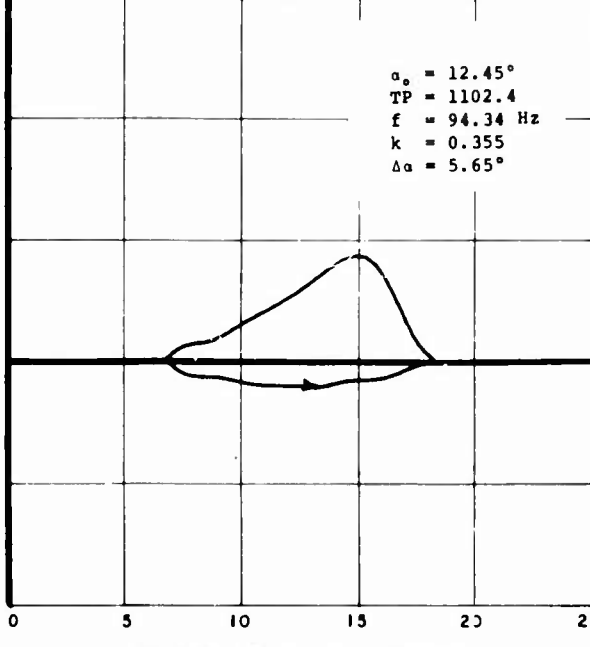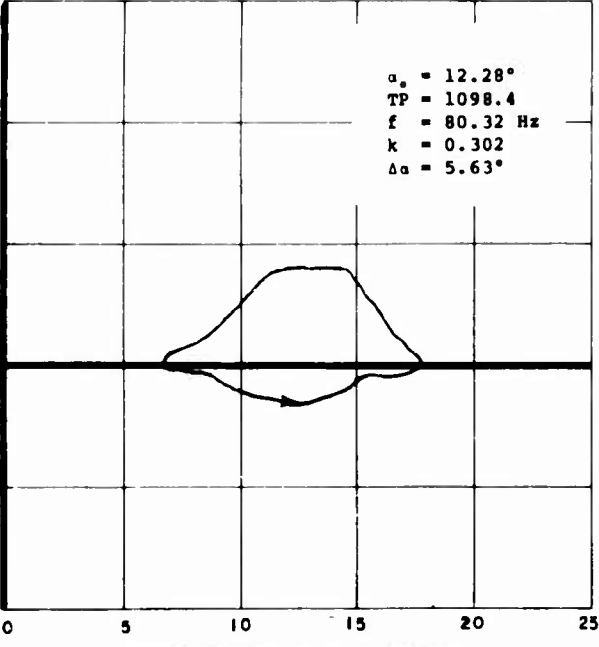Figure 59.   Variation of Incremental Work With Oscillation
Frequency for the Vertol 23010-1.58 Airfoil at
$M = 0.4, \alpha_0 = 12.25°$, and $\Delta\alpha = 5°$.
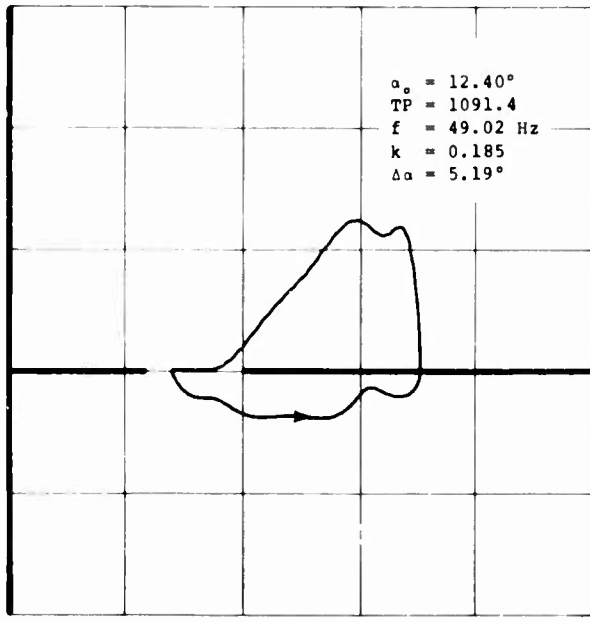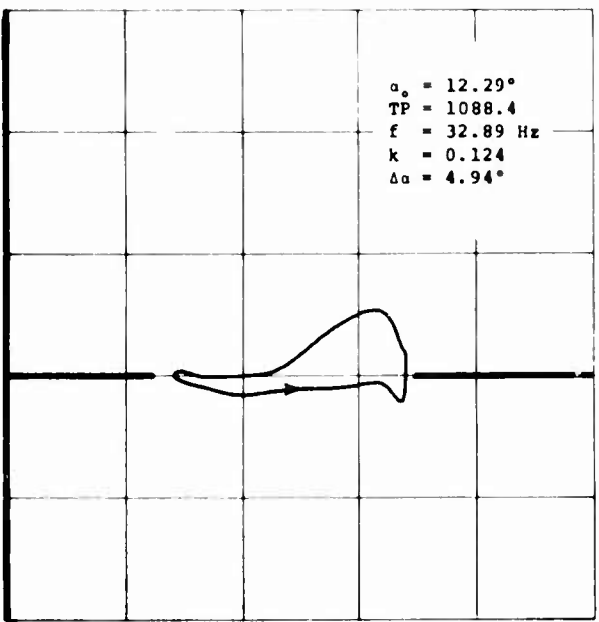
123

A₁

$\alpha_o$ = 12.29°
TP = 1088.4
f = 32.89 Hz
k = 0.124
$\Delta\alpha$ = 4.94°

$\alpha_o$ = 12.40°
TP = 1091.4
f = 49.02 Hz
k = 0.185
$\Delta\alpha$ = 5.19°

$\alpha_o$ = 12.28°
TP = 1098.4
f = 80.32 Hz
k = 0.302
$\Delta\alpha$ = 5.63°

$\alpha_o$ = 12.45°
TP = 1102.4
f = 94.34 Hz
k = 0.355
$\Delta\alpha$ = 5.65°

.22°
085.4
.38 Hz
.062
.83°

2.33°
092.4
3.37 Hz
.238
.31°

20          25

0          5          10          15          20          25

ANGLE OF ATTACK ($\alpha$) - DEGREES

0          5          10          15          20          25

ANGLE OF ATTACK ($\alpha$) - DEGREES

cremental Work With Oscillation
he Vertol 23010-1.58 Airfoil at
.25°, and $\Delta\alpha$ = 5°.

123
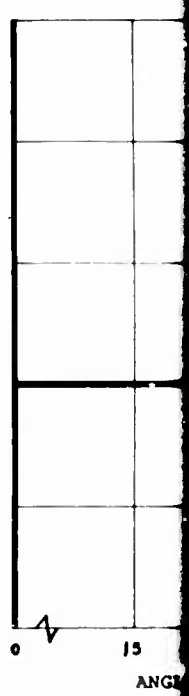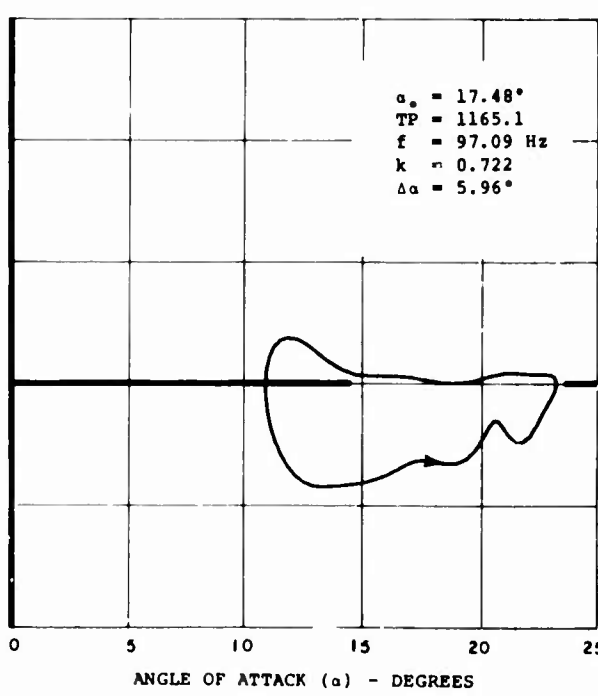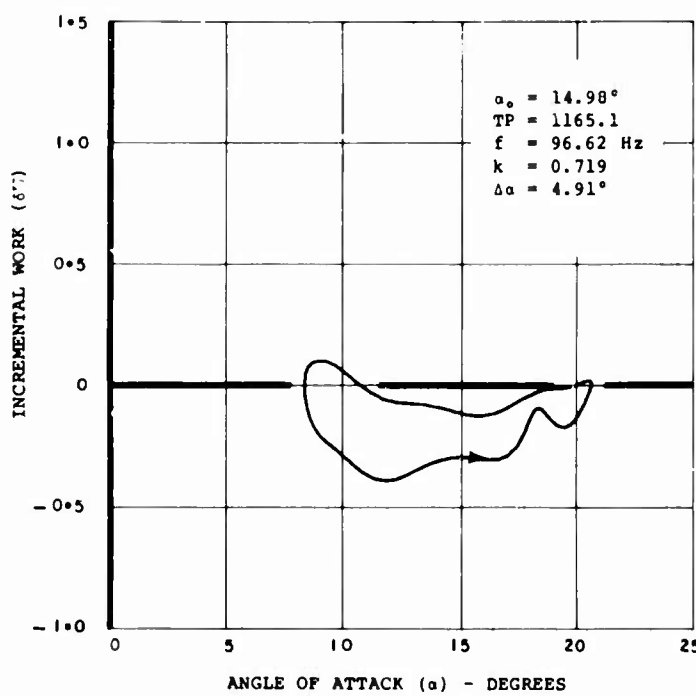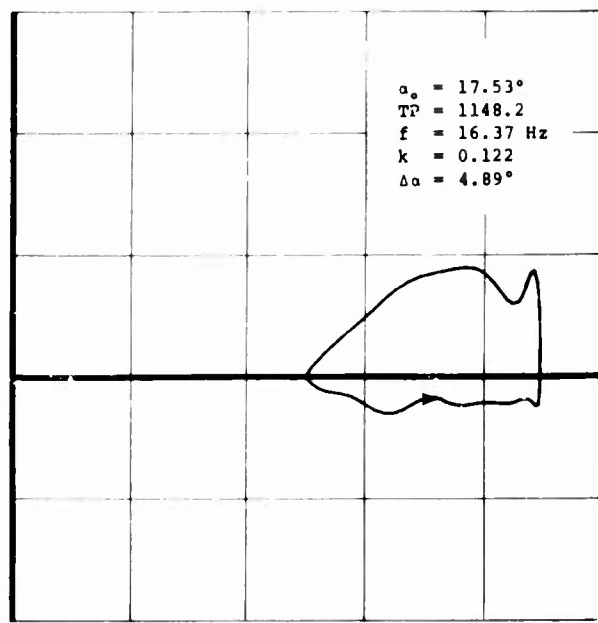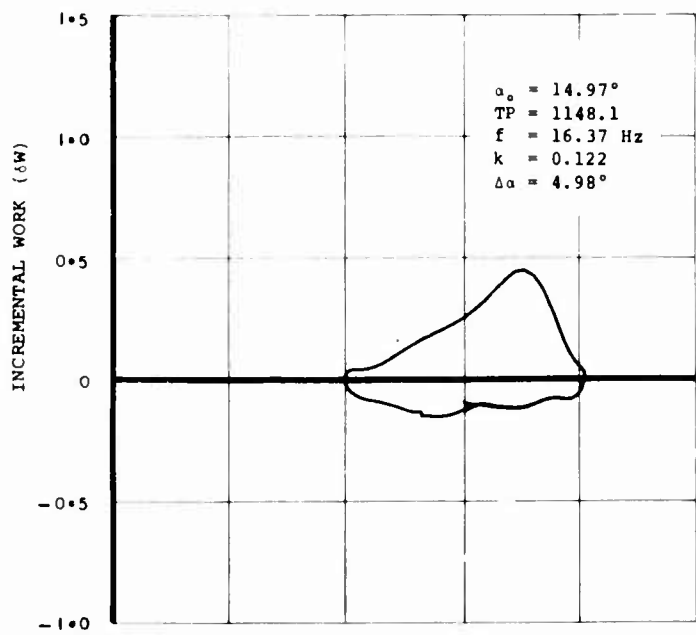
Figure 60.   Variation of Incremental Work for the Vertol
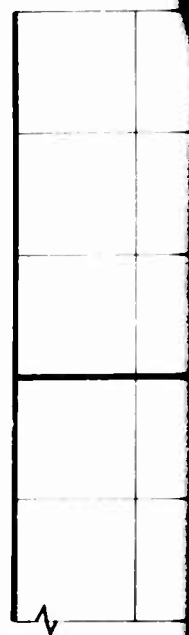            23010-1.58 Airfoil at M = 0.2, f = 16 and
            96 Hertz, and $\Delta\alpha = 5°$.

125

$A_1$
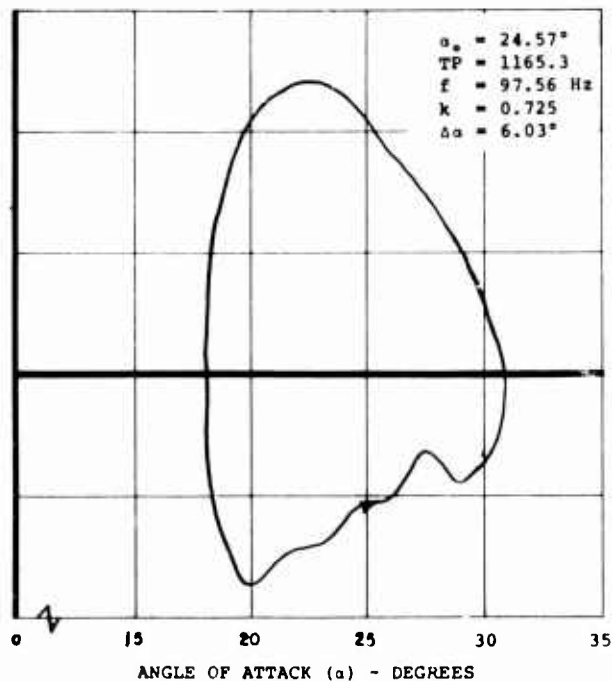
Incremental Work for the Vertol
rfoil at M = 0.2, f = 16 and
Δα = 5°.

125

B.

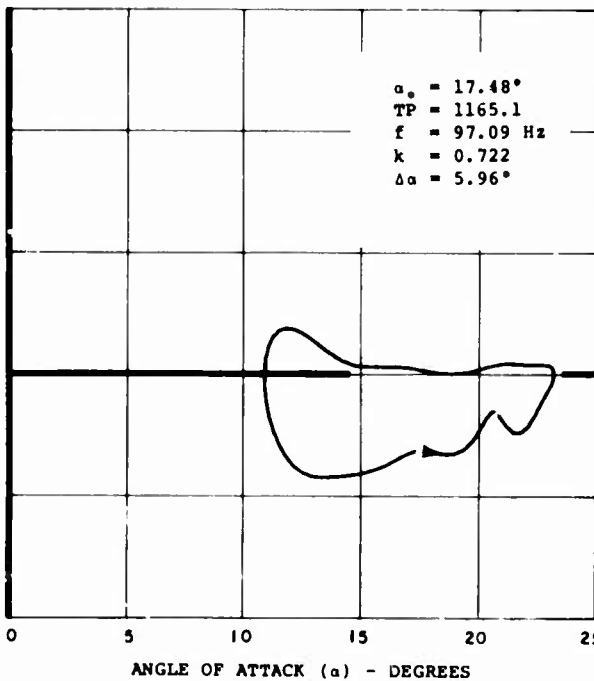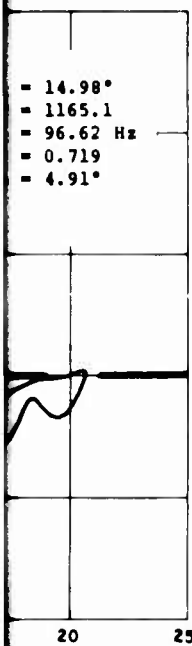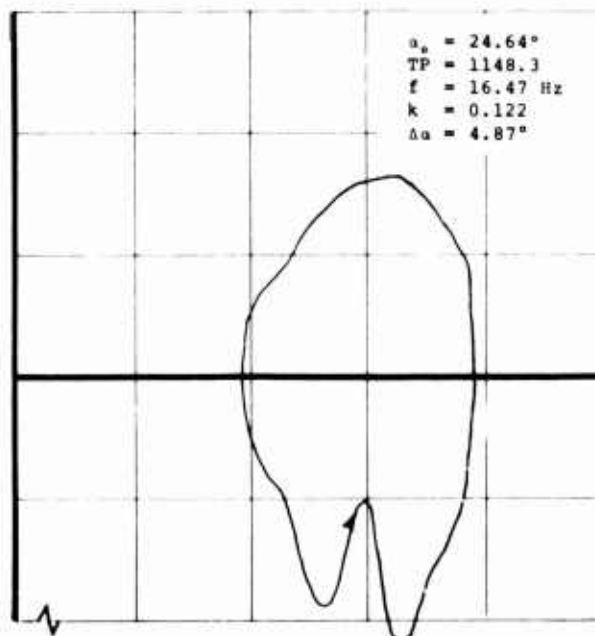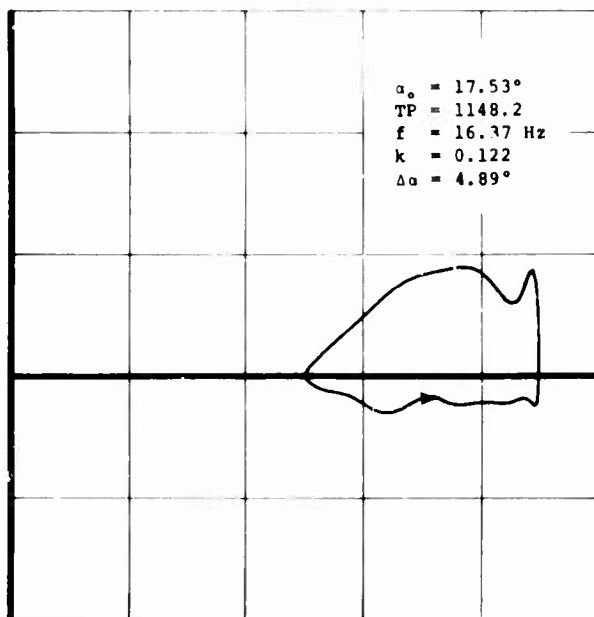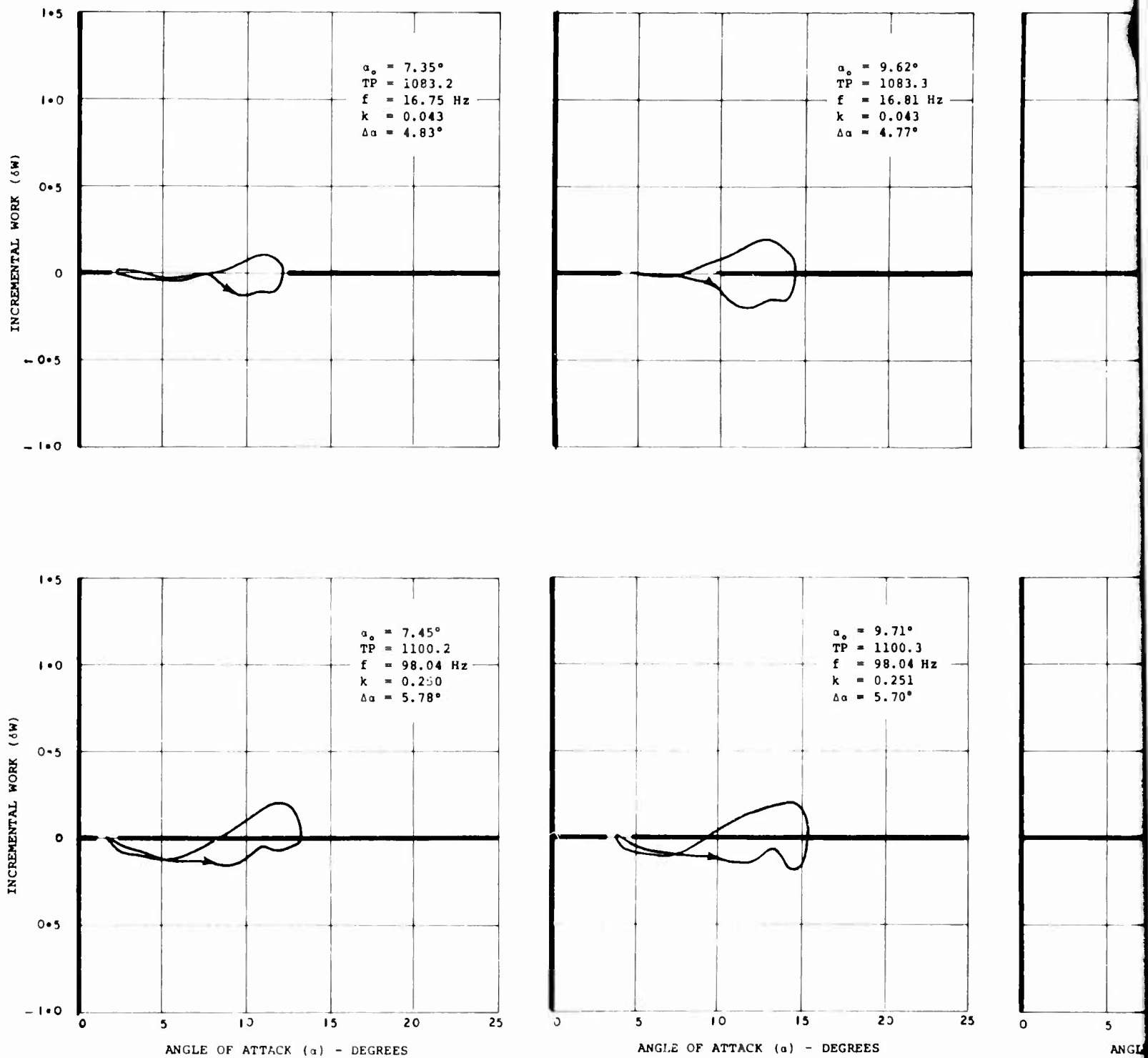Figure 61.  Variation of Incremental Work for the
Vertol 23010-1.58 Airfoil at M = 0.6,
f = 16 and 96 Hertz, and Δα = 5°.
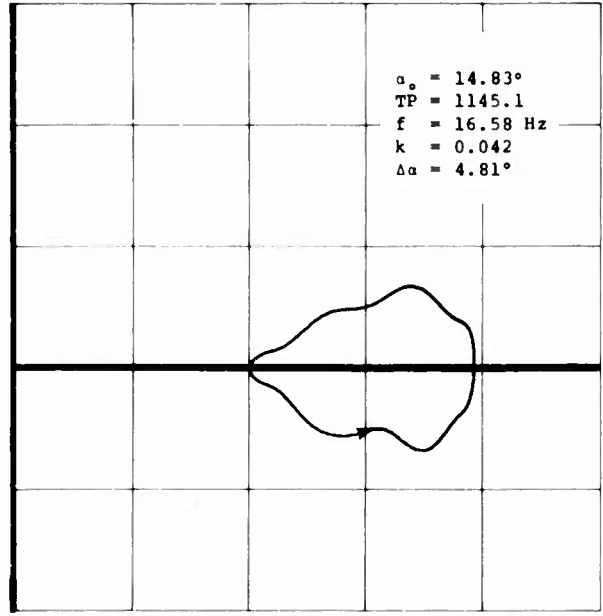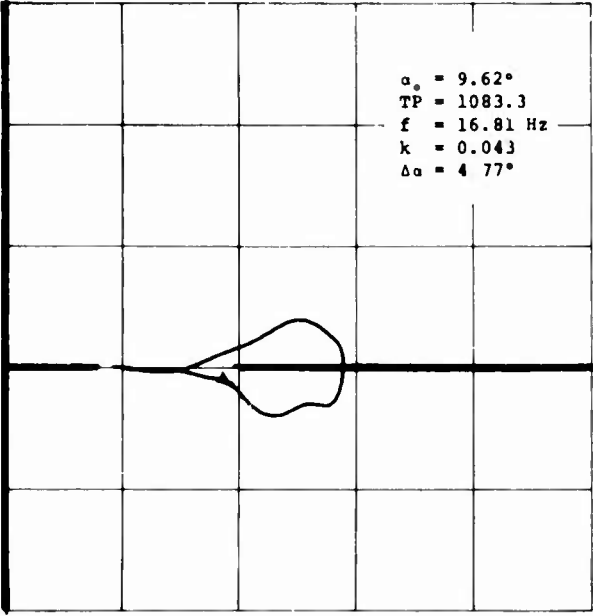
127

A.

Upper left panel:

35°
83.2
.75 Hz
043
83°

Upper middle panel:

$\alpha_o$ = 9.62°
TP = 1083.3
f = 16.81 Hz
k = 0.043
$\Delta\alpha$ = 4.77°

Upper right panel:

$\alpha_o$ = 14.83°
TP = 1145.1
f = 16.58 Hz
k = 0.042
$\Delta\alpha$ = 4.81°

Lower left panel:

45°
00.2
.04 Hz
250
78°

Lower middle panel:

$\alpha_o$ = 9.71°
TP = 1100.3
f = 98.04 Hz
k = 0.251
$\Delta\alpha$ = 5.70°

Lower right panel:

$\alpha_o$ = 14.93°
TP = 1164.1
f = 97.09 Hz
k = 0.248
$\Delta\alpha$ = 5.75°
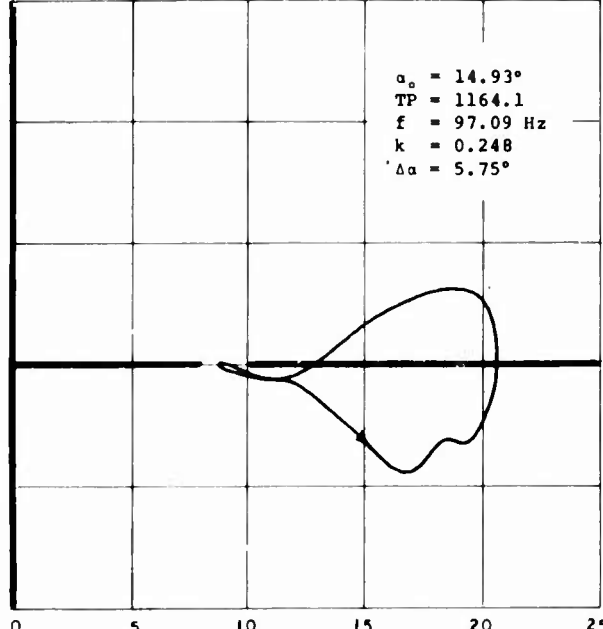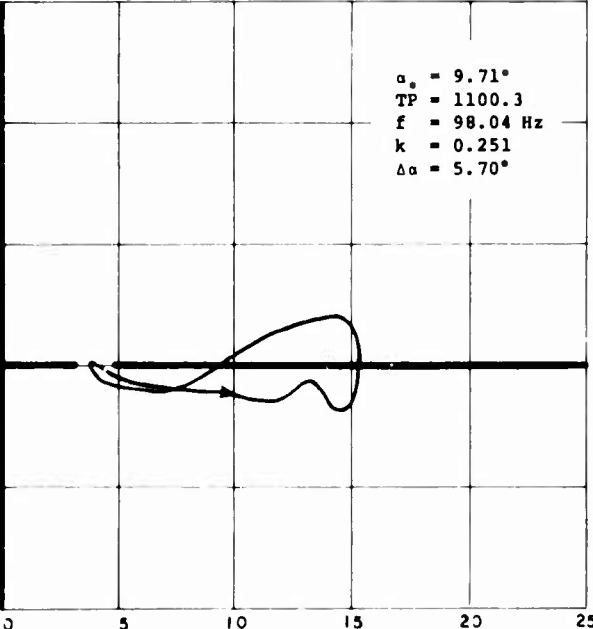
ANGLE OF ATTACK ($\alpha$) - DEGREES    ANGLE OF ATTACK ($\alpha$) - DEGREES

Incremental Work for the
-1.58 Airfoil at M = 0.6,
Hertz, and $\Delta\alpha$ = 5°.

27

B.
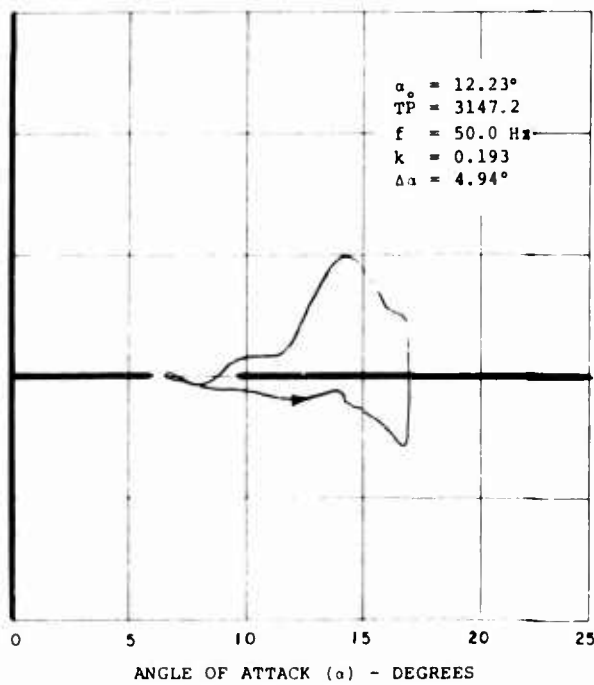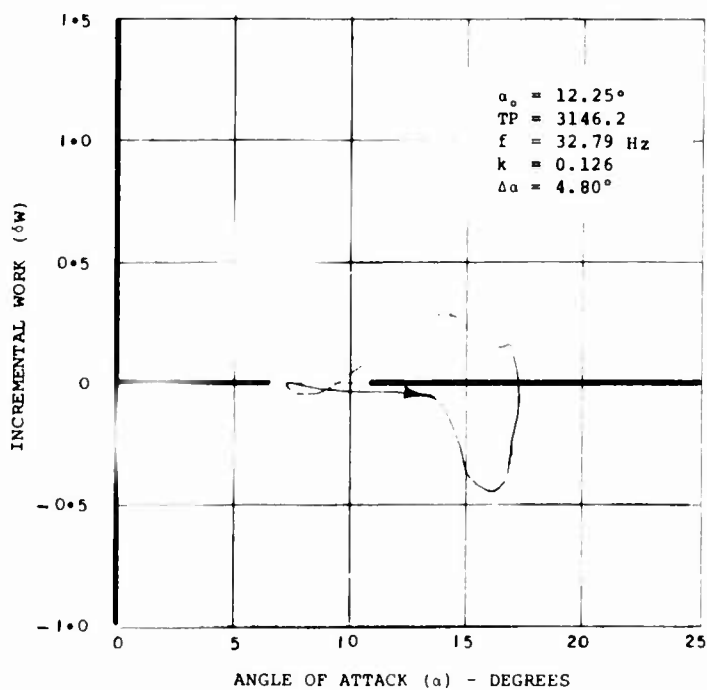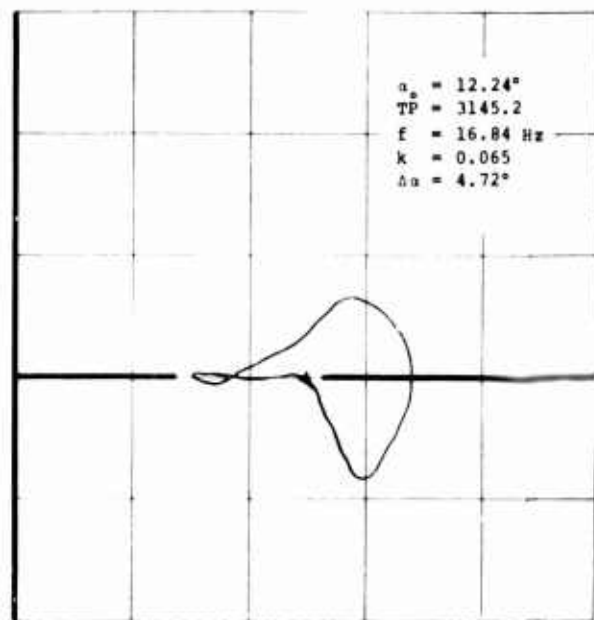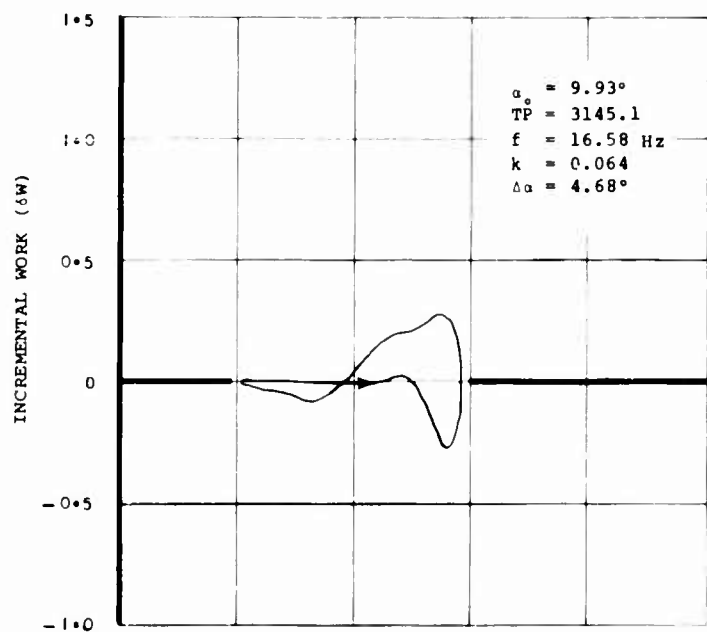
Figure 62.    Variation of Incremental Work for NACA 0012
              (Modified) Airfoil at M = 0.4.

129

A.

9.93°
3145.1
16.58 Hz
0.064
4.68°

$\alpha_o$ = 12.24°
TP = 3145.2
f = 16.84 Hz
k = 0.065
$\Delta\alpha$ = 4.72°
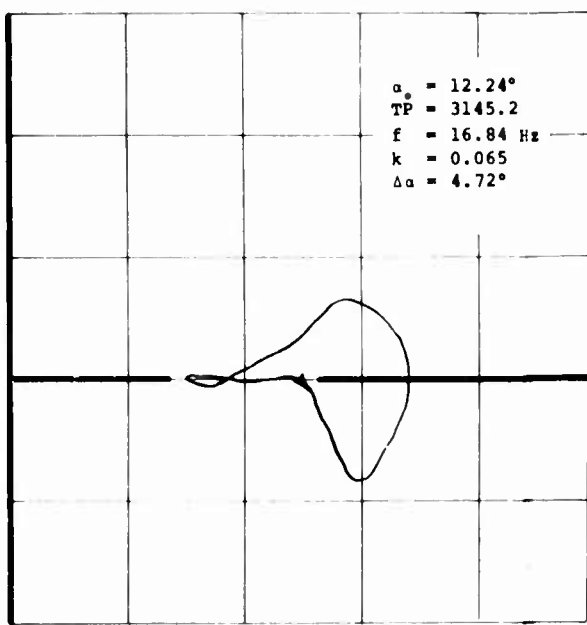
$\alpha_o$ = 14.7°
TP = 3145.3
f = 16.56 Hz
k = 0.064
$\Delta\alpha$ = 4.69°
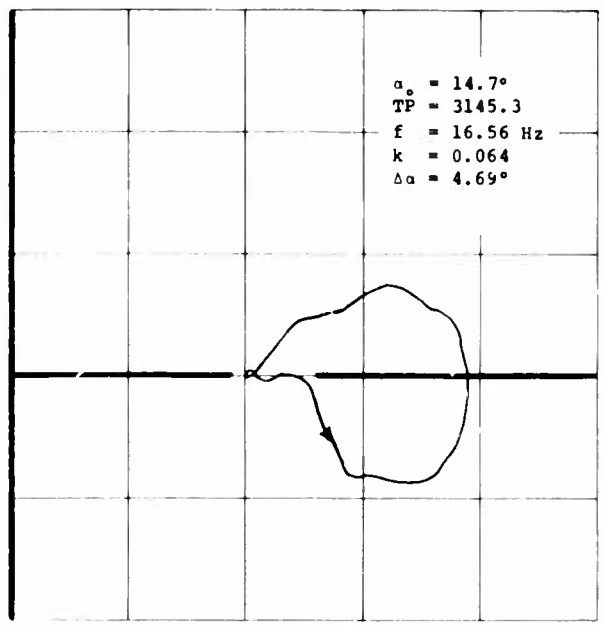
12.25°
3146.2
32.79 Hz
0.126
4.80°

$\alpha_o$ = 12.23°
TP = 3147.2
f = 50.0 Hz
k = 0.193
$\Delta\alpha$ = 4.94°
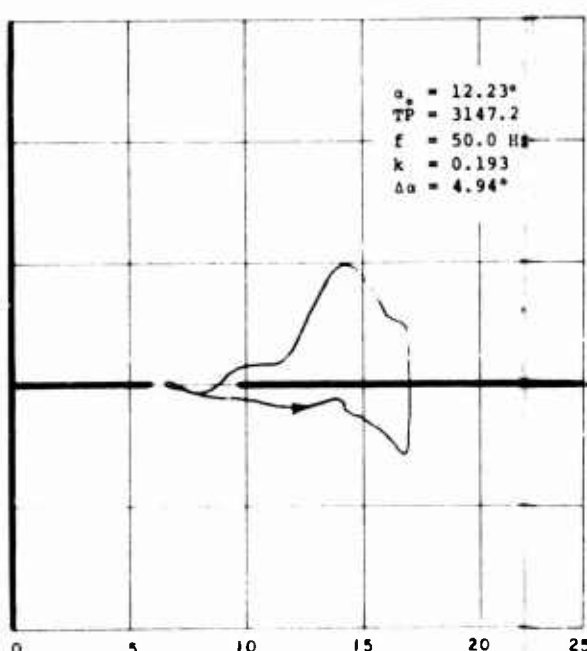
$\alpha_o$ = 11.80°
TP = 3191.4
f = 97.09 Hz
k = 0.371
$\Delta\alpha$ = 5.98°

20    25          0      5      10     15     20     25          0      5      10     15     20     25

ES          ANGLE OF ATTACK ($\alpha$) - DEGREES          ANGLE OF ATTACK ($\alpha$) - DEGREES

Incremental Work for NACA 0012
airfoil at M = 0.4.

129

$\mathcal{B}$

**DOCUMENT CONTROL DATA - R&D**

*(Security classification of title, body of abstract and indexing annotation must be entered when the overall report is classified)*

| 1. ORIGINATING ACTIVITY (Corporate author) | 2a. REPORT SECURITY CLASSIFICATION |
|---|---|
| The Boeing Company | Unclassified |
| Vertol Division | 2b. GROUP |
| Philadelphia, Pennsylvania | |

3. REPORT TITLE

Two-Dimensional Tests of Airfoils Oscillating Near Stall
Volume I    Summary and Evluation of Results

4. DESCRIPTIVE NOTES (Type of report and inclusive dates)

Final Technical Report

5. AUTHOR(S) (Last name, first name, initial)

Liiva, Jaan                     Gray, Lewis
Davenport, Franklyn J.          Walton, Ivor C.

| 6. REPORT DATE | 7a. TOTAL NO. OF PAGES | 7b. NO. OF REFS |
|---|---|---|
| April 1968 | 148 | 17 |

| 8a. CONTRACT OR GRANT NO. | 9a. ORIGINATOR'S REPORT NUMBER(S) |
|---|---|
| DA 44-177-AMC-438(T) | |
| b. PROJECT NO. | USAAVLABS Technical Report 68-13A |
| Task 1F125901A14231 | |
| c. | 9b. OTHER REPORT NO(S) (Any other numbers that may be assigned this report) |
| d. | Boeing Document D8-0678-1 |

10. AVAILABILITY/LIMITATION NOTICES

| 11. SUPPLEMENTARY NOTES | 12. SPONSORING MILITARY ACTIVITY |
|---|---|
| Volume I of a 2-volume report | U.S. Army Aviation Materiel Laboratories, Fort Eustis, Virginia |

13. ABSTRACT

An experimental investigation into rotor blade dynamic stall was
conducted.  Two typical airfoils, the NACA 0012 (modified) and the
Vertol 23010-1.58, were tested by measuring the differential
pressures acting during pitching and translatory oscillations over
a range of angles of attack covering the stall regime.  There were
two main objectives.  The first was to determine the influence of
stall on the aerodynamic pitching moment of an airfoil executing
pitching motions corresponding to the elastic torsional oscillations
of a rotor blade.  The second was to determine the extent to which
time-varying angle of attack could affect the maximum aerodynamic
lift that a rotor blade can develop.  The cambered profile remained
free of negative damping for 3 to 6 degrees beyond the point where
the symmetrical section encountered negative damping in the Mach
0.2 to 0.4 range.  The cambered section exhibited higher attainable
$C_N$'s than the symmetrical section under all conditions of motion,
except for the highest frequency tested at Mach 0.6.

**DD** FORM 1473
JAN 64

| 14. KEY WORDS | LINK A | | LINK B | | LINK C | |
|---|---|---|---|---|---|---|
| | ROLE | WT | ROLE | WT | ROLE | WT |
| Airfoil | | | | | | |
| Blade Stall | | | | | | |
| Blade Damping | | | | | | |
| Cambered Profile | | | | | | |
| Symmetrical Profile | | | | | | |
| Translatory Oscillation | | | | | | |
| Pitching Oscillation | | | | | | |

## INSTRUCTIONS

1. **ORIGINATING ACTIVITY:** Enter the name and address of the contractor, subcontractor, grantee, Department of Defense activity or other organization (*corporate author*) issuing the report.

2a. **REPORT SECURITY CLASSIFICATION:** Enter the overall security classification of the report. Indicate whether "Restricted Data" is included. Marking is to be in accordance with appropriate security regulations.

2b. **GROUP:** Automatic downgrading is specified in DoD Directive 5200.10 and Armed Forces Industrial Manual. Enter the group number. Also, when applicable, show that optional markings have been used for Group 3 and Group 4 as authorized.

3. **REPORT TITLE:** Enter the complete report title in all capital letters. Titles in all cases should be unclassified. If a meaningful title cannot be selected without classification, show title classification in all capitals in parenthesis immediately following the title.

4. **DESCRIPTIVE NOTES:** If appropriate, enter the type of report, e.g., interim, progress, summary, annual, or final. Give the inclusive dates when a specific reporting period is covered.

5. **AUTHOR(S):** Enter the name(s) of author(s) as shown on or in the report. Enter last name, first name, middle initial. If military, show rank and branch of service. The name of the principal author is an absolute minimum requirement

6. **REPORT DATE:** Enter the date of the report as day, month, year; or month, year. If more than one date appears on the report, use date of publication.

7a. **TOTAL NUMBER OF PAGES:** The total page count should follow normal pagination procedures, i.e., enter the number of pages containing information.

7b. **NUMBER OF REFERENCES** Enter the total number of references cited in the report.

8a. **CONTRACT OR GRANT NUMBER:** If appropriate, enter the applicable number of the contract or grant under which the report was written.

8b, 8c, & 8d. **PROJECT NUMBER:** Enter the appropriate military department identification, such as project number, subproject number, system numbers, task number, etc.

9a. **ORIGINATOR'S REPORT NUMBER(S):** Enter the official report number by which the document will be identified and controlled by the originating activity. This number must be unique to this report.

9b. **OTHER REPORT NUMBER(S):** If the report has been assigned any other report numbers (*either by the originator or by the sponsor*), also enter this number(s).

10. **AVAILABILITY/LIMITATION NOTICES:** Enter any limitations on further dissemination of the report, other than those imposed by security classification, using standard statements such as:

(1) "Qualified requesters may obtain copies of this report from DDC."

(2) "Foreign announcement and dissemination of this report by DDC is not authorized."

(3) "U. S. Government agencies may obtain copies of this report directly from DDC. Other qualified DDC users shall request through

_____."

(4) "U. S. military agencies may obtain copies of this report directly from DDC. Other qualified users shall request through

_____."

(5) "All distribution of this report is controlled. Qualified DDC users shall request through

_____."

If the report has been furnished to the Office of Technical Services, Department of Commerce, for sale to the public, indicate this fact and enter the price, if known.

11. **SUPPLEMENTARY NOTES:** Use for additional explanatory notes.

12. **SPONSORING MILITARY ACTIVITY:** Enter the name of the departmental project office or laboratory sponsoring (*paying for*) the research and development. Include address.

13. **ABSTRACT:** Enter an abstract giving a brief and factual summary of the document indicative of the report, even though it may also appear elsewhere in the body of the technical report. If additional space is required, a continuation sheet shall be attached.

It is highly desirable that the abstract of classified reports be unclassified. Each paragraph of the abstract shall end with an indication of the military security classification of the information in the paragraph, represented as *(TS)*, *(S)*, *(C)*, or *(U)*

There is no limitation on the length of the abstract. However, the suggested length is from 150 to 225 words.

14. **KEY WORDS:** Key words are technically meaningful terms or short phrases that characterize a report and may be used as index entries for cataloging the report. Key words must be selected so that no security classification is required. Identifiers, such as equipment model designation, trade name, military project code name, geographic location, may be used as key words but will be followed by an indication of technical context. The assignment of links, rules, and weights is optional.

AFLC–WPAFB–JUL 66 3M